

DEVELOPMENT OF A BIOMIMETIC IN VITRO SKELETAL MUSCLE TISSUE MODEL

A Dissertation

Submitted to the Faculty of
WORCESTER POLYTECHNIC INSTITUTE.


in partial fulfillment of the requirements of:

Degree of Doctor of Philosophy in Biomedical Engineering.

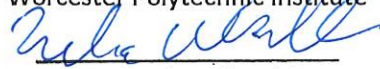
February 15, 2017

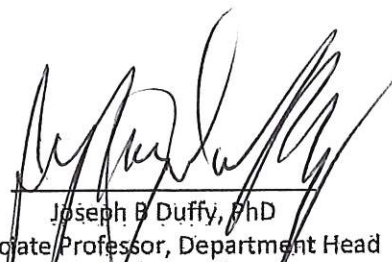
By

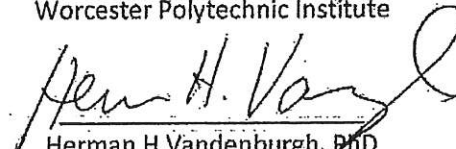

Jason M Forte


Raymond L Page, PhD
Professor of Practice (Advisor)
Biomedical Engineering
Worcester Polytechnic Institute


Kristen L Billar, PhD
Professor, Department Head (Committee Chair)
Biomedical Engineering
Worcester Polytechnic Institute


Marsha W Rolle, PhD
Associate Professor
Biomedical Engineering
Worcester Polytechnic Institute


Joseph B Duffy, PhD
Associate Professor, Department Head
Biology and Biotechnology
Worcester Polytechnic Institute


Herman H Vandenburg, PhD
Professor Emeritus
Pathology and Laboratory Medicine
Brown University School of Medicine

Acknowledgments

I would like to thank my advisor, Raymond Page for all of his help, support, mentoring, and guidance over the course of my project.

I would like to thank my dissertation committee: Kristen Billiar, Marsha Rolle, Joseph Duffy, and Herman Vandenburg, for their guidance, feedback, and mentoring.

Additional thanks to Sakthikumar Ambady, Tanja Dominko, and George Pins for assistance, mentoring, and guidance.

I would like to thank the following past and present graduate students who have helped me with this project: Jonathan Grasman, Denis Kole, Alexandra Grella, Alyssa Fianza, Katrina Hansen, Joshua Gershlak, Heather Cirka, Frank Benesch-Lee, and Hannah Strobel.

I would like to thank Dr. John Keaney and Siobhan Craige in the Department of Cardiovascular Medicine, UMASS Medical School for the use and assistance with their Wire Myograph.

Additional staff at WPI including Microscopy Technician Victoria Huntress and Histologist Hans Snyder for their expertise and assistance.

Finally, a special thanks to my friends and family, who have helped and supported me through this process. Most importantly, to my wife, Olivia O'Connell - without her loving support, I never would have been able to complete this process.

Contents

Chapter 1: Overview	12
1.1 Introduction	12
1.2 Project Objectives	14
1.3 Conclusions:	17
1.4 References	17
Chapter 2: Background	19
2.1: Clinical Need	19
2.1.1 Muscular Dystrophies	19
2.1.2 Dystrophin Protein Malfunction Leads to Progressive Weakening and Loss of Muscle Function	21
2.1.3 Muscular Dystrophy Lacks a Clinical Treatment	22
2.1.4 Non-Target Drugs Induce Muscle Myalgias and Myopathies	22
2.1.5 Current Drug Development Process/FDA Timeline	23
2.1.5 Statement of Clinical Need	28
2.2: Background - Skeletal Muscle Anatomy, Function, and Repair	29
2.2.1 Skeletal Muscle Anatomy and Structure	29
2.2.2 Development of Muscle - Embryogenesis and Myogenesis	34
2.3 Benchtop Models of Skeletal Muscle.....	38
2.3.1 Salient Features and Guidelines for Successful 3D Benchtop Models.....	38
2.3.2 Current Benchtop Model Systems: Overview, Benefits, and Pitfalls.....	45
2.3.3. Drawbacks of Current Model Systems.....	53
2.4 References	54
Chapter 3: The Generation and characterization of entirely cellular biomimetic 3D skeletal muscle tissue constructs, <i>in vitro</i>	60
3.1 Introduction	60
3.2 Methods	62

3.2.1 Isolation, Derivation, and Characterization of a Primary Skeletal Muscle Cell Line	62
3.2.2. Cell Culture.....	62
3.2.3 Immunocyto- and Immunohistochemistry	64
3.2.4 Myoblast Assembly into Contiguous Tissue Rings.....	67
3.2.5 Mitogen-Reduction Media Induces Myoblast Differentiation.....	69
3.2.6. Decreasing Cell Number Seeded into 3D Tissue Rings	71
3.2.7. Incorporation of Fibroblasts to Improve ECM Production	71
3.2.8. Statistics.....	75
3.3 Results.....	76
3.3.1. A Defined Culture System Prolongs Myogenic Potential, <i>In Vitro</i>	76
3.3.2. Cell Culture and Preparation for Tissue Ring Seeding	78
3.3.3. Myoblasts Fail to Assemble into Contiguous 3D Tissue Rings	78
3.3.4. Mitogen-reduction Induces Myoblast Terminal Differentiation	79
3.3.5. Differentiation Prior to Ring Seeding Improves Ring Formation Efficiency.....	81
3.3.6. Minimizing Cell Number Decreased Tissue Ring Necrosis.....	83
3.3.7. Fibroblasts Improve Tissue Compaction and Nuclear Alignment.....	85
3.4 Discussion.....	91
3.4.1. Growth Factors Coupled with Selective Sub-Culturing Maintain Myogenic Potential	91
3.4.2. Myoblasts Fail to Self Assemble in 3D Culture	94
3.4.3. Mitogen-reduction Induces 2D Terminal Differentiation.....	94
3.4.4. Rationale for Fibroblasts Improving Tissue Compaction and Cellular Alignment	96
3.5 References	98
Chapter 4: The modulations of culture conditions, supplements, and tissue shape improve tissue integrity and enable long-term culture while increasing contractile and ECM protein production.	100
4.1 Introduction	100
4.2 Methods.....	102

4.2.1. Mold Redesign with Slanted Wells and Sloped Posts.....	102
4.2.2. Ascorbic Acid 2-Phosphate Supplementation.....	104
4.2.3. IGF-1 Supplementation.....	106
4.2.4 Statistics.....	106
4.3 Results.....	107
4.3.1. A Mold Redesign Prevents 3D Muscle Tissues Cultured Failure.....	107
4.3.1.4 Mold Redesign Improves 3D Tissue Ring Longevity in Culture.....	114
4.3.2. Ascorbic Acid 2-Phosphate Improves ECM Production During 3D Culture.....	116
4.3.3. IGF-1 Supplementation Improves Contractile Protein Production During 3D Culture.....	118
4.4 Discussion.....	121
4.4.1. Allowing Tissue Constructs to Relax During Maturation Allows for Contractile Protein Development While Preventing Tissue Failure.....	121
4.4.2. The Increase in ECM Production Strengthens Cell-ECM Connections.....	123
4.4.3. Rationale for Myotube Diameter Increase Following IGF-1 Supplementation.....	124
4.5 Conclusion.....	126
4.5 References.....	127
Chapter 5: Functional contractile and mechanical properties are improved following culture and mold modifications.....	129
5.1 Introduction.....	129
5.2 Methods.....	130
5.2.1. Tissue Mechanical Strength Quantification.....	130
5.2.2. Active Tetanic Contractile Force Quantification.....	133
5.2.3. Statistics.....	136
5.3 Results.....	137
5.3.1. Culture Mold and Supplement Modifications Improve Functional Mechanical Strength and Tensile Properties of 3D Tissue Rings.....	137
5.3.2. Active Tetanic Contractile Force Production is Increased for Supplemented Tissues.....	142

5.4 Discussion.....	144
5.4.1. Culture Mold Modifications Improve Mechanical Strength and Tensile Properties of 3D Tissue Rings.....	144
5.4.2. Contractile Function is Improved and Correlated with Culture Mold and Supplement Modifications	147
5.5. Conclusions	149
5.6. References	150
Chapter 6: Downstream Translation of Benchtop Muscle Technology	151
6.1 Overview	151
6.2 Collagen Gel	151
6.3 Dystrophic Tissue Generation	154
6.4 Conclusions	156
6.5 References	157
Chapter 7: Conclusions and Future Work	158
7.1 Overview	158
7.2 Future Work	159
7.2.1 Translating Model into a High-Throughput System.....	159
7.2.2. Translating to a Linearly-Aligned Model System	160
7.2.3. Dystrophic Modeling - Translation	161
7.2.4. Mechanical and Electrical Conditioning to Improve Maturation	161
7.3 Contribution to Science	162
7.4 References	164
Appendix	165
Hematoxylin and Eosin Staining Protocol:.....	165
Pre-IHC Tissue Hydration Protocol:.....	166
IHC Staining Protocol - HRP Polymer Detection.....	167

Table of Figures

Figure 1: Structure of Skeletal Muscle	30
Figure 2: Skeletal Muscle Sarcomere	32
Figure 3: Schematic of BrdU Incorporation for 2D and 3D Assays	70
Figure 4: Schematic of Fluorescently-labeled Nuclei and Subsequent Nuclear Angle Calculation	74
Figure 5: 2D Proliferative Culture of Primary Myoblasts	76
Figure 6: Differentiation of Passage 8 versus Passage 17 Primary Myoblasts	77
Figure 7: Schematic of Primary Myoblast Culture and Expansion Process	77
Figure 8: The Effect of Mitogen-reduced Media and Timing on Cell Cycle Analysis	79
Figure 9: Quantification of the Effect Mitogen-reduced medium has on Myoblast Proliferation and Differentiation	80
Figure 10: Proliferating Cells following 3 Days of 3D Culture	81
Figure 11: The Effect of Pre-differentiation on Ring Formation Efficiency	82
Figure 12: Contiguous Tissue Ring Formed Around Central Post Following 7 Days Culture	82
Figure 13: Tissue Rings Formed with Varying Cell Numbers	83
Figure 14: Ring Formation Efficiency with Varying Cell Seeding Numbers	84
Figure 15: Percentage of Diameter of Malaligned Nuclei with Decreasing Cell Number	84
Figure 16: Fibroblast Incorporation Into Myoblast Rings	86
Figure 17: Fibroblast Incorporation Quantification of 7 Day Tissue Rings	87
Figure 18: Ring Nuclear Alignment Following 25% Fibroblast Addition	88
Figure 19: Fibroblast Supplementation Increase Myosin in 3D	89
Figure 20: 14 Day 2D Differentiation of Myoblasts and Fibroblast-Supplemented Myoblast Cultures ..	90
Figure 21: Human Myoblast Cells Implanted into Mouse Following Muscle Injury	92
Figure 22: Post Redesign Incorporating Conical Posts and Sloped Wells	103
Figure 23: Ring Failure During 3D Culture	108
Figure 24: 2D Myoblast Differentiation for 7 and 14 Days	109
Figure 25: Ring Formation Efficiency for the Annular and New Angle Wells	110
Figure 26: Ring Formation Efficiency with 300,000 Cells Seeded	111
Figure 27: Tissue Rings on 87.5° Posts	111
Figure 28: Hematoxylin and Eosin of New Angle Tissue Rings	112
Figure 29: Ring Diameter From New Angle Tissue Rings Molds	113
Figure 30: Ring Retention Annular vs. Sloped Post Tissue Rings	114
Figure 31: Myosin and Hematoxylin and Eosin Staining at 14 Days in New Angled Post Tissue Rings	115
Figure 32: Myosin-Positive Nuclei 14 Days New Angle Posts	116
Figure 33: The Effects of Ascorbic Acid on ECM Synthesis	117
Figure 34: Lower and Higher Concentration Ascorbic Acid Supplementation	118
Figure 35: Hematoxylin and Eosin Images of IGF-1 Supplemented Tissue Rings	119
Figure 36: Myosin Staining of IGF-1 Supplemented Tissue Rings	119
Figure 37: IGF-1 Increases Myotube Diameter	120
Figure 38: Mechanical Testing Setup	131
Figure 39: Side-View of Mechanical Testing Setup Showing Ring Anchored Between Glass Hooks	132
Figure 40: Image and Schematic of DMT Myograph and Electric Field Setup	135
Figure 41: Load vs. Extension Graph	138
Figure 42: Failure Load of Tissue Rings	139
Figure 43: Cross-Sectional Area of Tissue Rings	139
Figure 44: Failure Extension of Tissue Rings	140
Figure 45: UTS of Tissue Rings	141
Figure 46: Failure Strain of Tissue Rings	142

Figure 47: Tetanic Contractile Force of Tissue Rings 143
Figure 48: Tensile Stress of Contractile Force Production 144
Figure 49: Failure Load of Tissue Rings 146
Figure 50: H&E Images of Collagen Gel Rings 153
Figure 51: Myosin Heavy Chain Staining of Collagen-Gel Tissue Rings 154
Figure 52: 14 Day Differentiation of FSHD Cells 155
Figure 53: FSHD Tissue Rings 156

Table of Tables

Table 1: Primary Antibodies Used for Immunocyto/histo-chemical Analysis	65
Table 2: Secondary Antibodies Used for Immunocytochemical Staining Detection	65
Table 3: Reagents used for IHC Analysis - HRP Peroxidase Staining and Detection	67
Table 4: Inner Ring Diameters From New Angle Tissue Ring Molds.....	113
Table 5: Ring Types and Supplements Used for Mechanical Testing	130
Table 6: 60mM K-PSS Bicarbonate Buffer Recipe.....	134

Abbreviations

AA - Ascorbic Acid 2-phosphate
AHs - Adult Horse Serum
BrdU - Bromodeoxyuridine
DM - Differentiation Medium
DMD - Duchenne's Muscular Dystrophy
DMEM - Dulbecco's Modification of Eagle's Medium
ECM - Extracellular Matrix
EGF - Epidermal Growth Factor
FBS - Fetal Bovine Serum
FCIII - FetalClonelll
FGF-2 - Fibroblast Growth Factor - 2 (basic)
FSHD - Facioscapulohumeral muscular dystrophy
H&E - Hematoxylin and Eosin
HGF - Hepatocyte Growth Factor
Hskm - Human Skeletal Muscle Cells
ICC - Immunocytochemistry
IHC - Immunohistochemistry
IGF-1 - Insulin-like Growth Factor - 1
IMDM - Iscove's Modification of Dulbecco's Medium
ITS - Insulin, Transferrin, Selenium
K-PSS - Physiologic salt solution - Potassium rich
MD - Muscular Dystrophies
MGM - Myoblast Growth Medium
MHC - Myosin Heavy Chain
MRF - Myogenic Regulator Factors
PBS - Phosphate Buffered Saline
UTS - Ultimate Tensile Strength
VML - Volumetric Muscle Loss

Abstract

Many congenital skeletal muscle disorders including muscular dystrophies are caused by genetic mutations that lead to a dysfunction in myocytes effectively binding to the extracellular matrix. This leads to a chronic and continuous cycle of breakdown and regeneration of muscle tissue, ultimately resulting in loss of muscle function and patient mortality. Such disorders lack effective clinical treatments and challenge researchers to develop new therapeutics. The current drug development process often yields ineffective therapeutics due to the lack of genetic homology between pre-clinical animal models and humans. In addition current engineered tissue models using human cells fail to properly emulate native muscle morphology and function due to necrotic tissue cores and an abundance undigested ECM protein. Thus, a more precise benchtop model of 3D engineered human muscle tissue could serve as a better platform for translation to a disease model and could better predict candidate drug efficacy during pre-clinical development.

This work presents the methodology for generating a high-content system of contiguous skeletal muscle tissue constructs produced entirely from human cells by using a non-adhesive hydrogel micro-molding technique. Subsequent culture and mold modifications confirmed by morphological and contractile protein analysis improve tissue longevity and myocyte maturation. Finally, mechanical strength and contractile force measurements confirmed that such modulations resulted in skeletal muscle microtissues that were more mimetic of human muscle tissue.

This cell self-assembly technique yielded tissues approximately 150 μ m in diameter with cell densities approaching that of native muscle. Modifications including seeding pre-differentiated myoblasts and the addition of ECM producing fibroblasts improved both tissue formation efficiency and cell alignment. Further culture modifications including supplementation of the culture medium with 50 μ g/ml ascorbic acid and 100ng/ml Insulin-like growth factor-1 coupled with a mold redesign that allowed tissue to passively contract during maturation while still remaining anchored under tension further improved ECM production, myogenic differentiation, and long-term longevity in culture. Further confirmation of the culture improvements were demonstrated by increases in mechanical strength and contractile force production.

In conclusion, this approach overcomes cell density limitations with exogenous ECM-based methods and provides a platform for producing 3D models of human skeletal muscle by making tissue entirely using cells.

Future work will attempt to translate the methodology used for tissue generation and long-term culture to create benchtop models of disease models of skeletal muscle, streamlining pre-clinical benchtop testing to better predict candidate drug efficacy for skeletal muscle diseases and disorders along with elucidating side effects of non-target drugs.

Chapter 1: Overview

1.1 Introduction

Muscular dystrophy is a group of nine main skeletal muscle disorders that affects upwards of 1 in 3000 individuals (primarily males) [1]. The disorder is autosomal or X-linked recessive genetic-based and depending on the type and severity, results in chronic muscle breakdown, ultimately leading to decreased muscle function, loss of patient ambulation and poor quality of life. In the case of the especially virulent Duchenne's muscular dystrophy (accounting for roughly half of the total cases), severe muscle loss ultimately becomes fatal, generally by the patient's mid-20's due to cardiac or respiratory failure, with milder variants of dystrophy manifest as non-fatal, but still depreciate quality of life [2, 3]. The disease origin is due to a malfunctioning 427kDa molecular weight dystrophin protein which is primarily responsible for anchoring the myocyte to the extracellular matrix (ECM) [1, 4, 5]. Such malfunction leads to myofiber breakdown and chronic regeneration, leading to progressive loss of regenerative capacity and ultimately, loss of muscle function [1, 3].

Currently, there is no cure for muscular dystrophy. Current therapeutics aim to treat only the symptoms of muscular dystrophy and are generally limited to glucocorticoids (prednisone) and physical therapy that aim to maintain muscle mass, prolonging patient ambulation. Such therapeutics aim to maintain quality of life, but are nevertheless temporary in relief and simply prolong the inevitable fatality [1]. Furthermore, side-effects of prednisone treatment include risk of hyperplasia and decreased bone density, increasing prevalence of fracture, necessitating the need for a proper therapeutic to be developed to treat muscular dystrophy [1].

Currently, drug-development for the treatment of muscular dystrophy has been unsuccessful. The drug-development process begins with initial benchtop discovery of drug compounds with further

translation to preclinical animal models. While a muscular dystrophy mouse model exists, the model only recapitulates disease phenotype and not the genetic makeup of the disease (due to lack of genetic homology between mice and humans), and unlikely will ever properly emulate muscular dystrophy [6-8]. Additionally, development of a benchtop model of skeletal muscle that could ultimately be translated to a dystrophic model system has been recently developed, to functionally allow for the bypass of poorly-predictive preclinical animal models [9, 10].

Unfortunately, while researchers have understood the salient morphological and functional attributes of native skeletal muscle including the crucial importance of the ECM during muscle embryogenesis and regeneration, to date, no model system currently exists that properly emulates human skeletal muscle. Additionally, past work demonstrates that researchers understand the importance of building anchored 3D models to mimic native tissue morphology and myotendinous junctions [9]. Current models integrate myoblasts atop or within 3D fibrin and collagen gels in an attempt to provide the myoblasts with sufficient ECM protein to direct differentiation and maturation [9, 11-13]. Further work has investigated mechanical conditioning and electrical stimulation, aimed at improving contractile function [11, 14]. Yet still, limitations of current models exist, limiting their effectiveness to serve as a model of native skeletal muscle. Such limitations include low cell density and potential necrotic/acellular tissue core, due to the large percentage of undigested exogenous ECM protein. Furthermore, the sub-native cell density results in low cell fusion and subsequently force production approximating 1-2% of that of native muscle [10, 15]. Finally, many of the current model systems utilize immortalized animal cell lines, resulting in data that does not translate to the clinic, and requiring re-verification with primary human cells. To date, preclinical animal models differ in genetic homology and current benchtop models fail to precisely mimic the morphology and function of native skeletal muscle.

As such, a clear need exists for a more precise benchtop model of skeletal muscle that is formed using human cells, emulates native morphology and crucial myocyte-ECM interaction. Such a model would provide researchers with a high-content, inexpensive drug screening tool to streamline and potentially bypass ineffective and costly preclinical animal models in the development of a treatment for muscular dystrophies. The following section highlights the main project goal and specific project objectives that were completed towards accomplishing this goal.

1.2 Project Objectives

The goal of this project was to develop a more mimetic model of human skeletal muscle tissue on the benchtop. Current benchtop models fail to recapitulate native skeletal muscle and current animal models used in preclinical testing are poorly-predictive of human skeletal muscle diseases and disorders, resulting in substantial time and money spent on elucidating effective therapeutics identified during investigative drug discovery. This model aims to improve upon past models in that it can be generated from a clinically-relevant cell source and free of tissue necrosis or undigested exogenous ECM. Furthermore, the tissue generation method is aimed to be conducted in an assay-like array, such that tissue generation is in a high-content system, decreasing reagent costs. Subsequent culture modulations may optimize the synthesis of ECM by co-culturing fibroblasts into the tissue constructs while maintaining native levels of protein composition and tissue morphology. Confirmation of categorical improvements can be confirmed by investigating tissue morphology, contractile protein expression, and by measuring both mechanical properties and contractile force generation of the tissues.

This benchtop model will therefore provide researchers with a better benchmark *in vitro* skeletal muscle tissue that can be further adapted to a disease model which can then be used as a more

precise model and subsequently streamline drug development and diagnostic testing of skeletal muscle disorders.

To address the challenges of developing a human skeletal muscle tissue mimetic model that more precisely represents the morphology and function of native muscle, the following three objectives were proposed and completed:

Objective 1: Generate and characterize entirely cellular biomimetic 3D skeletal muscle tissue constructs, *in vitro*

The first objective of this thesis was to use a novel self-assembly technique to generate a minimal functional unit of skeletal muscle. Subsequent experimentation and characterization was completed to determine the benefits and pitfalls of using this technique. Further optimization of the 3D tissue cultures involved minimizing cell number to minimize necrosis as well as incorporating ECM-producing fibroblasts to mediate ECM synthesis, increase cell fusion and tissue maturation, while maintaining a high level of tissue formation. To analyze the effects of such culture modification, we used quantitative immunohistochemistry (IHC) staining for contractile protein accumulation (myosin heavy chain), coupled with morphological histological analysis to identify changes in cell density and tissue maturation. The results of these studies will demonstrate that a self-assembly system can be validated and optimized for the production of 3D skeletal muscle tissue constructs, *in vitro*. The results of this objective suggest that 3D mimetic models of skeletal muscle could be generated using a self-assembly process, and that modulations to cell seeding number and inducing differentiation prior to construct seeding reduced tissue necrosis and improved overall tissue formation efficiency.

Objective 2: Modulate culture conditions, supplements, and tissue shape to improve tissue integrity and enable long-term culture while increasing contractility and ECM protein production

The first objective outlined methodology for generating viable 3D skeletal muscle tissue constructs, yet limitations in functionality and long-term culture remained an issue, with many cultures

failing to maintain contiguity beyond 10 days in culture. The second objective of this thesis was to couple both culture modifications with a system that promotes long-term culture beyond 7 days, and more native levels of tissue maturation. Such modulations involved a mold redesign to enable initial tissue relaxation, preventing self compaction-related tissue failure, thus promoting long-term tissue culture. Furthermore, this objective involved supplementing the constructs with Ascorbic Acid to increase collagen secretion, and IGF-1 to increase myotube diameter and maturation. To analyze the effects of such modulations, quantitative IHC for myosin heavy chain along with salient ECM proteins found in native skeletal muscle identified the effect that reducing tension and supplementation had on long-term culture and protein production. The results of this objective suggest that long-term culture can be improved and that optimization experiments for both ascorbic acid and IGF-1 supplements can improve ECM production and myosin-positive myotube diameters.

Objective 3: Determine if culture and mold modifications improve mechanical strength and contractile function of muscle tissues, *in vitro*

The prior two objectives have demonstrated that categorical improvements through both culture and mold modifications result in 3D tissue that more closely mimics native skeletal muscle. The goal of this objective was to correlate the morphological improvements to mechanical strength analysis via uniaxial tensile testing and to functional force production by electrically-stimulating the tissues to contract and measure the resulting contractile force. We demonstrated that the addition of ascorbic acid and IGF-1 result in a statistical improvement in failure load and ultimate tensile strength (UTS) following uniaxial tensile testing. Furthermore, similar improvements in contractile force production were quantified, where supplemented tissue constructs produced statistically more force when subjected to an isometric tetanic force contractility test.

1.3 Conclusions:

In conclusion, this thesis describes novel methodology for generating an entirely cellular 3D skeletal muscle tissue constructs in a platform that promotes high-content generation of tissue constructs, minimizing cell number and reagent requirements compared to past research. Such tissue constructs were then subjected to culture and mold modifications that improved long-term culture integrity along with the production of salient contractile protein and ECM protein production during extended culture. Finally, mechanical testing and contractile force measurements correlated the categorical improvements with quantitative functional data.

This skeletal muscle model system may provide researchers with a more adept system capable of being adapted to a patient-specific disease model of skeletal muscle disorders, potentially streamlining the development of therapeutics and reducing the need for costly and poorly-predictive pre-clinical animal modeling.

1.4 References

1. Malik, V., L.R. Rodino-Klapac, and J.R. Mendell, *Emerging drugs for Duchenne muscular dystrophy*. *Expert Opin Emerg Drugs*, 2012. **17**(2): p. 261-77.
2. Eagle, M., et al., *Survival in Duchenne muscular dystrophy: improvements in life expectancy since 1967 and the impact of home nocturnal ventilation*. *Neuromuscular Disorders*, 2002. **12**(10): p. 926-929.
3. Muntoni, F., S. Torelli, and A. Ferlini, *Dystrophin and mutations: one gene, several proteins, multiple phenotypes*. *The Lancet Neurology*, 2003. **2**(12): p. 731-740.
4. Ervasti, J.M. and K.P. Campbell, *A Role for the Dystrophin-Glycoprotein Complex as a Transmembrane Linker between Laminin and Actin*. *Journal of Cell Biology*, 1993. **122**(4): p. 809-823.
5. Goyenvalle, A., et al., *Prevention of dystrophic pathology in severely affected dystrophin/utrophin-deficient mice by morpholino-oligomer-mediated exon-skipping*. *Mol Ther*, 2010. **18**(1): p. 198-205.
6. Dellorusso, C., et al., *Tibialis anterior muscles in mdx mice are highly susceptible to contraction-induced injury*. *J Muscle Res Cell Motil*, 2001. **22**(5): p. 467-75.
7. Friedrich, O., et al., *Microarchitecture is severely compromised but motor protein function is preserved in dystrophic mdx skeletal muscle*. *Biophys J*, 2010. **98**.

8. Partridge, T.A., *The mdx mouse model as a surrogate for Duchenne muscular dystrophy*. FEBS J, 2013. **280**(17): p. 4177-86.
9. Vandenburg, H., et al., *Drug-screening platform based on the contractility of tissue-engineered muscle*. Muscle Nerve, 2008. **37**(4): p. 438-47.
10. Mudera, V., et al., *The effect of cell density on the maturation and contractile ability of muscle derived cells in a 3D tissue-engineered skeletal muscle model and determination of the cellular and mechanical stimuli required for the synthesis of a postural phenotype*. J Cell Physiol, 2010. **225**(3): p. 646-53.
11. Powell, C.A., et al., *Mechanical stimulation improves tissue-engineered human skeletal muscle*. Am J Physiol Cell Physiol, 2002. **283**(5): p. C1557-65.
12. Huang, Y.C., et al., *Rapid formation of functional muscle in vitro using fibrin gels*. Journal of Applied Physiology, 2005. **98**(2): p. 706-713.
13. Cheema, U., et al., *3-D in vitro model of early skeletal muscle development*. Cell Motil Cytoskeleton, 2003. **54**(3): p. 226-36.
14. Langelaan, M.L., et al., *Advanced maturation by electrical stimulation: Differences in response between C2C12 and primary muscle progenitor cells*. J Tissue Eng Regen Med, 2011. **5**(7): p. 529-39.
15. Martin, N.R., et al., *Factors affecting the structure and maturation of human tissue engineered skeletal muscle*. Biomaterials, 2013.

Chapter 2: Background

2.1: Clinical Need

There is a significant population that is affected by muscular diseases and disorders that currently lack effective clinical treatment. Such disorders include a variety of muscular dystrophies that often result in reduced mobility, often leading to patient dependence on wheelchairs and depending on the type and severity of the disease, can be terminal. Additionally, a variety of drugs and therapeutics have been discovered to have severe side effects affecting skeletal muscle that clinical testing failed to elucidate, leading to drug recalls and significant health and financial losses. The following section will review the type and severity of muscular disorders, describe the current methodology of disease treatment along with the current disease research being conducted to develop a therapeutic treatment, and finally, present incidences of unwanted side effects of drugs not targeted to treat skeletal muscle disorders. This chapter will present a clear clinical need for the generation of a more precise skeletal muscle model that can serve as a therapeutic testing tool for a variety of applications.

2.1.1 Muscular Dystrophies

2.1.1.1. Duchenne Muscular Dystrophy

Duchenne's muscular dystrophy (DMD) is the most common form of muscular dystrophy in children. As this genetic disease is an X-linked recessive trait, disease presentation is only seen in boys, affecting roughly 1/3,500 [1, 2]. The disease progression is relentless such that ambulation is lost around age 12 and subsequent teen years result in a poor quality of life where patients often suffer from skeletal deformities, and occasionally cognitive deficiencies [1, 3]. Consequently, Duchenne's muscular

dystrophy is 100% fatal, often by the patients early to mid-20's, often due to respiratory or cardiac failure [4].

2.1.1.2 Becker Muscular Dystrophy

Becker muscular dystrophy is considered a milder form of muscular dystrophy with better prognosis. Disease symptoms are similar to those of Duchenne's, except the timeline of disease progression is elongated [3]. Often times, ambulation can be retained for decades with the disease progression ultimately turning fatal later in life (generally between the fourth and sixth decades of life) [1-3]. Similar to Duchenne, the patients' quality of life is reduced over their lifespan, however, not due to the severity and virulence, as Becker muscular dystrophy is believed to only affect a subset (46%) of the dystrophin protein, allowing the patient to retain some muscle function [5]. As such, the mild progression of Becker muscular dystrophy results in patients requiring significant care and assistance towards the later stages of the disease, and in some instances results in higher medical costs, due to the longevity of the disease progression, resulting in the burden of significant health care costs [3].

2.1.1.3 Facioscapulohumeral Muscular Dystrophy

Facioscapulohumeral muscular dystrophy (FSHD) presents symptoms similar to other muscular dystrophies, except the muscular degeneration is localized to groups of muscles in the patients' face, arms and pectoral regions, and in many instances presents as asymmetrical weakness in the muscle groups. FSHD is characterized as an autosomal dominant disease associated with a loss of part of the D4Z4 repeat sequence in the terminal region of chromosome 4 gene (4q35). Loss of repeat sequences leads to expression of the *dux4* gene, which is not normally expressed in skeletal muscle [6, 7]. Expression of this protein in muscle cells is thought to render the affected myocytes susceptible to

oxygen mediated cytotoxicity, although the severity of the malfunction is substantially less virulent and localized to facial muscles [7]. FSHD presents a timeline of symptoms similar to that of Becker's muscular dystrophy, with the far more common adult-onset form beginning to present symptoms by the patients 20's. However, while FSHD can result in a decreased quality of life, it is rarely fatal [6].

2.1.1.4. Bethlem Myopathy and Ullrich Congenital Muscular Dystrophy

Prior work has described skeletal muscle diseases and disorders that originate from dystrophin protein malfunction. In contrast, disorders including Bethlem myopathy (mild) and Ullrich Congenital muscular dystrophy (severe) are due to collagen-based disorders [8, 9]. Such disorders can originate from a variety of pathogenic variants that result in premature termination of collagen VI codons including frameshift-inducing deletions and splice changes [8]. While the incidence of such disease is less common than other dystrophies, averaging 1:100,000 births, the origin of the disease stems from collagen type VI, a protein found throughout all layers of extracellular matrix (ECM) within skeletal muscle. While specific functions of collagen type VI are not completely understood, prior research has postulated that collagen VI plays a role in cell attachment, differentiation and the prevention of apoptosis [9]. Secretion of collagen VI during native development and regeneration has previously been attributed to skeletal muscle interstitial fibroblasts, highlighting the importance of the collagen VI synthesizing fibroblasts within native skeletal muscle to produce the appropriate milieu [9].

2.1.2 Dystrophin Protein Malfunction Leads to Progressive Weakening and Loss of Muscle Function

The common connection between these and other types of muscular dystrophy involves dystrophin, a protein found in muscle tissue [10]. Specifically, dystrophin is a very large, 427 kDa protein (with a primary transcript in muscle measuring 2,100 kilobases), protein that is part of a protein complex

connecting the ECM to the cytoskeleton of the muscle fiber [1, 3, 10]. Briefly (and explained in depth in the following section), muscular dystrophies share a common trait consisting of a genetically-malfunctioning dystrophin protein, leading to constant breakdown and remodeling of the skeletal muscle, and ultimately to the loss of repair and regeneration capability, leading to the progressive weakening and loss of skeletal muscle function, as previously described with the various types of muscular dystrophy [10].

2.1.3 Muscular Dystrophy Lacks a Clinical Treatment

There is no current cure for any muscular dystrophy. Hundreds of clinical trials for DMD drugs and therapeutics have all failed due to lack of efficacy in target patients [1]. Patients suffering from this disease are offered therapeutics aimed at improving the quality of life, but do not treat or inhibit the disease progression. Yet still, only one treatment has consistently shown benefit in prolonging quality of life for patients suffering from decreased muscle function. Treatments using glucocorticoids (steroids) only serve to increase or simply maintain muscle tone and slow the degeneration progression [1, 5, 11]. Other treatments include orthopedic appliances, and in some cases, orthopedic surgery to improve quality of life [5]. Yet still, there is no cure for the disease, and generally, the treatment methods described above do not permanently curb the disease progression, often leading to years, and sometimes decades (in the case of the slower-progressing types of muscular dystrophy), of very poor quality of life for the patient [1, 5]. As such, a therapeutic treatment of muscular dystrophy is necessary.

2.1.4 Non-Target Drugs Can Induce Myalgias and Myopathies

Recently, a variety of prescription drugs including antibiotics and statins have been strongly correlated to a variety of muscle-based side effects including pain and tendonitis. In many cases, these drugs have been on the market for decades and prescribed to tens of millions of patients [12].

A recent FDA warnings issued in 2016, advised that there are correlative serious side effects of a class of strong antibiotics called fluoroquinolones [12]. While in many cases, the benefits of the drug outweigh the risks, these antibiotics have been known to cause disabling and sometimes permanent side effects to patients that result in serious muscle pain and weakness. Additionally, injuries to the skeletal system including tendon ruptures and joint pain have been correlated with the use of the fluoroquinolones [12, 13].

Cholesterol-reducing statins have also been shown to have deleterious side effects on skeletal muscle. A recent recall of a Baycol - a cholesterol drug statin produced by the pharmaceutical company Bayer was attributed to the drugs rare side effect of rhabdomyolysis [14]. This side effect destroys muscle cells and releases resultant byproducts into the bloodstream, leading to severe muscle pain and in some cases, fatal kidney failure [13, 14].

2.1.5 Current Drug Development Process/FDA Timeline

Currently, the FDA drug development process is long and arduous; requiring substantial testing and validation using a variety of methods, prior to any initial human clinical testing can be conducted. Initially, laboratory discovery must take place, in which benchtop high-throughput assays are conducted to identify a variety of drug compounds that have potential success for a certain disease [15, 16]. The entire drug development process can take between 10-15 years and the current platform for development incurs high costs, and low-approval rate, driving up the price of approved drugs, with the average drug exceeding \$400 Million in costs during development [15, 17].

However, the benchtop response of drug targets in 2D cell cultures and subsequent experiments do not always accurately recapitulate the native 3D environment. Therefore, prior to introducing the new drug into humans, a variety of preclinical *in vivo* studies are conducted using animal models [18, 19]. While the choice of animal models used, along with specific animal strains, etc. can vary based on

the drug/disease being developed, generally preclinical animal testing begins with small animals (mice or rats), and depending on the success of the therapeutic, can progress into larger, more complex organisms, and ultimately to the primate order. This progression of animal studies more effectively utilizes time and resources to best predict clinical efficacy following translation to humans [15, 18]. The progression of drug testing on preclinical animal models strive to elucidate the pharmacodynamics of the drug, (e.g. mechanism of action), as well as the pharmacokinetics (e.g. drug absorption, interaction, etc.), to determine how the drug functions within a living system [16].

If, following all *in vitro* and *in vivo* preclinical testing, the drug proves effective and safe, the development can then begin to progress into early stage clinical trials. Initial clinical trials (Phase 1) test mainly for toxicity and dosing, generally testing between 50-100 healthy individuals [15, 16]. Thus, the first stage in clinical trials does not strive for drug efficacy as an output, but instead simply to determine if the drug causes health issues with humans that were not previously identified with animal clinical trials [16]. A select few examples of drugs have caused serious health problems, with over 40% of the drugs approved for Phase 1 clinical trials being removed from research due to toxicity and inappropriate pharmacokinetics, despite the fact that this stage in clinical trials utilizes microdosing, often delivering 1/100th of the expected therapeutic dose to healthy individuals [15, 20].

Phase 2 clinical trials begin to test the drug on individuals (generally between 100-300 individuals) that suffer from the disease but is not a blinded study, indicating that the researchers and the patients are aware that they are being given a treatment for the disease [16]. Additionally, phase 2 clinical trials will also elucidate any side effects from the drug interaction with patients [21]. If the drug proves effective, progression to the scaled-up and double-blinded phase 3 clinical trial can occur, which can involve up to 5,000 individuals and if the drug proves effective, is the final step prior to FDA review and subsequent drug approval [16, 21]. This progression through the drug development process - initially starting at benchtop discovery and progressing through preclinical and clinical trials - is the

current mandate by the FDA in the US for drug development, and has been in place and largely unchanged since the 1960's [21].

Even when drugs progress through the phase 1 clinical trials, demonstrating that they do not pose a toxic threat to humans, a large percentage of drugs - upwards of 90% of investigative new drugs - fail during the phase 2 and 3 clinical trials [22, 23]. This failure is often attributed to the drug resulting in a lack of efficacy when targeted to the diseased patient. This lack of efficacy can be attributed to the lack of genetic homology between the pre-clinical animal models used to identify target drugs, and humans tested in clinical trials [24]. It is probable that the current drug development process utilizes improper and non-precise methods to identify drugs that are effective on both benchtop *in vitro* models and animal models, neither of which precisely mimics the response that is seen in humans. While recent promising work has demonstrated that large animals including sheep can be quite useful for modeling a variety of genetic disorders, due to their phenotypic relevance to humans, similar benefit is not observed with smaller animals (mice/rodents) [24]. Unfortunately, current preclinical research must begin and prove effective with smaller animals prior to progressing to larger and expensive animal model systems [24]. The current drug development process possibly fails to identify drugs that could be effective in humans, because they failed to be effective in preclinical animal models.

There are some drawbacks and concerns regarding this drug development process - especially when considering a genetic disorder such as muscular dystrophy. Currently, initial benchtop discovery and development often uses analogues that do not precisely recapitulate native tissue and the subsequent native response, *in vitro*, potentially neglecting a certain compound that would have a therapeutic benefit, and similarly, accepting a certain compound that ultimately will lack effectiveness during future clinical trials [16]. Currently, the benchtop models that exist, and the testing parameters used to identify candidate drugs do a poor job of mimicking the response seen *in vivo*, as in many cases, certain tests and assays are standard to the drug development protocol but can provide erroneous data

as a consequence [15]. Perhaps the most compelling argument necessitating the need for a better assay system involves the fact that upwards of 75% of the cost of developing a new drug is spent during the investigative stages of development [15].

Perhaps more profoundly, animal models can also fail to accurately recapitulate the human response to a therapeutic [25]. As mentioned previously, all drugs are subjected to showing safety and efficacy in animals prior to human clinical trials, generally starting with smaller animals and moving to larger species, as appropriate. This disconnect between pre-clinical animal models and subsequent translation to human clinical trials where drug efficacy is lost has been well characterized in the literature and is present across a variety of diseases and disorders beyond muscular dystrophy [25-28]. In the case of muscular dystrophy, the mutated gene for the dystrophin protein - a genetically inherited trait - is only accurately recapitulated in the primate order [29]. Therefore, initial validation and efficacy determination for muscular dystrophy therapeutics using small animal species (mice, rats, etc.) cannot effectively mimic clinical response, as an appropriate model of muscular dystrophy cannot be created in those species. Although, it is worthwhile to note that a Duchenne muscular dystrophy mouse model (mdx mouse) does exist, this model only replicates the phenotype of the diseases, namely the chronic breakdown and decrease in skeletal muscle mass [30, 31]. However, the genetic mutation for this muscle breakdown results in a milder-symptom presentation, likely due to the inherent differences in the molecular composition and regenerative capacity of skeletal muscle between species [30]. Nevertheless, preclinical efficacy utilizing the mdx mouse has been achieved for molecular-based therapeutics for treatment of muscular dystrophy [32, 33]. However, none of the pre-clinical data on drug efficacy has shown any promise of effectiveness during early stage clinical trials. Further, while the symptoms of the mouse are similar to those of humans, the disease is not a precise replication. Therefore, it is possible that even though a treatment for the disease is identified as effective in the animal model, subsequent translation to human patients may not yield similar beneficial results [30].

Very recent and preliminary research exists on the ability to use genomic editing technology CRISPR/Cas9 in attempt to create a rhesus-monkey model of DMD [34]. While the genomic editing technology is still in its infancy, preliminary work demonstrated that such targeting has lead to 87% of mosaic mutations in the dystrophin alleles in the monkey [34]. Overall, a crucial disconnect exists, where the preclinical models used to test and validate certain therapeutics do not accurately model the human disease, therefore erroneous data and false trends/efficacy findings may be created [31].

There have also been numerous examples of non-target drugs resulting in muscle-based side effects. Such side effects were never elucidated during either pre-clinical animal trials or during any of the clinical trial phases, due to the lack of current guidelines aimed at looking for long-term side effects in tissues that are not the target of the drug or therapeutic. A more precise benchtop model of skeletal muscle may provide researchers with the ability to identify such toxic side effects during earlier stages of drug development, affording the pharmaceutical industry the ability to alleviate the side effects prior to investing costly time and money in pre-clinical and clinical trials.

In summary, the current FDA guidelines have been minimally changed in decades, not representing the current advances and understandings in science [19, 21]. The current benchtop discovery and subsequent preclinical animal modeling can be beneficial in guiding more effective drugs to clinical trials; however, this process is plagued with being poorly designed and adaptable to certain diseases. In the case of muscular dystrophy, the simple fact that the animal models researchers use cannot accurately recapitulate the disease question their functionality as an appropriate model system, as well as the translational effectiveness of the therapeutic to humans. Furthermore, there is significant time and cost associated with completing both benchtop modeling along with preclinical animal models, with no guarantee that the findings will translate to effectiveness during human clinical trials [24]. Staggering out-of-pocket costs associated with the entire drug development process coupled with the cost of abandoned compounds have resulted in astronomical costs associated with drug development,

with pre-approval costs approaching \$1 Billion per drug [17]. One such example of this lack of translation involves statistics taken from clinical trial drug failure rates, which highlighted that upwards of 90% of investigative new drugs fail at some point during clinical trials [22]. This high failure rate is certainly due to a variety of factors including safety and strategic failures, however, the majority of these failures are due to a lack of efficacy [22, 23]. This high failure rate due to lack of therapeutic efficacy likely indicates that the preclinical metrics used to identify effective compounds, do not precisely translate to humans [29]. This lack of homology between both benchtop modeling and preclinical animal testing, when compared to the human response generate a need for a better therapeutic drug development process. Finally, a new model system could allow for benchtop identification of deleterious side effects of non-target drugs during the early stages of drug development.

2.1.5 Statement of Clinical Need

In summary, the overarching need for the development of a therapeutic to treat muscular dystrophy likely involves the development and validation of a biomimetic model of dystrophic human muscle. A muscle model may be capable of producing a more precise native response, yielding a benchtop platform that outperforms the current benchtop models, and potentially is a better predictive tool when compared to animal modeling. To aid in the development of a dystrophic muscle model, the developing of a precise biomimetic model of healthy human skeletal muscle should be completed first. As such, the goal of this project is to design and validate a platform methodology for the development of a biomimetic model of healthy human skeletal muscle tissue *in vitro*.

2.2: Background - Skeletal Muscle Anatomy, Function, and Repair

2.2.1 Skeletal Muscle Anatomy and Structure

Skeletal muscle consists of a hierarchical cable-like structure that is capable of voluntary contraction generating force through shortening of these fiber structures. As shown in *Figure 1*, a total muscle consists of various bundled groups termed fascicles, with each fascicle containing a large group of muscle cells or myofibers [35, 36]. Each myofiber contains multiple myofibrils, in which each myofibril contains the contractile proteins actin and myosin, which together comprise a sarcomere - the functional unit of skeletal muscle, and discussed in detail in a later section [36]. An individual myofibril contains a large percentage of contractile function protein and very few nuclei, with nuclei in mature and functional muscle positioned at the periphery of individual myofibrils [35, 37]. This hierarchal morphology results in multiple layers of contractile proteins, allowing for a variety of different force production values, based on the number of myofibers that are innervated and instructed to contract at any given instant [36].

In parallel with the hierarchal layers of contractile proteins, there are also layers of ECM protein that envelop each subsequent fiber layer. While the ratio of ECM to skeletal muscle is relatively low, the presence of the ECM within skeletal muscle is crucially important towards contractile function [38]. During *de novo* formation, ECM is synthesized endogenously by the resident fibroblasts present within the muscle tissue [39]. Briefly, the epimysium wraps around the entire muscle group, whereas the perimysium and endomysium envelop the muscle fascicles and individual myofibers respectively [38, 40]. While researchers often characterize ECM based on the location within skeletal muscle, often, the distinguishing characteristics between different layers of muscle are arbitrary, since one layer blends into the next [38]. Similarly, while there are known proteins that comprise the skeletal muscle ECM, they are not uniformly segregated to a certain location within the muscle, and their exact ratios and how the interplay between different proteins plays a role in overall muscle function still remains poorly

understood [38]. Briefly, human skeletal muscle is known to contain a variety of ECM proteins. Concentric sheaths of ECM protein organize around different hierarchal layers of skeletal muscle, as shown below in *Figure 1*. Various ECM layers containing different ECM proteins envelope different layers of the skeletal muscle fiber [40]. Of note, the endomysium consists of a highly-ordered network of ECM proteins that wrap around individual myofibers and deform nonlinearly during the changing sarcomeric length due to muscle contraction [41]. The transmission of force is believed to occur by shear through the endomysium and thus highlights the importance of the ECM protein for generating native levels of functionality along with rationale for previous study on constitutive modeling of muscle endomysium ECM [38, 41, 42]. The various layers of ECM protein are shown in *Figure 1* below.

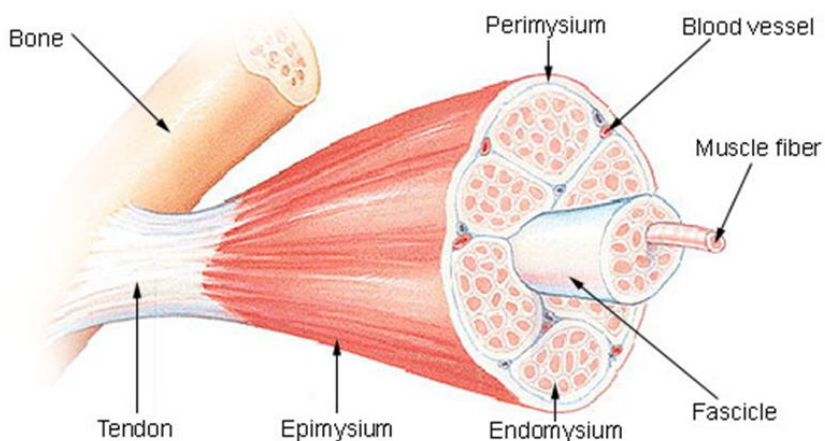


Figure 1: Structure of Skeletal Muscle

Hierarchal Structure of Skeletal Muscle showing cable-like structure on individual fascicles and muscle fibers. Layers of skeletal muscle ECM and location within skeletal muscle are also highlighted. (Wikimedia Commons)

The organization and location of ECM proteins within the different layers of ECM in skeletal muscle have been previously studied, yet becomes quite complicated due to transition zones between layers and between skeletal muscle-tendon interfaces (myotendonous junctions), where a variety of ECM proteins converge [41, 43]. Largely, skeletal muscle consist of collagens, where fibrillar types I and III dominate in the mature endo-, peri-, and epimysium [43]. Yet, during muscle development, a variety of other collagens including basement membrane collagens IV and VI dominate the endomysium during development [38, 40, 44]. Such basement membrane collagens are crucially up-regulated during

development due to the crucial interaction between developing muscle fibers and the ECM, as explained in depth below. Additionally, many glycoproteins including laminin-211 function as linker molecules between the basement membrane collagens (namely collagen IV) and the sarcolemma, further indicating the importance of laminin-211 in skeletal muscle development and function [38, 44, 45]. Furthermore, it has been hypothesized, that some degree of ECM protein content customization occurs across muscle of varying functional force production, indicating that there is a plastic relationship between the contractile muscle and the surrounding ECM [38, 41]. While the exact ratios of ECM proteins within skeletal muscle and their relationship towards functional and regenerating muscle have not yet been quantified in a human system, the presence of salient basement membrane proteins coupled with crucial glycoproteins demonstrate that certain specific ECM proteins play a crucial role in muscle development and function [38, 40, 45].

As mentioned previously, the symbiotic relationship that exists between the skeletal muscle and the resident ECM surrounding the various muscle layers is crucial for contractile function. In fact, it is well postulated that the ECM within skeletal muscle bears the majority of the passive load of force transmission during a muscle contraction [41, 42]. Furthermore, a variety of skeletal muscle disorders, including muscular dystrophy, as described previously, originate in the ECM, and are due to a malfunctioning dystrophin ECM protein that leads to a progressive and chronic muscle-ECM disconnect, leading to aforementioned chronic regeneration and repair, ultimately leading to a loss in muscle tissue [1, 3, 5].

2.2.1.1 Contractile Apparatus Structure and Function - Sarcomeric Physiology

As mentioned previously, actin and myosin proteins comprise the contractile functional unit of muscle, termed the sarcomere [35, 46]. A single sarcomere consists of an array of overlapping thick myosin protein overlapping with the thin actin filaments, as shown below in *Figure 2*. These sarcomeres repeat in series longitudinally down the length of the myofiber [46, 47]. During a contraction, the

myosin heads attach to the actin filaments and undergo a conformational change, increasing the degree of overlap between the two proteins, and thus shortening the overall length of the sarcomere (termed the distance between two neighboring Z-disks - or endpoints of the individual sarcomere) [48]. With muscle contraction, there is an optimal length-tension relationship between the degree of overlap of the actin and myosin filaments, where the strongest force production can occur due to a contraction, this optimal length occurs when the sarcomere is roughly $2\mu\text{m}$ in length, whereas higher or lower degrees of overlap lead to sub-optimal levels of contractile force [48].

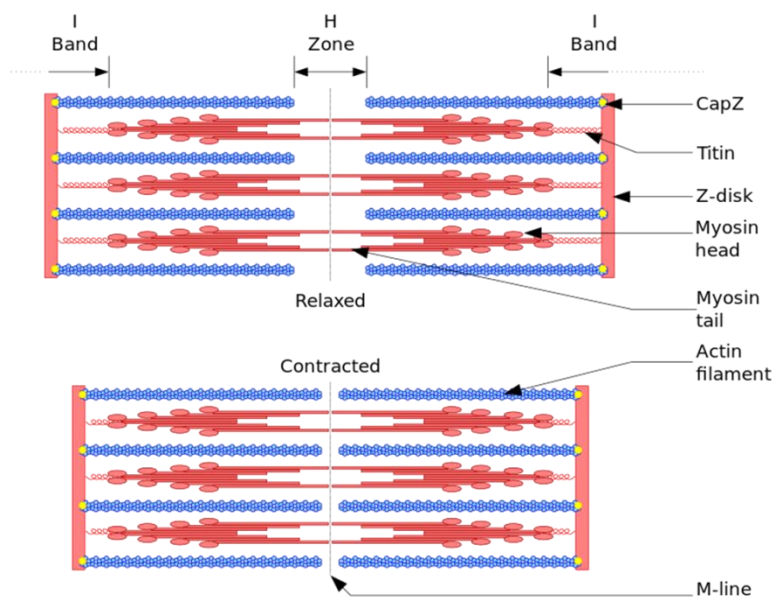


Figure 2: Skeletal Muscle Sarcomere.

Sarcomeric structure highlighting thin actin and thick myosin protein filaments along with associated structural regions (Wikimedia Commons)

A muscle contraction begins with the motor neuron releasing the neurotransmitter acetylcholine, which binds to an acetylcholine receptor, initiating a conformational change that allowing an inward flow of sodium ions, initiating an action potential [49]. This action potential activates voltage-gated calcium channels that initiates a mechanism termed calcium-induced calcium release. While the physiological reason for the complexity of this phenomenon remains loosely understood, the end result of the outward flow of calcium ions promotes the myosin heads to contact the actin filaments [49]. Adenosine triphosphate (ATP) bound to the myosin head is then hydrolyzed into adenosine diphosphate

(ADP) plus an inorganic phosphate ion, resulting in the myosin head conversion from a high energy state to a lower energy state, resulting in the final conformational change, termed the sliding filament theory, where the actin and myosin filaments increase their overlap, leading to a muscle contraction due to the shortening of the overall muscle length [35, 47, 49].

Native skeletal muscle consists of greater than 90% myosin-positive tissue, with the remaining tissue consisting of sheaths of ECM along with vascular and nervous system networks throughout the tissue [35]. On average, myofibers range between 10-100 μm in diameter (depending on muscle tissue group and location, although often myofiber diameters are closer to 100 μm , with only low force muscles, e.g. eyelids, containing myofibers approximating 10 μm in diameter), and contain heavily-striated regions (sarcomeres), as described previously [35, 46]. The fiber length is approximately 1cm in humans, depending on the muscle group they are within. However, the overall length of an individual fiber is not considered to be an important criteria in determining the overall functionality or maturity of the muscle, since sarcomeres align in series, as described previously [35]. Researchers have attempted to elucidate the average force that a single muscle fiber can produce during contraction. However, due to the exceedingly small size of a myofiber, coupled with the fact that myofibers within a single muscle are bundled in 3D - it is challenging to isolate a single myofiber. Nevertheless, benchmarks on muscle fiber contractile force do exist, but such values contain several fibers, necessitating the need for cross sectional area measurements to normalize the contractile force measurements. In the case of healthy and mature muscle, since the tissue is greater than 90% myosin-positive, generally, the cross sectional area can be considered the actual area that is participating in the tissue contraction. Research groups have determined that for individual muscle fibers that were excised from healthy volunteers, observed force production has been observed to range between 0.5 and 2 mN of force on fibers that consist of a cross sectional area of between 4000 and 12,000 μm^2 [50]. Similar work completed by a different group also returned force values in the 0-2mN force range for similarly-sized tissues, and both groups indicated

that substantial patient-patient variation for factors including patient sex, age, and lifestyle, including exercise can influence the force production values of skeletal muscle fibers [50, 51].

2.2.2 Development of Muscle - Embryogenesis and Myogenesis

The development of skeletal muscle during embryogenesis, a process termed myogenesis, occurs mainly during prenatal development and can be divided into two discrete phases, primary and secondary myogenesis [52]. During primary myogenesis, a committed pool of stem cells arising mainly from a mesenchymal cell lineage contribute to form a small number of primary muscle fibers, which serve as guides for further muscle fiber development during the secondary phase of myogenesis. These committed myogenic precursors express paired box (Pax) 3 and Pax 7 regulatory proteins which induce the expression of myogenic regulatory factors (MRFs), leading to myogenic differentiation and muscle tissue formation [40, 52-54]. Many MRFs have a temporal response of expression, including MyoD, which is a transcription factor that regulates myogenic differentiation and Myogenin expression, another transcription factor that regulates skeletal myogenesis - generally with temporal expression following cell fusion and the beginning of muscle tissue formation [40, 52, 54, 55]. Following more maturation, expression of myosin heavy chain, a marker for the myosin protein found within mature sarcomeres begins to express and remains expressed following complete maturation. Such temporal myogenic regulatory factors have allowed researchers to quantify the specific stages of differentiation, based on the relative expression of certain temporal factors [40, 52]. In fact, the majority of skeletal muscle fibers are formed during the secondary myogenesis process, with very minimal new tissue formation occurring postnatal, (as myonuclei are post-mitotic and are not able to divide), where only myofiber size is modulated, with minimal net gain in myofibers occurring [54, 56]. During the adult stage, new muscle fiber development occurs to replace or repair injured myofibers as a result of a traumatic or chronic injury [54, 56].

During the muscle fiber development and embryogenesis, simultaneous formation of the ECM that surrounds the various muscle fibers is equally critical for complete and native levels of maturation [38, 40, 57]. Such ECM synthesis is modulated endogenously by the resident fibroblasts within skeletal muscle tissue. As described previously, there is a temporal relationship between both the myogenesis of new muscle fibers and the synthesis of the supporting ECM [38, 39]. Skeletal muscle fibroblasts rapidly proliferate during the early stages of regeneration to lay down sufficient provisional basement membrane matrix consisting of basement membrane ECM that allow the skeletal muscle myoblasts to make crucial cell-ECM connections that drive both muscle formation and subsequent muscle function [9, 38, 58, 59]. Following such cell-ECM binding, myoblasts can continue to fuse and subsequently mature into multinucleated myotubes, following which myotube hypertrophy (diameter thickening and contractile force-increasing) occurs and following maturation, nuclei migrate from a central position to the periphery of the newly formed myofiber [58, 60].

2.2.2.1 De Novo repair of skeletal muscle

Skeletal muscle injuries consist of two main types, large and small injuries [61]. For large injuries, often the result of a volumetric muscle loss, such as those sustained in combat, create a wound size that cannot be healed, thus intrinsic regeneration cannot occur [62]. Instead, rapid proliferation of fibroblasts deposit non-functional scar tissue to close the wound; however, this prevents functional regeneration of the tissue, and in large-scale cases, can severely impact quality of life [62]. For small injuries including shearing injuries common with sports-based injuries, where the muscle fiber delaminates from the basal lamina or small lacerations, both of which can rupture capillaries resulting in localized tissue death, skeletal muscle has the ability to intrinsically regenerate [54, 63]. However, large scale injuries caused by traumatic injury (termed Volumetric Muscle Loss - VML) or chronic injuries that maintain a constant state of repair, coupled with basement membrane destruction and depletion of the growth factor reservoir needed for intrinsic repair, leading to non-functional scar formation [62].

Small muscle injuries can be intrinsic repair of small skeletal muscle wounds begins with the activation and proliferation of normally-dormant muscle progenitor cells, termed satellite cells, that reside between the sarcolemma and the basal lamina, actively migrate towards the injury [54, 64-66]. Once at the injury site, satellite cells proliferate, exiting the normally dormant Gap 0 (G_0) phase of the cell cycle, and enter G_1 phase to begin proliferation to generate a higher number of cells capable of participating in regeneration [66, 67]. However, this stage of muscle regeneration also involves self-renewal of the satellite cells, whereas a small sub-population of the proliferating satellite cells generate daughter cells that return to the pool of progenitor cells, and return to a quiescent state, thus preserving the innate ability of the satellite cells to direct future repair and regeneration [54, 68, 69]. Once expanded to a sufficient number to facilitate myofiber repair, satellite cells undergo cell division where the remaining (differentiation-competent) sub-population exit the replicative cell cycle and begin to differentiate into myoblasts, where expression of temporally-regulated transcription factors transitions into myogenic regulatory factors [54, 67, 70]. As described previously, following terminal differentiation, myoblasts fuse with the existing damaged myofiber structure along with the and basement membrane ECM secreted by interstitial fibroblasts, leading to muscle regeneration. Following structural repair, a variety of myogenic regulatory factors are temporally expressed, as described previously, and subsequent maturation involves the strengthening of the newly formed myofiber and the ultimate migration of the myofiber nuclei from the center of the fiber to the periphery, indicating terminal and complete repair of the injured muscle [54, 66, 71]. Such regeneration initially yields small (neonatal-like) myofibers that can mature and strengthen over time (due to exercise or other external stimuli) combined with positive-feedback loops for terminal differentiation regulatory factors, ultimately regaining the original pre-injury functionality and strength [54, 72].

2.2.2.2 Chronic Injuries deplete satellite cell pool

While muscle regeneration occurs throughout a person's lifetime (elderly can heal from a muscle injury), the timing and speed of regeneration is not maintained. Like many other regeneration processes in the body, younger people heal quicker than the elderly, due to the available pool of progenitor cells capable of participating in regeneration [66]. Regeneration of skeletal muscle is no different, whereas younger muscle heals at a quicker rate than older muscle if subjected to a similar type of injury, as the younger person has more progenitor cells available, expediting the healing process [54].

However, one exception involves muscular diseases such as muscular dystrophy. In the case of muscular dystrophy, as described previously, the pathogenesis stems from the malfunctioning myocyte protein dystrophin which is involved in anchoring the myocyte to the ECM [3, 10]. As dystrophin is chiefly responsible for connecting the cytoskeleton of each myofiber to the underlying basal lamina, this malfunction leads to an increase in calcium penetration into the cell, creating an ionic gradient and hence causing water to enter, resulting in mitochondrial swelling and ultimately bursting and lysing the cell [73]. Although poorly understood, it is hypothesized that mitochondrial bursting leads to an increase in reactive oxygen species (ROS) production, that damages the sarcolemma, eventually leading to cell death[73]. In summary, the malfunctioning dystrophin protein leads to a constant and chronic breakdown of muscle triggering constant regeneration [3, 31]. While repair via the innate satellite cell activation, proliferation, and self-renewal process, as described previously, takes place, the constant and chronic nature of the dystrophy depletes the regenerative capacity of muscle significantly quicker than non-disease related injuries - as such injury occurrence is far less in frequency [31]. As such, as the patient ages, (and depending on the type and severity of the dystrophy), eventually, the ability to regenerate muscle is lost, leading to system organ failure and death [1, 10].

2.3 Benchtop Models of Skeletal Muscle

Prior to discussing the current benchtop models of skeletal muscle, it is important to understand some salient features and attributes that a benchtop model must possess, to ensure that such model has the capability to precisely mimic the morphology and function of native muscle and serve as a useful model system for drug screening and therapeutic testing for the development of a treatment for muscular disorders in humans [74]. Previous sections highlighted the need for more effective therapeutic development and demonstrated that the current method of utilizing animal models in preclinical testing is poorly-predictive of the human response and is extremely costly and time-consuming [74]. Such lack of homology has led to upwards of 90% of investigative new drugs failing during early-stage clinical trials for efficacy [22]. As such, developing a more precise model of skeletal muscle on the benchtop could then be adapted to streamline drug development and therapeutics for the treatment of skeletal muscle diseases and disorders. To develop a more precise benchtop model of skeletal muscle, the following section outlines salient features and attributes that must be employed and/or emulated.

2.3.1 Salient Features and Guidelines for Successful 3D Benchtop Models

2.3.1.1 2D vs. 3D Tissue Engineered Models

Currently, 2D culture is widely accepted as the most efficient way to expand a cell population, *in vitro*, as cells can be controllably handled and expanded via exponential growth until the desired cell number is achieved. Furthermore, homeostatic conditions (humidified, 37°C, pH 7.4) can be emulated on the benchtop to create a *pseudo-in vivo* environment to optimize growth kinetics [75, 76]. But, beyond cell expansion, there are significant drawbacks associated with 2D culture - there are very limited native applications of 2D cells - perhaps with the only example involving capillaries where gas and nutrients are exchanged across a membrane barrier that is one cell layer thick [75]. Namely, cells

grown in monolayer culture are directed to attach to a plastic surface that possesses a stiffness several orders of magnitude higher than any native tissue, and present a cell morphology much more spread out and flattened compared to how cells grow within 3D cultures and within *in vivo* environments [75, 77]. Furthermore, crucial cell-cell and cell-ECM contacts are generally not made during traditional 2D monolayer culture, as cell-cell contacts can direct cells out of replicative cell cycle, and cell-ECM contacts are not present because the majority of ECM-producing cells synthesize substantially less ECM in 2D culture, compared to the native 3D environment [75, 78].

Recently, 3D cell culture has been adopted as the better predictive for drug screening and diagnostic testing as the cells comprising the 3D tissue are placed in a physical environment that better mimics native tissue [75, 78, 79]. Cells within a 3D gel make crucial cell-cell and cell-ECM connections, (of which in 2D culture, the latter is discouraged by researchers, as it leads to contact inhibition, while the former occurs less in 2D than 3D for a variety of cell types), that better mimic the architecture and morphology of native tissue [75, 78].

Furthermore, in the case of skeletal muscle, 3D culture allows myofibers to make crucial connections with the underlying basement membrane, facilitating the crucial cell-ECM bonds that facilitate force transmission [38, 54, 80]. To relate the importance of a 3D culture environment to skeletal muscle tissue constructs and their use as a drug screening and diagnostic testing tool, it is also paramount to note that the 3D environment better emulates the *in vivo* response to drugs or therapeutics, as the diffusion rate of drugs through 3D tissue (vs. 2D cells) better approximates native response [75, 78]. A 2D culture may have a faster (non-predictive of native tissue) response to drugs due to the different cell morphology and the manner in which cells interact with the culture medium.

In summary, 3D models are rarely used during initial drug discovery and development, yet there are clear benefits indicating that such models could serve as a better overall predictive tool of the clinical response [75, 78]. This connection between preclinical benchtop testing and efficacy in clinical

trials has been hypothesized to better streamline drug development and lower the percentage of drug failures (currently ~90%) that fail in clinical trials due to lack of efficacy [22]. The following sections highlight salient attributes that such 3D models must possess in order to serve as better predictive modeling tools.

2.3.1.2 Clinically-Relevant Cell Source

The initial component of building a better benchtop model of skeletal muscle involves choosing a cell type that will facilitate differentiation and maturation, *in vitro*. Choosing a cell type from a certain source can result in a 3D tissue that better emulates the native response, thus function as a more predictive preclinical benchtop model.

Immortalized cell lines of murine origin have been popular in skeletal muscle research for decades. Initially developed in the 1977 by David Yaffe and Ora Saxel [81, 82], and then subcloned further by Helen Blau [83, 84], the immortalize murine myoblast cell line C2C12 is a common heavily-used immortalize cell line for skeletal muscle research. The C2C12 cell line benefits from the ease of culture and rapid expansion of the cells, with a doubling time of 18-20 hrs and requiring a low-cost, commonly-used basal medium (e.g. DMEM) supplemented only with 10% FBS [85]. As an immortalized cell line, senescence is never reached, allowing for infinite numbers of cells to be expanded in culture. The C2C12 cell line is highly myogenic (>90% - providing appropriate growth conditions are maintained), allowing for the myogenic capability of the cell line to be retained during exponential expansion [84, 85]. Finally, by utilizing a cell line that originates from a single source, separate research groups can make comparisons between their data, removing the cell source as a potential variable influencing their results. Such growth conditions and media requirements, make the C2C12 line desirable to researchers, as low-cost, low-maintenance cells can be expanded to any desired number and used for benchtop assays [86, 87]. Unfortunately, immortalized murine cell lines translate poorly to the clinic, as they can

respond differently to a variety of external stimuli including therapeutic treatment, therefore, requiring pre-clinical translation to primary human cells [88].

On the contrary, primary human cells would provide a smoother clinical translation as there would be no species differences from preclinical research, however, there are a multitude of limitations that must be addressed prior to utilizing these cells. Firstly, human primary cells must be isolated from a willing donor, or obtained from discard tissue following a skeletal muscle surgical procedure. Although neither of which draw substantial ethical concern, there are associated risks including unwanted disease transmission, that are introduced into researchers that utilize tissue biopsies as cell sources [66]. A major limitation associated with deriving myogenic cells from human skeletal muscle, involve the propensity of the biopsy and isolation process to activate quiescent satellite cells and subsequently initiate terminal differentiation [66, 89]. As the cells are cultured in *ex vivo*, the satellite cells lose their ability to self-renew, often resulting in a myogenic level that immediately begins to irreversibly decrease, during *in vitro* culture. This limitation, along with the relative scarcity of the percentage of available progenitor cells within native human skeletal muscle, makes it difficult for researchers to obtain a useful number of cells such that a clinically-useful experiment can be conducted [66, 90]. Additionally, while improved methods of culturing human primary skeletal muscle cells to maintain the progenitor cell population for an extended time in culture exist, such procedures involve the use of prohibitively-expensive ready-to-use media kits, and have only been verified to maintain the level of myogenic potential for 8-10 doublings [91, 92]. Even with the costly media kits, primary skeletal muscle cells grow significantly slower than their immortalized counterparts, with a doubling time ranging between researchers and isolations, but, tend to range between 36-44 hrs [92]. Finally, since primary isolations and derivation sources and methodologies are different between research groups, there is a potential lack of reproducibility that is created by using primary myoblast cultures.

In summary, there are clear benefits to utilizing human primary skeletal muscle cells for preclinical benchtop work, yet challenges remain to be addressed before the use of these cells can generate clinically-relevant data [25, 30]. If these challenges associated with primary myoblasts can be addressed, there is potential for a beneficial improvement relevant data generation during preclinical work that could lead to a higher success rate of drug development. Ultimately, the best clinical data may be generated using patient-specific cells, however, the timing of such work along with the logistics are beyond the scope of this work [93].

2.3.1.3 Mimic Native Tissue Structure and Morphology

Another attribute that 3D skeletal muscle tissue should exhibit involves generating a tissue morphology that mimics that of native tissue. Native muscle consists of a 3D tissue that contains anchored and aligned myofibers, as described previously, along with layers of ECM protein that allow the cells to make crucial cell-ECM connections, permitting the transmission of force during contraction [35, 38]. A mimetic benchtop model would emulate the anchorage to generate aligned tissue, along with mimicking the native relationship between the myofibers and the layers of ECM sheaths observed surrounding various fibers within native muscle [35, 36, 38].

2.3.1.4 Generate a Small Minimal Functional Unit

Skeletal muscle is a highly functional tissue, thus requiring an abundance of nutrients. Not surprisingly, this tissue is highly innervated and vascularized, to ensure that the tissue health and viability is maintained during periods of heavy workload [35]. The purpose of most 3D skeletal muscle constructs is not to recapitulate the complex vascular and nervous system components integrated into native muscle (although, that is a future outlook, but beyond the scope of this work), but instead, to recapitulate the functional component of muscle, namely in terms of myosin protein force production and mediated by cell-ECM interaction . As such, in the absence of innervation and vascularization the

tissue must not exceed a thickness in which passive diffusion of nutrients takes place. In skeletal muscle, the diffusion limit of nutrients is roughly 100-150 μm , indicating that 3D skeletal muscle tissue constructs should not exceed 300 μm in thickness, assuming free diffusion of nutrients can be supplied from both sides of the tissue [94, 95].

2.3.1.5 Generate Tissue that Produces Force Similar to Native Muscle

As mentioned previously, the role of skeletal muscle is to produce contractile force, shortening the overall length of the muscle and facilitating skeletal movement. As such, skeletal muscle is capable of imparting a varying amount of force, depending on the action required, and in cases of heavy workload, skeletal muscle is capable of producing between 0.5-2mN per fiber bundle of approximately 4,000-12,000 μm^2 in area [50]. Entire muscle units can produce force several orders of magnitude higher, but developing a full-thickness muscle analogue is beyond the scope of this work, as this project only aims to develop a minimal functional unit of muscle - aimed at matching the functionality per unit area. To create an analogous benchtop model of skeletal muscle, it is important that the model is capable of functioning in a similar manner to that of native muscle [35]. A benchtop model should contain gross morphology consisting of striated fibers within the range of native muscle (10-100 μm), and being to display sarcomeric structures, indicating that significant late-stage maturation is taking place during culture [35].

2.3.1.6 Generate a High-Throughput Tissue Generation System

Another vital component to generating a useful benchtop model of skeletal muscle involves generating tissue within a mold platform that promotes functionality for high-content screening [74]. Traditional screening assays utilize microtiter plates that contain between 96 and 1536 wells/plate. Such plates are useful as they occupy minimal space within the lab, but allow for dose and drug-dependent variables to be tested within the same plate (minimizing plate-to-plate and experiment-to-experiment

variables that often result in high batch-to-batch errors), making them quite useful for high-throughput assays [74]. It may be beyond the scope of this work to engineer micro-skeletal muscle tissue capable of fitting into microtiter plates; however, it may be possible to generate tissue within such a platform that minimizes the use of both the space and media required to culture each tissue, creating a more cost-effective system for high-throughput testing [74, 96].

2.3.1.7 Summary of Benchtop Features Needs

Overall, there are a variety of features and attributes that, if applied correctly in practice, should result in the generation of a more mimetic tissue model of skeletal muscle. One overarching principle involves the benefits of generating 3D tissues on the benchtop and the more practical clinical translation such a model may have [74, 96]. Such a 3D system provides the researcher with a more precise model of native architecture, along with the crucial cell-cell and cell-ECM bonds that play a vital role in native contractile function. Another important attribute involves the cell source used for 3D tissue generation. While immortalized cell lines are readily available and easy/inexpensive to maintain *in vitro*, in many instances, including the genetic makeup that causes muscular dystrophy, they differ from human primary cells. As such, data produced from tissues comprised of immortalized animal cell lines may be poorly-predictive of the response seen during clinical trials due to salient differences in the species that the drug was initially tested within.

There are also attributes involving the specific methodology used to generate 3D tissues that contribute to the generation of a more mimetic tissue, *in vitro*. Namely, these muscle tissue analogues should mimic the morphology of native tissue, including the high ratio of contracting myofibers to ECM, along with anchorage points to mimic the myotendonous junctions and thus produce linearly-aligned microtissues [35, 97, 98]. Furthermore, in the absence of a vascular or nervous network, there is a crucial maximal size that these tissues can reach before free passive diffusion of nutrients fails to maintain viable tissue. Free diffusion can occur through dense tissue between 100-150 μm , indicating

that if such microtissues are avascular but surrounding in nutrient-rich media, that their maximal size in any dimension cannot exceed 300 μ m [94, 95]. While these microtissues likely will not create a similar force to an entire native muscle, it is fair to extrapolate the force/unit area that native muscle generates, and compare such values to the force production of benchtop muscle analogues. Finally, to generate a platform technology that is useful to the drug development industry, creating a high content platform that produces tissues in an array format to minimize media use and create a setup that is conducive for high throughput screening of drug compounds [74, 96].

In summary, if the above attributes can be applied correctly to a benchtop model of skeletal muscle, the result could be the production of a more mimetic tissue model that can serve as a more effective starting point for the development of a dystrophic model and thus the more apt testing of treatments and therapeutics, leading to more effective drug development for the treatment of muscular dystrophy. The following section outlines the current state-of-the-art models of 3D skeletal muscle tissue, including their benefits and pitfalls.

2.3.2 Current Benchtop Model Systems: Overview, Benefits, and Pitfalls

Over the past decade, researchers have worked to generate a benchtop model of skeletal muscle. Largely, researchers have understood the importance of three salient components, firstly, the benefit of generating 3D tissue, secondly, the importance of including ECM protein(s) into the 3D construct to promote cell-ECM interaction in 3D, and thirdly, the importance of generating anchored tissue to promote cellular alignment and mimic native myotendinous junctions. The following sections highlight the work completed by various groups towards the generation of a benchtop 3D model of skeletal muscle.

2.3.2.1 Collagen Gel-Based 3D Muscle Tissues

Collagen is the most abundant ECM protein in the human body and the main structural protein in the ECM space, comprising approximately 30% of whole body protein content, and serves as the main structural protein within the connective tissue of the majority of tissues [99]. Collagen consists of consisting of 28 different types of collagen, however, type 1 is by far, the most abundant, comprising 90% of all collagen in the body. Within skeletal muscle, collagen is a major component of the endomysium the inner-most layer of ECM that envelops the individual myofibers and contribute to the force transmission following muscle contraction [38, 100]. As such, researchers have investigated the use of type 1 collagen in aiding 3D tissue formation and providing an appropriate platform for muscle cell differentiation and maturation, *in vitro*.

To facilitate 3D tissue formation, prior research has demonstrated the ability to adjust the pH of a type 1 collagen gel to stabilize the pH into the physiologic range (as collagen is stabilized for storage at an acidic pH) to prevent immediate cell lysis. Initial generation of benchtop models of skeletal muscle began in the late 1980's where researchers developed a method to culture avian myoblasts embedded within a collagen gel to generate a 3D tissue [101]. Further investigation demonstrated that if such 3D cultures were maintained under tension between either stainless steel mesh or nylon support systems, that the myosin heavy chain protein accumulation was 2-3 times greater, compared to tissues cultured under no tension [101], with the structure of the myotubes reported to be similar structurally to that of neonatal myofibers, likely consisting of a smaller diameter and lacking large sarcomeric structures indicative of adult mature muscle tissue [101]. This initial work highlighted the benefit of combining an ECM protein with myoblasts to both aid in 3D tissue formation and also promote native cell-ECM connections, promoting myoblast differentiation and maturation.

More recent research from the same group identified various exogenous supplements such as Insulin Like Growth Factor-1 (IGF-1) that at a defined concentration of 50ng/ml, result in a statistical

increase in the diameter of the myotubes within the cultured collagen gel scaffolds [94]. Further work demonstrated that the modulation of both cell number along with the concentration of the collagen gel led to a varying degree of overall construct tension, indicating that such parameters can be optimized to yield a tissue that best promotes maturation [94].

In a similar fashion, Cheema et al. [97] along with Mudera et al. [102, 103] also created a 3D gel consisting of collagen populated with an immortalized murine myoblast cell line. The cells were harvested and mixed with the collagen gel, creating a collagen gel solution that was then cast into a plate between two anchor points. Following gelation at 37°C for 1 hour, the gel was flooded with media and cultured as a 3D tissue between the two anchor points and cultured in a similar manner to traditional 2D tissue culture [97, 102, 103]. These collagen gel constructs resulted in viable cells within the gel, but at a very diffuse cell density and much lower than that of native muscle during the regeneration phases. The presence of two anchor points result in a 3D gel constrained between two points of tension, resulting in cellular alignment and differentiation along the axis of strain created by the anchor points [97]. The research group also showed that visualization of filamentous actin by phalloidin staining is possible, indicating the beginning of contractile protein apparatus production. However, it is important to note that actin filaments should be seen within cells that are constrained between anchor points, as the cells are subjected to constant stress due to the anchorage [97].

More recent work has begun to utilize human primary myoblasts to generate 3D skeletal muscle tissue. For this work, briefly an acellular collagen scaffold was prepared from porcine bladder submucosa, cut into thin strips (1.5cm x 1.5cm), and sterilized such that cells can then be seeded onto the scaffold and cultured, *in vitro* [104]. Following sterilization, primary myoblasts (60×10^6 total cells) were seeded onto each scaffold. In a similar manner, following 7 days in culture, tissues were harvested and stained using immunofluorescence techniques for myosin protein. As stated previously, and

observed with this research once again, tissues expressed myosin protein, but morphologically lacked mature multinucleated contractile myotubes nor contained any sarcomeric structures [104].

In summary, collagen gels provide 3D scaffold for which myoblasts can be embedded into. The researchers hypothesized that due to the abundance of available ECM protein, sufficient cell-ECM bonds could be made such that maturation occurs in a similar fashion as it does within native muscle during development or repair [97, 103].

2.3.2.2. Fibrin Gel-Based 3D Muscle Tissues

Over the past decade, additional ECM proteins have been investigated for their use as a scaffold that can guide 3D skeletal muscle tissue formation and promote crucial cell-ECM bonds during myoblast maturation. Fibrin is a fibrous, non-globular protein chiefly responsible for blood clotting and formed from the polymerization of thrombin protease and fibrinogen [105]. Additionally, fibrin hydrogels have the advantage of binding growth factors including IGF-1, that promote native levels of myogenesis, further rationalizing their use as an exogenous ECM protein for 3D muscle tissue formation [106]. Following a large-scale muscular injury, blood loss is inhibited through the formation of a fibrin clot. During the natural regeneration process, fibroblasts initially infiltrate the fibrin matrix and synthesize collagen [39, 64]. While collagen synthesis is synonymous with scar tissue formation, the process of fibroblast infiltration also precludes functional muscle regeneration [105, 107]. As such, past researchers have investigated the use of fibrin scaffolds as a provisional 3D matrix for which to promote 3D muscle tissue formation and maturation, *in vitro* [108, 109].

The utilization of a fibrin scaffold was done in a different manner than how collagen scaffolds were utilized. In an attempt to provide the myoblasts sufficient cell-cell contact - a crucial component to promoting cell fusion -the initial stage of differentiation and maturation, myoblasts were seeded atop (vs. within, as done with the collagen gel scaffolds) a polymerized fibrin matrix, hence allowing the myoblasts to differentiate and initiate cell fusion at a high cell density monolayer setting [109, 110]. For

this experiment, primary rat myoblasts were isolated and expanded in culture, using a combination of a pre-plating step to remove quickly-adherent fibroblasts, yielding a more pure myoblast culture, confirmed using immunofluorescent staining for myogenic precursor marker MyoD [109]. Pre-plating to selectively purify a myogenic subpopulation from a primary biopsy has been used effectively in prior work [111]. A 35mm plate was coated with fibrin gel and 1×10^5 cells were seeded atop the fibrin gel and allowed to expand in proliferative medium for 2 additional days, following which, a transition to a defined mitogen-reduced medium was conducted, and the constructs were cultured for up to 14 days [109]. Macroscopic analysis of the tissues demonstrate that starting at 2 days (and completing at 8 days), the cell layer attached to the fibrin gel and following complete confluency of the cells atop the fibrin gel, the cells along with the fibrin gel released from the surface of the culture vessel and began to contract. As two individual anchor pins were previously adhered into the culture vessel, the contracting gel formed a linear cylindrical-shaped tissue between the two anchor pins [109].

Histologically, cross-sectional images showed that the cells contract the fibrin gel and form a contiguous 3D construct between the two anchor points. These constructs had an average diameter of $180\mu\text{m}$, yet contained a relatively low cell density along with an abundance of undigested fibrin matrix, observed at upwards of $100\mu\text{m}$ of fibrin gel with the absence of any nuclei [109]. As such, morphological analysis identified various regions of gel fraying - potentially identifying areas that did not receive nutrients through passive diffusion indicating cell death, with the majority of the viable cells observed towards the periphery of the 3D fibrin gel construct, indicating that the gel construct was too thick and did not promote sufficient nutrient diffusion to maintain cell viability towards the center of the construct [109]. Finally, such tissue constructs did produce a contractile force, when electrically stimulated, with maximal tetanic force production achieving $805\mu\text{N}/\text{construct}$ [109].

Additional work completed utilizing fibrin scaffolds as guides for muscle tissue formation and/or regeneration have focused on tuning the properties of both the fibrin gel along with protease

supplements that attempt to optimize the synthesis and remodeling of the exogenous fibrin matrix with cell-produced ECM, more effectively mimicking *de novo* muscle tissue formation and regeneration. While significant advancements have been made over the years, including novel methods to tune the structural properties of fibrin scaffolds, a succinct example of such timing and subsequent optimization and the effect that such timing has on cell function, has yet to be completed [112].

Furthermore, much of the promising work completed with fibrin gel scaffolds still utilize immortalized murine cell lines, potentially requiring further optimization and modulation prior to determining if such a model system accurately recapitulates native human skeletal muscle [98]. Namely, the MagnaTissue™ Bioreactor applies the concept of mechanical conditioning to strengthen their fibrin gel-based tissue constructs in an incubator setting. Such process, as described in detail here [98], although functionally similar to past fibrin gel procedures, involves seeding immortalized murine myoblasts within a fibrin gel, following which the gel was anchored to two hooks, generating a tissue that can be maintained under tension, promoting linearly-aligned differentiation [98]. Results of such culture methodology and the benefits of mechanical conditioning showed that multinucleated myotubes containing visible sarcomeres can be generated following 14 days in culture. However, the researchers fail to elucidate the role that the exogenous ECM had on the tissue thickness and whether or not the entire tissue contains viable contractile myotubes, compared to just the periphery [98]. Horizontal sections of the mechanically-strained tissues indicate that there are visible sarcomeric striations stained positive for myosin heavy chain, however, cross-sectional images of the tissues was not presented in the article, indicating that the differentiation observed in the horizontal tissues may not be indicative of the full-thickness differentiation of the entire 3D tissue, and may present scale-up challenges for drug screening [98].

2.3.2.3. Inclusion of Fibroblasts to Endogenously-Synthesize ECM

Prior work has eluded to the benefit of either embedding cells within or atop ECM proteins, to provide a pro-myogenic environment, allowing cells to make crucial cell-ECM contacts that impact their capability to differentiate and mature [39, 58]. However, the exogenous inclusion of ECM protein has been done at a crucial cost of reducing overall cell density along with the retention of unwanted exogenous ECM that results in a tissue size that is beyond the capability of passive free diffusion of nutrients, often resulting in a necrotic/non-functional tissue core. One promising improvement may involve utilizing fibroblasts - a cell type that natively synthesizes ECM protein - and is chiefly responsible for the ECM protein synthesis during *de novo* muscle development, to synthesize ECM within a benchtop muscle model [58, 59, 113]. More recently, some limited literature has investigated the role that fibroblasts have in the synergy of muscle development, *in vitro* [58, 114, 115].

The following research was conducted in a similar manner to previously described fibrin gel work, whereas cells were seeded atop a fibrin gel and allowed to contract along with the gel around two structural pins, creating an anchored and aligned 3D construct. The iteration in research involved the use of two different cell types in the generation of the tissue. Primary mouse myoblasts were derived as described here and their myogenic potential confirmed via a Desmin stain (a marker for myoblasts) which indicated 98% of the cells were Desmin-positive [58]. In addition to the myoblasts, the research group isolated mouse embryonic fibroblasts and expanded those cells along with the myoblasts in separate culture vessels. As described previously, cells were seeded atop the fibrin gel, but done so in varying ratios of myoblasts:fibroblasts (1:0.5, 1:1, or 1:2), to attempt to elucidate the role that a varying percentage of fibroblasts will have on both the maturation potential of the tissue along with the active remodeling of the fibrin matrix [58].

Results of such fibroblast-inclusion studies indicated that the addition of fibroblasts improved the myotube formation compared to purely-myoblast cultures. Monolayer differentiation of pure

myoblast cultures began to degrade and release from the surface following 18 days of culture, whereas fibroblast supplemented myoblast 2D differentiation cultures maintained intact with the culture surface, with multinucleated myotubes visible [58]. This observation indicates that the myoblasts alone cannot synthesize sufficient ECM to promote improved and complete maturation and sustained attachment to the culture vessel surface [58, 103]. As described previously, the crucial cell-ECM connections are vital for directing complete and terminal differentiation and maturation of skeletal muscle, and that the supplementation of fibroblasts in a benchtop monolayer model system appears to generate a more *in vivo* like environment that allows for continued long-term culture of differentiated myoblasts, *in vitro* [40, 58].

A similar outcome occurred during 3D tissue formation. Entirely myoblast constructs did not reproducibly roll and form a contiguous rod-shaped tissue between the two anchor points, whereas the formation efficiency and tissue compaction was improved with the addition of the fibroblasts into the fibrin gel tissue construct [58]. Such observations are likely due to the myoblasts' inability to make sufficient cell-ECM connections in a shortened time period as required for the 2D to 3D translation and subsequent tissue formation, whereas the constructs supplemented with fibroblasts were able to connect sufficiently with the ECM beneath the cells and result in the entire cell-gel construct maintaining contiguity during the 3D transition, resulting in a contiguous 3D tissue[40, 58].

Furthermore, the constructs containing the fibroblasts demonstrated an accelerated capability to degrade the excess exogenous fibrin matrix - a phenomena not addressed with previous 3D cells in gel muscle tissue models [58]. Finally, the constructs containing the fibroblasts resulted in an increase in myotube formation - an interesting observation because of the overall fewer number of myoblasts/construct - indicating that there perhaps is a symbiotic relationship between the myoblasts and fibroblasts, and such cellular crosstalk (more mimetic of native muscle tissue), results in a higher degree of myoblast differentiation and maturation [58, 103].

2.3.3. Drawbacks of Current Model Systems

As summarized previously, there are a variety of different methodologies that have been used to generate 3D benchtop models of skeletal muscle, however, significant limitations and drawbacks to such methods prevent the current benchtop models from mimicking native tissue morphology and achieving native levels of functionality. Notably, collagen gel-based systems allow for some myotube formation, however the resulting morphology indicates significant tissue necrosis towards the center of the tissues due to a lack a free diffusion of nutrients through the large tissue, along with a decrease in overall force production (roughly 1% of that of native tissue), due to the low density of myotube formation within the collagen gel, inhibiting crucial cell-cell connections that result in differentiation and maturation [94].

Similarly, collagen and fibrin gel-based systems result in an abundance of undigested fibrin matrix, also yielding a cell density within the tissue that is far below that of native tissue, similarly resulting in construct functionality multiple orders of magnitude below that of native skeletal muscle tissue [109]. Furthermore, the presence of an abundance of an ECM matrix within a tissue construct that is supposed to be promoting muscle regeneration may in fact inhibit *de novo* regeneration, due to the presence of collagen and/or fibrin, an abundant protein during non functional scar tissue generation following injury [100]. While cells can remodel injured tissue, generally, in the case of muscle tissue, myogenic cells do not synthesize and remodel scar tissue to restore functionality.

Salient limitations to both types of ECM protein-based 3D muscle tissue constructs firstly involve the inability of the cells through the entire construct to differentiate fully, as nutrients cannot reach the center of the tissues, creating a gradient of differentiation and nutrient delivery. Such inability of full-thickness differentiation has also been shown to lead to necrotic and/or non-functional tissue cores, inherit limitations associated with the methodology of using gel-based ECM proteins to aid in 3D tissue generation [94, 109]. Furthermore, the previously described approaches utilizing exogenous ECM

proteins only used a single kind of protein. During native muscle development and repair, a variety of different ECM proteins participate in the various stages of regeneration, and as such, incorporating a variety of ECM proteins into a 3D tissue construct may better promote native levels of regeneration and functional restoration. The use of skeletal muscle fibroblasts perhaps best approximate the native ECM environment [58]. Past work has shown that fibroblasts can more rapidly remodel the exogenous ECM matrix, thus making them useful to incorporate within ECM gel-based tissue constructs [109]. But furthermore, as native fibroblasts endogenously synthesize a variety of ECM proteins, perhaps instructing skeletal muscle fibroblasts to synthesize ECM, which can then be used to promote myoblast differentiation and maturation would better emulate the process of native ECM synthesis during *de novo* muscle formation and regeneration.

In summary, the importance of the cell-ECM interaction coupled with the pro-regenerative capability of ECM-producing fibroblasts is clear, yet, salient limitations regarding creating a full-thickness functionality, utilizing a clinically-relevant cell source, and tuning culture conditions to promote long-term culture and native levels of maturation remain. The goal of this project is to improve upon the limitations of prior work and develop methodology for the generation of a more precise mimetic *in vitro* model of skeletal muscle such that future translation to disease model can provide more useful data for skeletal muscle disorders.

2.4 References

1. Malik, V., L.R. Rodino-Klapac, and J.R. Mendell, *Emerging drugs for Duchenne muscular dystrophy*. Expert Opin Emerg Drugs, 2012. **17**(2): p. 261-77.
2. Muntoni, F., S. Torelli, and A. Ferlini, *Dystrophin and mutations: one gene, several proteins, multiple phenotypes*. The Lancet Neurology, 2003. **2**(12): p. 731-740.
3. Le Rumeur, E., *Dystrophin and the two related genetic diseases, Duchenne and Becker muscular dystrophies*. Bosn J Basic Med Sci, 2015. **15**(3): p. 14-20.
4. Eagle, M., et al., *Survival in Duchenne muscular dystrophy: improvements in life expectancy since 1967 and the impact of home nocturnal ventilation*. Neuromuscular Disorders, 2002. **12**(10): p. 926-929.

5. England, S.B., et al., *Very Mild Muscular-Dystrophy Associated with the Deletion of 46-Percent of Dystrophin*. *Nature*, 1990. **343**(6254): p. 180-182.
6. Statland, J. and R. Tawil, *Facioscapulohumeral muscular dystrophy*. *Neurol Clin*, 2014. **32**(3): p. 721-8, ix.
7. Zhang, Y., et al., *Improved characterization of FSHD mutations*. *Ann Genet*, 2001. **44**(2): p. 105-10.
8. Bertini, E., et al., *Congenital muscular dystrophies: a brief review*. *Semin Pediatr Neurol*, 2011. **18**(4): p. 277-88.
9. Biggar, W.D., et al., *Long-term benefits of deflazacort treatment for boys with Duchenne muscular dystrophy in their second decade*. *Neuromuscul Disord*, 2006. **16**(4): p. 249-55.
10. Graedon, J., *New FDA Warning For Popular Cipro and Levaquin Antibiotics!* The Peoples Pharmacy, 2016.
11. Holder, K., *Myalgias and Myopathies: Drug-Induced Myalgias and Myopathies*. *FP Essent*, 2016. **440**(23): p. 7.
12. Pozniak, A., *Cholesterol Drug Pulled From Market*. ABC News, 2001.
13. Marchetti, S. and J.H. Schellens, *The impact of FDA and EMEA guidelines on drug development in relation to Phase 0 trials*. *Br J Cancer*, 2007. **97**(5): p. 577-81.
14. Umscheid, C.A., D.J. Margolis, and C.E. Grossman, *Key concepts of clinical trials: a narrative review*. *Postgrad Med*, 2011. **123**(5): p. 194-204.
15. DiMasi, J.A., R.W. Hansen, and H.G. Grabowski, *The price of innovation: new estimates of drug development costs*. *Journal of Health Economics*, 2003. **22**(2): p. 151-185.
16. Witten, C.M., R.D. McFarland, and S.L. Simek, *Concise Review: The U.S. Food and Drug Administration and Regenerative Medicine*. *Stem Cells Transl Med*, 2015. **4**(12): p. 1495-9.
17. Deyo, R.A., *Gaps, tensions, and conflicts in the FDA approval process: implications for clinical practice*. *J Am Board Fam Pract*, 2004. **17**(2): p. 142-9.
18. DiMasi, J., *Risks in new drug development: Approval success rates for investigational drugs*. *Clinical Pharmacology & Therapeutics*, 2001. **69**(5): p. 297-307.
19. Temple, R., *Current definitions of the phases of investigation and the role of the FDA in the conduct of clinical trials*. *American Heart Journal*, 2000. **139**(4): p. 133-135.
20. Arrowsmith, J., *Trial watch: Phase II failures: 2008–2010*. *Nat Rev Drug Discov*, 2011. **10**(5): p. 328-329.
21. Arrowsmith, J., *Trial watch: Phase III and submission failures: 2007–2010*. *Nat Rev Drug Discov*, 2011. **10**(2): p. 87-87.
22. Pinnapureddy, A.R., et al., *Large animal models of rare genetic disorders: sheep as phenotypically relevant models of human genetic disease*. *Orphanet J Rare Dis*, 2015. **10**: p. 107.
23. Mak, I.W.V., I. Evaniew, and M. Chert, *Lost in translation: animal models and clinical trials in cancer treatment*. *Am J Transl Res*, 2014. **6**(2): p. 114-118.
24. Philip, M., et al., *Methodological quality of animal studies of neuroprotective agents currently in phase II/III acute ischemic stroke trials*. *Stroke*, 2009. **40**(2): p. 577-81.
25. Benatar, M., *Lost in translation: treatment trials in the SOD1 mouse and in human ALS*. *Neurobiol Dis*, 2007. **26**(1): p. 1-13.
26. Landis, S.C., et al., *A call for transparent reporting to optimize the predictive value of preclinical research*. *Nature*, 2012. **490**(7419): p. 187-91.
27. Mah, J.K., et al., *A Systematic Review and Meta-analysis on the Epidemiology of the Muscular Dystrophies*. *Canadian Journal of Neurological Sciences / Journal Canadien des Sciences Neurologiques*, 2016. **43**(1): p. 163-177.
28. Partridge, T.A., *The mdx mouse model as a surrogate for Duchenne muscular dystrophy*. *FEBS J*, 2013. **280**(17): p. 4177-86.

29. Sacco, A., et al., *Short telomeres and stem cell exhaustion model Duchenne muscular dystrophy in mdx/mTR mice*. Cell, 2010. **143**(7): p. 1059-71.
30. Goyenvalle, A., et al., *Prevention of dystrophic pathology in severely affected dystrophin/utrophin-deficient mice by morpholino-oligomer-mediated exon-skipping*. Mol Ther, 2010. **18**(1): p. 198-205.
31. Mann, C.J., et al., *Antisense-induced exon skipping and synthesis of dystrophin in the mdx mouse*. Proc Natl Acad Sci U S A, 2001. **98**(1): p. 42-7.
32. Chen, Y., et al., *Functional disruption of the dystrophin gene in rhesus monkey using CRISPR/Cas9*. Hum Mol Genet, 2015. **24**(13): p. 3764-74.
33. Frontera, W.R. and J. Ochala, *Skeletal muscle: a brief review of structure and function*. Calcif Tissue Int, 2015. **96**(3): p. 183-95.
34. Ottenheijm, C.A. and H. Granzier, *Lifting the nebula: novel insights into skeletal muscle contractility*. Physiology (Bethesda), 2010. **25**(5): p. 304-10.
35. Hikida, R.S., *Aging changes in satellite cells and their functions*. Curr Aging Sci, 2011. **4**(3): p. 279-97.
36. Gillies, A.R. and R.L. Lieber, *Structure and function of the skeletal muscle extracellular matrix*. Muscle Nerve, 2011. **44**(3): p. 318-31.
37. Kuhl, U., et al., *Role of muscle fibroblasts in the deposition of type-IV collagen in the basal lamina of myotubes*. Differentiation, 1984. **28**(2): p. 164-72.
38. Chaturvedi, V., et al., *Interactions between Skeletal Muscle Myoblasts and their Extracellular Matrix Revealed by a Serum Free Culture System*. PLoS One, 2015. **10**(6): p. e0127675.
39. Grounds, M.D., L. Sorokin, and J. White, *Strength at the extracellular matrix-muscle interface*. Scand J Med Sci Sports, 2005. **15**(6): p. 381-91.
40. Purslow, P.P. and J.A. Trotter, *The morphology and mechanical properties of endomysium in series-fibred muscles: variations with muscle length*. Journal of Muscle Research & Cell Motility, 1994. **15**(3): p. 299-308.
41. Passerieux, E., et al., *Physical continuity of the perimysium from myofibers to tendons: involvement in lateral force transmission in skeletal muscle*. J Struct Biol, 2007. **159**(1): p. 19-28.
42. Urciuolo, A., et al., *Collagen VI regulates satellite cell self-renewal and muscle regeneration*. Nat Commun, 2013. **4**: p. 1964.
43. Ervasti, J.M. and K.P. Campbell, *A Role for the Dystrophin-Glycoprotein Complex as a Transmembrane Linker between Laminin and Actin*. Journal of Cell Biology, 1993. **122**(4): p. 809-823.
44. Luther, P.K., *The vertebrate muscle Z-disc: sarcomere anchor for structure and signalling*. J Muscle Res Cell Motil, 2009. **30**(5-6): p. 171-85.
45. Martin, N.R., et al., *Factors affecting the structure and maturation of human tissue engineered skeletal muscle*. Biomaterials, 2013.
46. Edman, K.A.P., *Contractile Performance of Striated Muscle*, in *Muscle Biophysics: From Molecules to Cells*, D.E. Rassier, Editor. 2010, Springer New York: New York, NY. p. 7-40.
47. Smith, L.R., G. Meyer, and R.L. Lieber, *Systems analysis of biological networks in skeletal muscle function*. Wiley Interdiscip Rev Syst Biol Med, 2013. **5**(1): p. 55-71.
48. Claflin, D.R., et al., *Effects of high- and low-velocity resistance training on the contractile properties of skeletal muscle fibers from young and older humans*. J Appl Physiol, 2011. **111**(4): p. 1021-30.
49. Roche, S.M., et al., *Measurement of Maximum Isometric Force Generated by Permeabilized Skeletal Muscle Fibers*. 2015(100): p. e52695.
50. Yan, X., et al., *Developmental programming of fetal skeletal muscle and adipose tissue development*. J Genomics, 2013. **1**: p. 29-38.

51. Calve, S., S.J. Odelberg, and H.G. Simon, *A transitional extracellular matrix instructs cell behavior during muscle regeneration*. *Dev Biol*, 2010. **344**(1): p. 259-71.
52. Dumont, N.A., et al., *Satellite Cells and Skeletal Muscle Regeneration*. *Compr Physiol*, 2015. **5**(3): p. 1027-59.
53. Punch, V.G., A.E. Jones, and M.A. Rudnicki, *Transcriptional networks that regulate muscle stem cell function*. *Wiley Interdisciplinary Reviews-Systems Biology and Medicine*, 2009. **1**(1): p. 128-140.
54. Tidball, J.G., *Inflammatory processes in muscle injury and repair*. *Am J Physiol Regul Integr Comp Physiol*, 2005. **288**(2): p. R345-53.
55. Duffy, R.M., Y. Sun, and A.W. Feinberg, *Understanding the Role of ECM Protein Composition and Geometric Micropatterning for Engineering Human Skeletal Muscle*. *Ann Biomed Eng*, 2016.
56. Li, M., et al., *The role of fibroblasts in self-assembled skeletal muscle*. *Tissue Eng Part A*, 2011. **17**(21-22): p. 2641-50.
57. Zou, Y., et al., *Muscle interstitial fibroblasts are the main source of collagen VI synthesis in skeletal muscle: implications for congenital muscular dystrophy types Ullrich and Bethlem*. *J Neuropathol Exp Neurol*, 2008. **67**(2): p. 144-54.
58. Murphy, M.M., et al., *Satellite cells, connective tissue fibroblasts and their interactions are crucial for muscle regeneration*. *Development*, 2011. **138**(17): p. 3625-37.
59. Hicks, M.R., et al., *Mechanical strain applied to human fibroblasts differentially regulates skeletal myoblast differentiation*. *Journal of Applied Physiology*, 2012. **113**(3): p. 465-72.
60. Jarvinen, T.A., M. Jarvinen, and H. Kalimo, *Regeneration of injured skeletal muscle after the injury*. *Muscles Ligaments Tendons J*, 2013. **3**(4): p. 337-45.
61. Grogan, B.F., J.R. Hsu, and C. Skeletal Trauma Research, *Volumetric muscle loss*. *J Am Acad Orthop Surg*, 2011. **19 Suppl 1**: p. S35-7.
62. Juhas, M. and N. Bursac, *Engineering skeletal muscle repair*. *Curr Opin Biotechnol*, 2013. **24**(5): p. 880-6.
63. Huard, J., Y. Li, and F.H. Fu, *Muscle injuries and repair: current trends in research*. *J Bone Joint Surg Am*, 2002. **84-A**(5): p. 822-32.
64. Boldrin, L., F. Muntoni, and J.E. Morgan, *Are human and mouse satellite cells really the same?* *J Histochem Cytochem*, 2010. **58**(11): p. 941-55.
65. Danoviz, M.E. and Z. Yablonka-Reuveni, *Skeletal muscle satellite cells: background and methods for isolation and analysis in a primary culture system*. *Methods Mol Biol*, 2012. **798**: p. 21-52.
66. Morgan, J.E. and T.A. Partridge, *Muscle satellite cells*. *Int J Biochem Cell Biol*, 2003. **35**(8): p. 1151-1156.
67. Feldman, J.L. and F.E. Stockdale, *Skeletal muscle satellite cell diversity: Satellite cells form fibers of different types in cell culture*. *Dev Biol*, 1991. **143**(2): p. 320-334.
68. Kalhovde, J.M., et al., *'Fast' and 'slow' muscle fibres in hindlimb muscles of adult rats regenerate from intrinsically different satellite cells*. *J Physiol*, 2005. **562**(Pt 3): p. 847-857.
69. Fukada, S., et al., *Molecular signature of quiescent satellite cells in adult skeletal muscle*. *Stem Cells*, 2007. **25**(10): p. 2448-59.
70. Ten Broek, R.W., S. Grefte, and J.W. Von den Hoff, *Regulatory factors and cell populations involved in skeletal muscle regeneration*. *J Cell Physiol*, 2010. **224**(1): p. 7-16.
71. Liu, N., et al., *Requirement of MEF2A, C, and D for skeletal muscle regeneration*. *Proceedings of the National Academy of Sciences*, 2014. **111**(11): p. 4109-4114.
72. Irwin, W.A., et al., *Mitochondrial dysfunction and apoptosis in myopathic mice with collagen VI deficiency*. *Nat Genet*, 2003. **35**(4): p. 367-71.
73. Nam, K.H., et al., *Biomimetic 3D Tissue Models for Advanced High-Throughput Drug Screening*. *J Lab Autom*, 2015. **20**(3): p. 201-15.

74. Edmondson, R., et al., *Three-dimensional cell culture systems and their applications in drug discovery and cell-based biosensors*. *Assay Drug Dev Technol*, 2014. **12**(4): p. 207-18.
75. Nelson, C.M. and M.J. Bissell, *Modeling dynamic reciprocity: engineering three-dimensional culture models of breast architecture, function, and neoplastic transformation*. *Semin Cancer Biol*, 2005. **15**(5): p. 342-52.
76. Gurski, L., et al., *3D Matrices for Anti-Cancer Drug Testing and Development*. *Oncology Issues*, 2010(Jan/Feb): p. 20-25.
77. Breslin, S. and L. O'Driscoll, *Three-dimensional cell culture: the missing link in drug discovery*. *Drug Discov Today*, 2013. **18**(5-6): p. 240-9.
78. Kinney, M.A., et al., *Engineering three-dimensional stem cell morphogenesis for the development of tissue models and scalable regenerative therapeutics*. *Ann Biomed Eng*, 2014. **42**(2): p. 352-67.
79. Auluck, A., et al., *A three-dimensional in vitro model system to study the adaptation of craniofacial skeletal muscle following mechanostimulation*. *European Journal of Oral Sciences*, 2005. **113**(3): p. 218-224.
80. Yaffe, D. and O. Saxel, *A Myogenic Cell Line with Altered Serum Requirements for Differentiation*. *Differentiation*, 1977. **7**(3): p. 159-66.
81. Yaffe, D. and O. Saxel, *Serial passaging and differentiation of myogenic cells isolated from dystrophic mouse muscle*. *Nature*, 1977. **270**(5639): p. 725-7.
82. Blau, H.M., C. Webster, and G.K. Pavlath, *Defective myoblasts identified in Duchenne muscular dystrophy*. *Proc Natl Acad Sci U S A*, 1983. **80**(15): p. 4856-60.
83. Blau, H.M., et al., *Differentiation properties of pure populations of human dystrophic muscle cells*. *Exp Cell Res*, 1983. **1**(144): p. 495-503.
84. Patz, T.M., et al., *Two-dimensional differential adherence and alignment of C2C12 myoblasts*. *Materials Science and Engineering: B*, 2005. **123**(3): p. 242-247.
85. Nagamine, K., et al., *Micropatterning contractile C2C12 myotubes embedded in a fibrin gel*. *Biotechnol Bioeng*, 2010. **105**(6): p. 1161-7.
86. Sharples, A.P., et al., *Reduction of myoblast differentiation following multiple population doublings in mouse C2C12 cells: A model to investigate ageing?* *J Cell Biochem*, 2011. **112**(12): p. 3773-3785.
87. Langelaan, M.L., et al., *Advanced maturation by electrical stimulation: Differences in response between C2C12 and primary muscle progenitor cells*. *J Tissue Eng Regen Med*, 2011. **5**(7): p. 529-39.
88. Merrick, D., et al., *Adult and embryonic skeletal muscle microexplant culture and isolation of skeletal muscle stem cells*. *J Vis Exp*, 2010(43).
89. Montarras, D., et al., *Direct isolation of satellite cells for skeletal muscle regeneration*. *Science*, 2005. **309**(5743): p. 2064-7.
90. Kikuchi, T. and T. Shimizu, *Selective Culture of Human Skeletal Myoblasts by Brefeldin*. *JSM Regen Med Bio Eng*, 2016. **4**(1).
91. Stern-Straeter, J., et al., *Evaluation of the effects of different culture media on the myogenic differentiation potential of adipose tissue- or bone marrow-derived human mesenchymal stem cells*. *Int J Mol Med*, 2014. **33**(1): p. 160-70.
92. Mordwinkin, N.M., A.S. Lee, and J.C. Wu, *Patient-specific stem cells and cardiovascular drug discovery*. *JAMA*, 2013. **310**(19): p. 2039-40.
93. Shansky, J., et al., *Paracrine release of insulin-like growth factor 1 from a bioengineered tissue stimulates skeletal muscle growth in vitro*. *Tissue Eng*, 2006. **12**(7): p. 1833-41.
94. Lovett, M., et al., *Vascularization Strategies for Tissue Engineering*. *Tissue Eng Part B* 2009. **15**(3): p. 353-370.

95. Boudou, T., et al., *A microfabricated platform to measure and manipulate the mechanics of engineered cardiac microtissues*. *Tissue Eng Part A*, 2012. **18**(9-10): p. 910-9.
96. Cheema, U., et al., *3-D in vitro model of early skeletal muscle development*. *Cell Motil Cytoskeleton*, 2003. **54**(3): p. 226-36.
97. Heher, P., et al., *A novel bioreactor for the generation of highly aligned 3D skeletal muscle-like constructs through orientation of fibrin via application of static strain*. *Acta Biomater*, 2015. **24**: p. 251-65.
98. Di Lullo, G.A., et al., *Mapping the ligand-binding sites and disease-associated mutations on the most abundant protein in the human, type I collagen*. *J Biol Chem*, 2002. **277**(6): p. 4223-31.
99. Mann, C.J., et al., *Aberrant repair and fibrosis development in skeletal muscle*. *Skelet Muscle*, 2011. **1**(1): p. 21.
100. Vandenburg, H., P. Karlisch, and L. Farr, *Maintenance of highly contractile tissue-cultured avian skeletal myotubes in collagen gel*. *In Vitro Cell Dev Bio*, 1988. **24**(3): p. 166-74.
101. Mudera, V., et al., *The effect of cell density on the maturation and contractile ability of muscle derived cells in a 3D tissue-engineered skeletal muscle model and determination of the cellular and mechanical stimuli required for the synthesis of a postural phenotype*. *J Cell Physiol*, 2010. **225**(3): p. 646-53.
102. Brady, M.A., M.P. Lewis, and V. Mudera, *Synergy between myogenic and non-myogenic cells in a 3D tissue-engineered craniofacial skeletal muscle construct*. *J Tissue Eng Regen Med*, 2008. **2**(7): p. 408-17.
103. Moon du, G., et al., *Cyclic mechanical preconditioning improves engineered muscle contraction*. *Tissue Eng Part A*, 2008. **14**(4): p. 473-82.
104. Janmey, P.A., J.P. Winer, and J.W. Weisel, *Fibrin gels and their clinical and bioengineering applications*. *J R Soc Interface*, 2009. **6**(30): p. 1-10.
105. Campbell, P.G., et al., *Insulin-like Growth Factor-binding Protein-3 Binds Fibrinogen and Fibrin*. *Journal of Biological Chemistry*, 1999. **274**(42): p. 30215-30221.
106. Page, R.L., et al., *Restoration of skeletal muscle defects with adult human cells delivered on fibrin microthreads*. *Tissue Eng Part A*, 2011. **17**(21-22): p. 2629-40.
107. Bian, W. and N. Bursac, *Engineered skeletal muscle tissue networks with controllable architecture*. *Biomaterials*, 2009. **30**(7): p. 1401-12.
108. Huang, Y.C., et al., *Rapid formation of functional muscle in vitro using fibrin gels*. *Journal of Applied Physiology*, 2005. **98**(2): p. 706-713.
109. Hinds, S., et al., *The role of extracellular matrix composition in structure and function of bioengineered skeletal muscle*. *Biomaterials*, 2011. **32**(14): p. 3575-83.
110. Qu-Petersen, Z., et al., *Identification of a novel population of muscle stem cells in mice: potential for muscle regeneration*. *J Cell Biol*, 2002. **157**(5): p. 851-64.
111. Grasman, J.M., et al., *Crosslinking strategies facilitate tunable structural properties of fibrin microthreads*. *Acta Biomater*, 2012. **8**(11): p. 4020-30.
112. Hinz, B., et al., *The myofibroblast: one function, multiple origins*. *American Journal of Pathology*, 2007. **170**.
113. Dennis, R.G., et al., *Excitability and contractility of skeletal muscle engineered from primary cultures and cell lines*. *American Journal of Physiology - Cell Physiology*, 2001. **280**(2): p. C288-C295.
114. Khodabukus, A. and K. Baar, *Regulating fibrinolysis to engineer skeletal muscle from the C2C12 cell line*. *Tissue Eng Part C Methods*, 2009. **15**(3): p. 501-11.

Chapter 3: The Generation and characterization of entirely cellular biomimetic 3D skeletal muscle tissue constructs, *in vitro*

3.1 Introduction

Genetic muscular disorders such as Muscular Dystrophy are the result of genetic mutations in molecules that mediate the interaction between myocytes and the surrounding ECM. Although these disorders differ in etiology and severity, the disrupted myocyte-ECM connection leads to cycles of constant muscle degeneration and repair, ultimately depleting the innate ability of the muscle to repair itself, leading to loss of function. Duchenne's muscular dystrophy - an example of this genetic based chronic muscle wasting disease - is 100% fatal muscular disease and affects roughly 1 in 3,500 males, is caused by a genetic mutation resulting in a signaling breakdown within the dystroglycan complex, which in healthy patients mediates crucial cell-ECM binding [1-4].

To understand how the disease progresses and what specific structures are affected, an understanding of muscle structure and physiology is important. Skeletal muscle is a highly organized and aligned tissue composed of parallel muscle fibers consisting of the proteins actin and myosin which combine to form sarcomeres, the functional motor unit of skeletal muscle [5]. During development or following small injuries, intrinsic regeneration and functional repair is driven by the activation, proliferation, and differentiation of normally-dormant satellite cells (SC) and ECM -synthesizing fibroblasts into the wound site [6, 7]. In mature muscle, the ECM tethers the muscle fibers through myotendonous junctions to transmit forces generated by muscle contraction to movement of the bones, and further provides elasticity to prevent rupture [8-12].

Development of therapeutic treatment for muscular dystrophy has been attempted, but unfortunately, the current drug development is hampered by the use of poorly-predictive preclinical animal modeling, and the inability of benchtop model systems to precisely model the structure and function of native skeletal muscle due to inappropriate cell sources and methodology used for tissue

formation and subsequent culture [8, 11, 13-15]. These pitfalls in the current development process necessitate the need for a more precise benchtop skeletal muscle model that could streamline candidate drug efficacy testing along with reduce time, cost, and usage of poorly-predictive animals during the development [16].

To this end, one novel approach to engineer more biomimetic benchtop skeletal muscle tissue constructs involves the use of cell self-assembly. Guided cell self-assembly utilizing non-adhesive hydrogels has been successful for a variety of applications while addressing application-dependent concerns regarding molecular transport, cell-ECM interaction, and tissue modeling, as reviewed here [17]. Prior work has demonstrated that ring-shaped tissues can be formed through an entirely self-assembly method by creating a hydrogel 2% agarose mold consisting of a central post surrounded by an annular well [18]. Additionally, other work has shown that the inclusion of ECM-producing fibroblasts into myoblast 3D constructs, can mediate endogenous ECM production [6, 19, 20]. Yet to date, no research has identified proper methodology for generating highly aligned and anchored self-assembled skeletal muscle tissue constructs while combining the beneficial function of endogenous ECM-production via fibroblasts, and generating a tissue that is free of necrosis and functionally biomimetic to native muscle. This chapter outlines methodology and optimization parameters for generating a more biomimetic 3D self-assembled skeletal muscle tissue scaffold that has a higher level of myoblast maturation and functionality than current model systems, which may allow this model system to ultimately be tuned from a healthy model to a patient-specific model of muscle-specific disorders.

3.2 Methods

3.2.1 Isolation, Derivation, and Characterization of a Primary Skeletal Muscle Cell Line

Previous work completed in the laboratory involved isolating and deriving a highly-myogenic myoblast population from a adult human skeletal muscle tissue. Briefly, surplus tissue from a latissimus dorsi skeletal muscle reconstruction procedure of a 58 year-old female patient was obtained from the operating surgeon and taken into the laboratory for cell line derivation. Initially, skeletal muscle was dissected from fat tissue, minced into small pieces and enzymatically digested at 37C for 30 minutes, as described previously [21]. Additional purification steps intended to remove fast-proliferating fibroblasts and immune cells from the culture were completed and described previously, resulting in a highly-myogenic population of myoblasts confirmed by positive Desmin (a muscle-specific intermediate filament protein) staining [21].

3.2.2. Cell Culture

Primary myoblast cells were cultured in the following proliferative growth media: a basal medium consisting of a 60:40 (v:v) blend of Dulbecco's modification of Eagle's medium (DMEM): Ham's F12 (F12) medium, supplemented with 10% FetalCloneIII (FCIII) serum substitute and 4mM L-Glutamine (Corning). This basal medium was further supplemented with growth factors which have been previously shown to improve cell proliferation and extend cell lifespan, while maintaining myogenic (stem-like) potential *in vitro*: fibroblast growth factor-basic (FGF-2) [4.0ng/ml]; insulin-like growth factor-1 (IGF-1) [5.0ng/ml]; hepatocyte growth factor (HGF) [2.5ng/ml]; and epidermal growth factor (EGF) [10ng/ml](All Peprotech) (Myoblast Growth Medium - MGM). Human dermal fibroblasts (ATCC CRL-2352) were expanded as recommended by the ATCC in standard 2D monolayer culture in culture medium consisting of Iscove's modified Dulbecco's medium (IMDM)(Corning), supplemented with 10% Fetal Bovine Serum (FBS) (HyClone) and 4mM L-glutamine (Corning) (IMDM media).

Immortalized murine myoblast cells - C2C12 (ATCC 1772) were expanded in a basal medium consisting of DMEM supplemented with 10% FCS and 4mM L-glutamine (C2C12 Proliferative Media).

Primary human skin fibroblasts (CRL-2097) were cultured in DMEM supplemented with 10% FBS and 2mM L-glutamine (2097 Proliferative Media).

For myoblast differentiation (for both primary and immortalized cells), a mitogen-reduced culture medium was used to direct cells to exit cell cycle and begin terminal differentiation. Media containing a 60:40 (v:v) blend of Dulbecco's modification of Eagle's medium: Ham's F12 medium, supplemented with 2% adult horse serum (AHS) and 1% Insulin, Transferrin, and Selenium (ITS), and 4mM L-Glutamine (Differentiation media) was used for myoblast differentiation, unless otherwise specified.

Primary patient-derived myoblast cells (hSkM 1201) were thawed from cryogenic storage using traditional cell culture methodology. Briefly, cells were removed from thawed cryogenic storage vial and transferred to a 15ml conical tube containing 5 ml of myoblast growth medium and centrifuged at 300g for 5 minutes. The supernatant was aspirated and the cell pellet was resuspended in 1ml fresh MGM and cells were plated at a density of 2,000 cells/cm² in a tissue culture coated vessel and maintained in a humidified environment at 37°C buffered with 5% CO₂.

hSkM 1201 cells were expanded in culture and fed every 48 hrs. by removing half of the volume of media, centrifuging, and resuspending in equal volume of fresh myoblast growth medium and replaced into the original culture vessel. All cultures were sub-cultured at, or below 70% confluency (retaining both adherent and non-adherent sub-populations of cells in culture), using 0.05% trypsin-EDTA to release the cells from monolayer culture, collected and counted, and then replated into a fresh culture vessel containing fresh media at a density of 2,000 cells/cm².

Immortalized C2C12 murine skeletal muscle myoblasts were initially seeded at 2,000 cells/cm² on standard tissue culture treated vessels in C2C12 proliferation media, and allowed to proliferate until

they reached 70% confluence, at which point, the adherent cells were harvested using 0.05% trypsin-EDTA, and then replated into a fresh culture vessel containing fresh media at a density of 2,000 cells/cm².

CRL-2097 fibroblasts were expanded in monolayer culture on tissue culture treated vessels in 2097 Proliferation Media. Once 80% confluent, cells were released from monolayer culture using 0.25% Trypsin-EDTA, collected and counted, then replated into a fresh tissue culture vessel containing fresh media at 4,000 cells/cm².

CRL-2352 fibroblasts were expanded in culture and fed every 48 hrs. with complete media exchanges. Cultures were sub-cultured at, or below 70% confluency by first rinsing cells in DPBS free of divalent cations and then using 0.05% trypsin-EDTA to release cells from monolayer culture, collected and counted, then replated into a fresh culture vessel containing fresh media at 4,000 cells/cm².

3.2.3 Immunocyto- and Immunohistochemistry

For fixation, cells and tissues were first washed in DPBS containing divalent cations (DPBS+) (Corning) to increase cell-surface adhesion, then fixed in 2% paraformaldehyde (methanol-free) (Polyscientific) for 20 minutes, then rinsed thrice in PBS and either stained immediately, or stored in PBS containing 0.05% Sodium Azide at 4°C wrapped in plastic to prevent evaporation. For immunocytochemical (ICC) staining, first, a step to permeabilize cell membrane with 0.1% Triton X-100 in PBS was completed, if appropriate, followed by blocking of non-specific binding using 5% serum diluted in PBS, from the species producing the fluorescent secondary antibody, following which, incubation in cell cycle, myogenic differentiation, or ECM markers diluted in PBS + 0.05% Tween-20 was completed, with all primary antibodies and associated dilutions shown in *Table 1*.

Table 1: Primary Antibodies Used for Immunocyto/histo-chemical Analysis

Primary antibodies used for cell/tissue labeling for all experimentation.

Primary Antibody	Supplier	Cat. #	Dilution	Isotype Specificity
Myosin Heavy Chain	Hybridoma Bank	MF-20	1:250	Human, Mouse
Neural Cell Adhesion Molecule (NCAM)	Hybridoma Bank	5.1H11-s	1:250	Human
Collagen I	SantaCruz	SC-8782	1:400	Human
Collagen IV	abcam	ab-6586	1:500	Human, Mouse
Collagen VI	abcam	ab-6588	1:500	Human, Mouse
Laminin-211	abcam	ab-140482	1:500	Human
Human Nuclear Antigen	Millipore	MAB4383	1:500	Human

Detection of the primary antibodies on 2D cells was performed using isotype-appropriate secondary antibodies labeled with Alexa Fluor® dye and counterstained, as described. Detailed information on the detection antibodies and subsequent fluorescent nuclear counterstains (Hoechst 33342, and 4',6-Diamidino-2-Phenylindole, Dihydrochloride - DAPI) are shown in *Table 2* below.

Table 2: Secondary Antibodies Used for Immunocytochemical Staining Detection

Secondary AlexaFluor antibodies used to bind to primary antibodies for fluorescent detection.

Secondary Antibody	Supplier	Cat. #	Dilution/Concentration	Species Reactivity
Alexa Fluor-488	Invitrogen	A-11055	1:500	Goat
Alexa Fluor-488	Invitrogen	A-21206	1:500	Rabbit
Alexa Fluor-488	Invitrogen	A-11029	1:500	Mouse
Alexa Fluor-568	Invitrogen	A-11036	1:500	Rabbit
Alexa Fluor-568	Invitrogen	A-11057	1:500	Goat
Hoechst	EMD	382065	0.5ug/ml	N/A
DAPI	EMD	268298	0.5ug/ml	N/A

For immunohistochemistry (IHC), tissues were rinsed in PBS and fixed in 2% paraformaldehyde for 2 hrs. Using standard histological procedures, tissues were processed through alcohols, cleared in

xylenes, embedded in paraffin wax, sectioned into 6µm slices, and mounted onto charged microscope slides. Standard protocols were followed for histological staining. For IHC analysis, a hydrogen-peroxidase reaction-based staining protocol was completed to visualize specific proteins on the tissue sections. Briefly, paraffin wax was removed from the tissue sections by 3 incubations in Xylene, followed by hydration in graded alcohols and a wash in diH₂O. Antigen retrieval was conducted in a pressure cooker for 20 minutes in a citrate-based antigen retrieval solution at a 1:100 dilution in diH₂O (Vector Labs, H-3300). Detection of the primary antibodies was achieved by Peroxidase (HRP) substrates (All Vector Labs).

Staining was completed using a highly-sensitive enzymatic (non-biotin) polymerized polymer reporter enzyme staining system using the above antibodies described in *Table 1* at the same concentrations shown, unless otherwise noted. Unless otherwise stated, nuclei were counterstained with Harris Hematoxylin, then dehydrated and permanently mounted prior to imaging on a Zeiss Axiovert inverted microscope. A table of reagent used for IHC antibody labeling and subsequent detection are summarized in *Table 3* below. Unless otherwise noted, all solutions were prepared and used at the recommended dilution and according to all manufactures protocols.

Table 3: Reagents used for IHC Analysis - HRP Peroxidase Staining and Detection

All hydrogen peroxidase reagents used for HRP labeling and subsequent enzymatic detection of primary antibodies.

IHC Reagent	Supplier	Cat. #	Dilution/Concentration
Antigen Retrieval Solution	Vector Labs	H-3300	1:100 in DiH ₂ O
HRP Anti-Rabbit IgG (Peroxidase)	Vector Labs	MP-7401	Per Manufacture Protocol
HRP Anti-Mouse IgG (Peroxidase)	Vector Labs	MP-7402	Per Manufacture Protocol
HRP Anti-Rat IgG (Peroxidase)	Vector Labs	MP-7404	Per Manufacture Protocol
Mouse on Mouse (M.O.M.) IMPRESS Kit	Vector Labs	MP-2400	Per Manufacture Protocol
ImmPACT DAB (Brown)	Vector Labs	SK-4105	Per Manufacture Protocol
ImmPACT VIP (Purple)	Vector Labs	SK-4605	Per Manufacture Protocol
ImmPACT SG (Silver/Grey)	Vector Labs	SK-4705	Per Manufacture Protocol

For histological analysis, tissues were fixed, processed, embedded, sectioned, and mounted on charged coverslips, as previously described for IHC analysis. Standard histological staining protocols were followed, unless otherwise noted for all histological analysis. Histological staining procedures used for all tissue morphological analysis along with tissue hydration processes used for preparation for IHC staining are shown in the Appendix section of this document.

3.2.4 Myoblast Assembly into Contiguous Tissue Rings

To generate 3D ring-shaped tissues, a non-adhesive hydrogel mold was adapted from a collaborator that has been previously used to generate vascular microtissues, *in vitro* [18]. Briefly, a polycarbonate mold generated using CAD software was used to cast a polydimethylsiloxane (PDMS) negative mold. The resulting PDMS negatives were then autoclave sterilized and aseptically used with sterile hot and liquefied 2% agarose in DMEM to cast ring-shaped molds. Molds were allowed to solidify at room temperature in a sterile environment for 30 minutes, and then removed from the reusable

PDMS molds and placed into individual wells of a 6-well plate and flooded with DM and allowed to equilibrate for a minimum of 24 hrs at 37°C prior to use. Each mold yields 5 ring-shaped molds containing annular wells with a measured volume of 55 μ L with a 2mm diameter cylindrical post in the center, and has been used previously to promote cell aggregation into 3D microtissues. A summary of the mold production process and a schematic of the tissue ring formation procedure is shown in Gwyther et al. [18].

To generate 3D ring shaped tissues, cells were trypsinized, harvested, and pelleted, as previously described. Cells were counted and resuspended at a density of [500,000cells/55 μ l] (unless otherwise specified), as described [18]. To prepare the molds for ring seeding, a percentage DM was removed such that the level of media was slightly below the top of the agarose mold (preventing cells from floating out of the ring mold immediately following seeding. Additionally, the annular well was gently aspirated, leaving the well empty and dry. For seeding of tissue rings, 55 μ l of cell suspension was pipetted into each well and gently mixed in a circular fashion to ensure uniform circumferential seeding. Cells/molds were placed back in the 37°C incubator for 24 hrs. to allow for cell aggregation into 3D tissues. Media diffusion occurs through the agarose mold, but because the fluid level does not exceed the mold height, cells remain within the mold wells. Following 24 hrs. the entire media in the well was gently changed and the tissues were gently flooded with DM, covering the molds and tissues. Media was exchanged daily, unless otherwise specified.

Heterogeneous rings consisting of myoblasts and fibroblasts were also made. To generate heterogeneous rings, both cell types were cultured separately and prepared for seeding as previously described. Both myoblasts and fibroblasts were resuspended separately at the same concentration [500,000cells/55 μ l], and then mixed at a defined volume ratio in a separate conical tube, yielding a heterogeneous population of myoblasts/fibroblasts, while maintaining the same cell density [500,000cells/55 μ l].

3.2.4.1 2D Culture Controls for 3D Tissue Ring Experimentation

There is debated opinion on whether data generated using a 2D culture system translates directly to 3D [22, 23]. For some applications, research and finding may be translatable, but for others, there are clear differences between 2D and 3D that inhibit the translation of findings. Completing appropriate 3D culture experiments involving simple variables, such as media supplementation, in 2D simultaneously may simply provide a confirmation of the trends and improvements observed during the 3D culture. As such, data presented from 3D experiments also strive to make comparisons between identically-treated 2D culture comparisons, and trends will be attempted to be correlated between both culture platforms. This correlation may provide insight as to whether or not 2D to 3D correlations should be acceptable when researching skeletal muscle development and regeneration.

For all instances of 2D differentiation, cells were initially seeded in growth medium (containing 10% FBS), to facilitate surface attachment. When cells reached 90% confluency, growth media was aspirated, the cells were thoroughly washed with DPBS free of divalent cations and the media was transitioned to Differentiation Media (formulation described previously). Cells were fed daily with complete media exchanges and cultured for 14 days, to mirror experimentation done in 3D. Following culture, cells were washed, fixed, and prepared for ICC, as previously described.

3.2.5 Mitogen-Reduction Media Induces Myoblast Differentiation

To determine the effect that reducing mitogens available to the cells in culture has on the proliferation and differentiation index of the cells, the following experiment was completed. Briefly, cells were harvested from standard proliferating conditions and seeded at a density of 20,000 cells/well into a 24-well plate. Cells were seeded in MGM and allowed to attach to the surface for 24 hrs. Following the attachment period, cells were washed with DPBS and the culture media was changed to DM. At each 24 hr interval for 4 subsequent days, BrdU labeling reagent (a synthetic nucleoside that incorporates into the DNA of cells during S-phase, thus is a marker of proliferation), was incorporated into the cultures for

a period of 1 cell cycle, at which point, the cells were fixed for ICC analysis. This was completed for each of the 4 time points, including a 5th time point for cells that were maintaining in proliferative MGM. To further allow for correlations to be drawn between 2D and 3D cultures, a similar assay was completed for 3D tissue rings, in which BrdU labeling reagent was incorporated into tissue rings following 3 days in culture. Similarly, tissue rings were fixed 1 cell cycle of time following the BrdU incorporation. This assay demonstrates the proliferative capacity of cells following the transition to mitogen-reduced differentiation medium and allow for comparative differences between cells differentiated in 2D and tissues differentiated in 3D in terms of proliferative capacity following induction of differentiation. A schematic of the experimental setup is shown below in *Figure 3*.

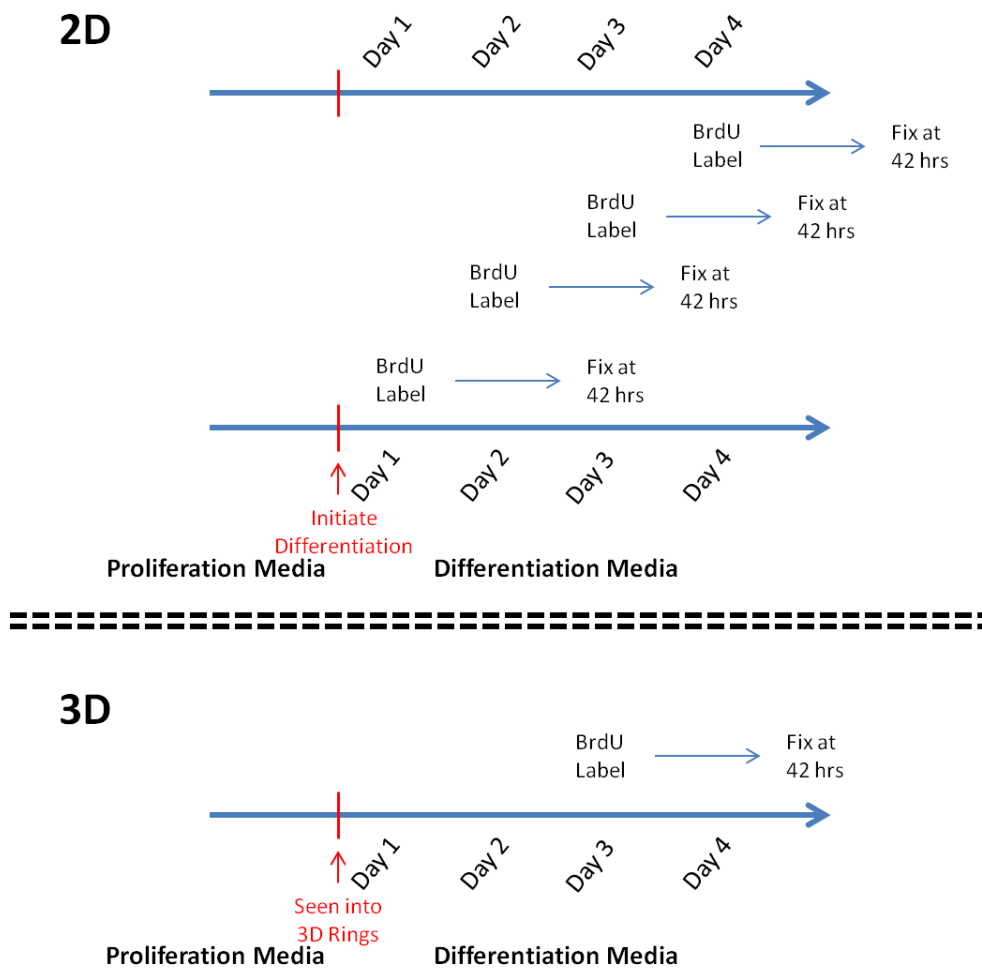


Figure 3: Schematic of BrdU Incorporation for 2D and 3D Assays

For 2D assays, BrdU labeling reagent was incorporated into differentiated myoblasts daily, starting at 1 day following induction of differentiation. For 3D tissues, BrdU labeling reagent was incorporated following 3 days in culture. All cells/tissues were fixed and analyzed 1 cell cycle (42 hrs) following BrdU incorporation.

In addition to completing ICC to identify BrdU (+) cells, the 2D cells were also stained for expression of surface marker NCAM protein (a marker for early-stage differentiation) [24]. Co-staining for both of these antigens on the same cells allowed for the identification of a proliferation/differentiation index for the cells when chemically-instructed to differentiate. Furthermore, the NCAM staining serves as an internal control as NCAM is only upregulated when the cells exit cell cycle, as such, NCAM(+) cells should not be BrdU(+) simultaneously (however, they would have been, if the BrdU labeling reagent was added prior to the induction of differentiation, but this was not done).

3.2.6. Decreasing Cell Number Seeded into 3D Tissue Rings

To minimize observed tissue necrosis that was observed with 3D rings seeded with 500,000 cells, a cell number optimization experiment was completed. To minimize tissue necrosis, the cell number seeded into the 3D rings was decreased to 400,000 and 300,000 total cells/ring, along with also repeating the 500,000 cells/tissue ring condition, while maintaining the same seeding volume of 55 μ l - resulting in 3D rings being formed with fewer cells. This experiment identified the minimal number of cells needed to form tissues at a high formation efficiency, while concurrently minimizing the number of non-function (potentially necrotic) regions of the tissue ring, as measured by identifying malaligned nuclei that did not align with the circumference of the tissue ring. For determination of the effectiveness of the cell number minimization, formation efficiency and percent of malaligned nuclei was measured and quantified for each of the three seeding conditions.

3.2.7. Incorporation of Fibroblasts to Improve ECM Production

Following improvements to overall tissue morphology, and the reduction of malaligned nuclei and potential tissue necrosis, further culture optimization involving fibroblast supplementation can

occur. The majority of current 3D skeletal muscle models involve an ECM protein hydrogel, as previously described, to provide an initial scaffold along with a provisional matrix upon which myoblast differentiation and maturation can occur. By utilizing self-assembly, pitfalls of ECM hydrogel methods, including necrotic tissue core and decreased cellular density are avoided - at the cost of not providing myoblasts with a sufficient ECM for which to initially digest and provide signaling cues for cell-mediated ECM synthesis [8, 25]. As such, incorporating ECM-producing fibroblasts into the culture at the time of 3D ring tissue seeding, to provide the myoblasts with a supplemental cell line that has both been shown to improve 3D culture cell alignment and synthesize endogenous ECM, may provide a better pro-maturation environment [6].

Initially, human dermal fibroblasts (CRL-2352) were cultured in standard monolayer culture in standard growth media, as previously described. Unlike the pre-seeding differentiation done with the myoblasts, the fibroblasts were maintained in a proliferative state up until 3D tissue seeding. At the time of seeding, both myoblasts and fibroblasts were harvested and counted separately and both cell lines were resuspended at a concentration of [400,000 cells/55 μ l] - (the seeding density previously optimized from the tissue thickness and necrosis study described previously with data presented in the results section).

To determine the percentage of fibroblasts that should be incorporated into the 3D tissue rings, a review of literature indicated that while there is a relatively low ratio myoblasts to fibroblasts in native healthy muscle (5-40%), a higher concentration of myoblasts may be needed, as this project aims to emulate the regeneration-phase of skeletal muscle, in which a high percentage of muscle-producing myoblasts is required [19]. During both development and tissue regeneration, the percentage of myoblasts per unit area greatly increases - only once muscle is mature, do the myoblasts migrate to the periphery of a myotube. Following hypertrophy and growth of the myotube, the overall percentage of area that is occupied by nuclei decreases. While the logical purpose of this fibroblast incorporation study

would be to incorporate fibroblasts at percentages that mimic native muscle, the actual purpose was to determine the minimal number of fibroblasts necessary to facilitate an improvement in tissue alignment and endogenous ECM synthesis. As previously described, a salient limitation of other 3D skeletal muscle tissue models involves sub-native levels of maturation, often due to the relative scarcity of differentiation-competent myoblasts/unit area. Such minimization of fibroblasts and maximization of myoblasts provides these tissue rings with the best platform to generate contractile protein.

At defined ratios including 0, 25, 50 and 75% fibroblasts, volumetric mixtures of the two cell suspensions was completed, such that the resulting heterogeneous cell suspensions contain the percentages of fibroblasts, while unchanging the cell density [400,000/55 μ l]. The aim of this experiment was to determine the minimal percentage of fibroblasts necessary to improve overall tissue alignment and increase endogenous fibroblast-mediated ECM synthesis.

3.2.7.1. Tissue Ring Nuclear Alignment Calculation

Following fibroblast incorporation, and subsequent 3D tissue ring culture, analysis of overall nuclear alignment was completed, as described here. Briefly, tissues were cultured to 14 days, fixed, processed, embedded in wax, and sectioned onto charged microscope slides, as previously described. Sections were then labeled with Hoechst nuclear dye, to visualize nuclei, and imaged under an inverted fluorescent microscope. Images were imported into ImageJ®, in which the blue channel was isolated from the image - providing high contrast of the stained nuclei against the tissue ring. The image was then thresholded to binarize the nuclei from the tissue ring - resulting in black punctate nuclei with a white background.

To quantify the alignment of the nuclei relative to the circumference of the tissue ring, a particle analyzer function within ImageJ was used to quantify the absolute direction of the long axis of each nucleus. This direction (between 0-180°), was then compared to the tangent to the ring circumference at the approximate location of the nuclei. To quantify the degree of such alignment between different

tissues and groups, measured nuclear alignment angles were binned in 10° increments. If a nucleus was perfectly aligned with the tangent to the ring circumference, the nuclear alignment angle would be 0°, whereas, if a nuclei was completely perpendicular to the tangent to the ring circumference, the nuclear angle would be returned as 90°. A schematic of the initial binarized nuclear-stained tissue ring with subsequent thresholding and nuclear angle measurement is shown below in *Figure 4*.

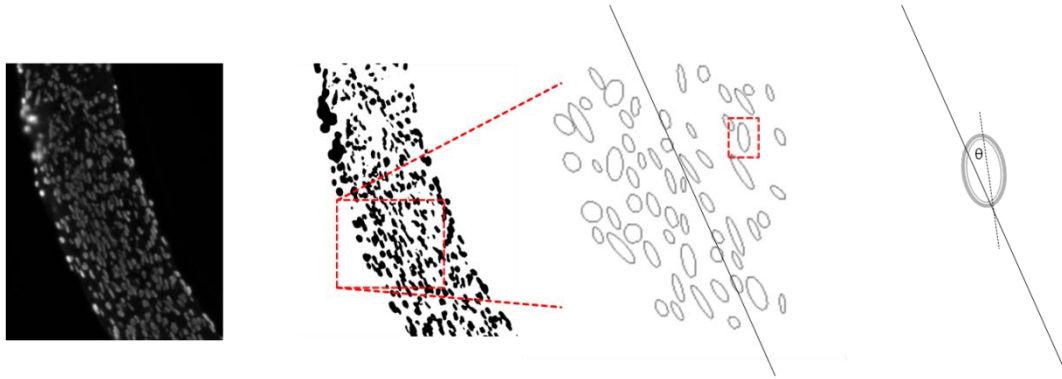


Figure 4: Schematic of Fluorescently-labeled Nuclei and Subsequent Nuclear Angle Calculation
Hoechst labeled tissues were imaged and binarized in ImageJ. Nuclear shape was quantified by determining the long axis of the nucleus and related to the tangent to the circumference of the tissue ring.

3.2.7.2. Myosin Heavy Chain Quantification

To quantify the amount of myosin protein that the tissues are producing, the following procedure and quantification parameters were used. Histological sections of tissue rings at 14 days were prepared, as previously described and stained using IHC for myosin heavy chain, using protocol, antibody, and dilutions, as previously described above and in *Table 1* and *Table 3*. Following hematoxylin counterstain, mounting, and visualization using an HRP staining system and DAB brown detection, tissues were imaged and analyzed as follows. The percentage of myosin-positive nuclei (quantification of cells that were either within or immediately adjacent to myosin protein, hence participating in the differentiation/production of contractile protein), were counted as "myosin positive cells". A ratio of myosin positive to negative nuclei was calculated for the tissue sections and compared across the

groups to determine if a higher percentage of nuclei were participating in the tissue differentiation/maturation during culture.

Similarly, a quantification of multi-nucleated myotubes, a marker of more downstream differentiation, was completed as follows. Any observed myotube that contained 3 or more nuclei was counted as a multinucleated myotube. Myotubes that contained either 1 or 2 nuclei were not counted. Thus, this parameter provided a simultaneous measure of tissue maturity, as compared to the number of nuclei adjacent to a myosin protein, which can be influenced by a variety of external factors, and may not be a true indication of differentiation potential.

3.2.8. Statistics

For all experimentation, sample sizes of tissue rings consisted of at least 12 rings per group. Fibroblast-incorporation validation studies had an n=6 for all groups. Nuclear alignment data consisted of n=4 tissue rings per group. All experimentation was completed at least in duplicate and the two groups were averaged prior to statistical analysis. All immunocytochemistry was completed in triplicate to ensure that presented data is accurate. All data is presented as mean \pm Standard Error of Measurement (SEM). For analysis of ring formation efficiency, and parameters involved in characterizing tissue morphology and protein production, a Student's t-test was used to determine significance between individual test groups, (at a critical p-value <0.05). To determine variation between groups of proliferation and differentiation index, as appropriate, a one-way ANOVA was used, with a Holm-Sidak post-hoc analysis, (at a critical p-value <0.05).

3.3 Results

3.3.1. A Defined Culture System Prolongs Myogenic Potential, *In Vitro*

Primary skeletal muscle myoblasts were cultured using methodology described previously. Culture in MGM resulted in a heterogeneous population of both substrate-adherent cells and non-adherent cells. Viability of the non-adherent population was confirmed by selectively sub-culturing only the non-adherent population into a fresh tissue culture vessel containing MGM, where a new heterogeneous population of adherent and non-adherent cells developed. Such selective sub-culturing can be repeated until cells reach senescence, indicating that the non-adherent population contains a continually viable and myogenic cell population. Shown in *Figure 5* below, hSkM-1201 cells in culture in MGM showing both viable adherent and non-adherent myoblasts, (bar = 50 μ m).

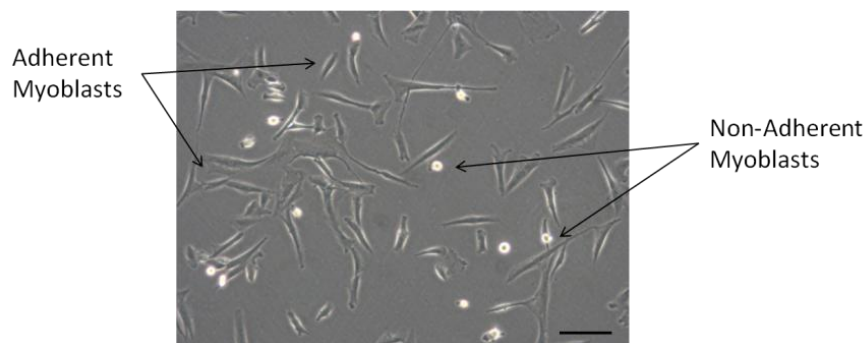


Figure 5: 2D Proliferative Culture of Primary Myoblasts

Adherent myoblasts are observed with characteristic spread morphology, whereas non-adherent myoblasts are observed with characteristic suspension culture morphology, bar = 50 μ m.

We observed that the selective propagation of only the non-adherent population maintains the myogenic potential of the skeletal muscle myoblasts longer than if only the adherent population was sub-cultured forward. Myosin protein using ICC staining methodology previously describes indicates that the differentiation potential of these myoblasts does not decrease when comparing early to late (passage 8 versus passage 17 - one passage prior to observed cell senescence). Shown in *Figure 6* below, 14 day differentiated myoblasts from passage 8 (left) and passage 17 (right) stained for myosin heavy

chain (red) and nuclei (blue) indicated that selective sub-culturing of the non-adherent population retained the myogenic potential for extended culture (bar = 50µm).

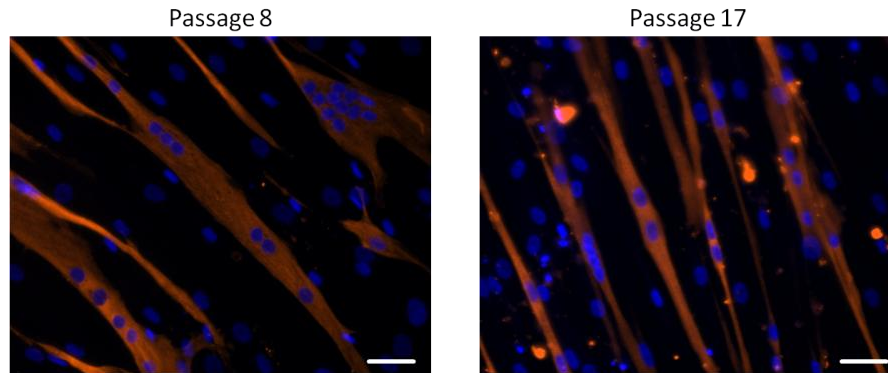


Figure 6: Differentiation of Passage 8 versus Passage 17 Primary Myoblasts
14 day differentiation of passage 8 myoblasts (left) vs. passage 17 myoblasts (right) demonstrating that myosin protein production (red) is not decreased with the extension of the culture lifespan via selective sub-culturing.

To maintain the myogenic potential during cell expansion, *in vitro* for subsequent experimentation, both the adherent and non-adherent populations were retained during sub-culturing, by first collecting the non-adherent cells (vs. aspirating away spent media), then trypsinizing and collecting the adherent cells. As shown in *Figure 7* below, non-adherent cells are collected and sub-cultured for expansion while adherent cells are trypsinized and used for experimentation. Due to the intrinsic maintenance of the myogenic population by selective forward propagation of the non-adherent cells, coupled with the cell number-limiting relationship with only using the non-adherent cells for 3D tissue ring seeding, protocols defined in *Figure 7* were used for all experimentation.

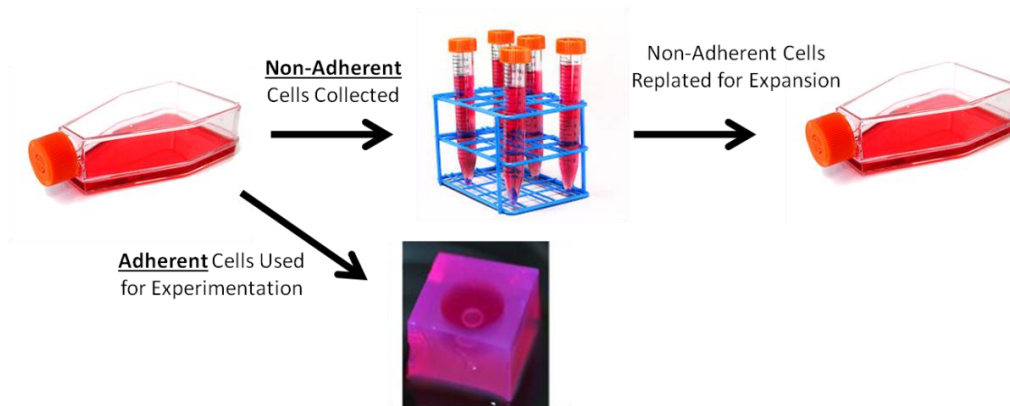


Figure 7: Schematic of Primary Myoblast Culture and Expansion Process

Myoblast expansion completed by selectively propagating the non-adherent cells forward to maintain the myogenic potential, while adherent cells are used for 3D tissue experimentation.

3.3.2. Cell Culture and Preparation for Tissue Ring Seeding

To ensure that a consistent population of cells were used for all experiments within these studies, cells were expanded from low passage stocks and used for experimentation between population doublings 15-28 (Passages 5-10). Cells that exceeded this doubling value were not used for any experimentation and were either discarded or frozen and preserved. This was done in order to prevent faster-proliferating fibroblasts from overtaking the myoblast culture, resulting in a culture that is incapable of myogenic differentiation.

During our culturing of the adherent population of hSkM cells, the calculated population doubling time was 42 hrs. The doubling time of the non-adherent cells was not calculated, as such a value was not relevant to subsequent 3D tissue construct culture. Subsequent experimentation involving mitogen-reduction-induced differentiation, cell cycle doubling time was considered to be 42 hrs.

3.3.3. Myoblasts Fail to Assemble into Contiguous 3D Tissue Rings

Initial experimentation involved mimicking previous work by harvesting myoblasts and seeding them into 3D ring tissues while maintaining them in their proliferative state. Previous published work by Gwyther et al. [18] demonstrated that rat-derived smooth muscle cells could be aggregated into 3D ring-shaped tissues while being maintained in high-serum growth medium [18]. However, initial experimentation to replicate such culture conditions with myoblasts failed to generate 3D tissues on a consistent basis, only forming contiguous tissues at a rate of 11% +/- 15% (n>6 groups >12 tissues/group). As such, investigation into pre-seeding differentiation was completed first in 2D culture to determine the effects initiating differentiation have on the culture characteristics, and second in 3D culture to determine the role that pre-differentiation has on ring formation efficiency.

3.3.4. Mitogen-reduction Induces Myoblast Terminal Differentiation

Following differentiation, BrdU incorporation and subsequent NCAM and BrdU ICC staining, clear differences were observed and can be seen in *Figure 8* below where cultures are incorporated with BrdU (top) and NCAM (bottom) starting with cultures in MGM (left) and assayed for daily time points of differentiation (days 1-4, from left to right).

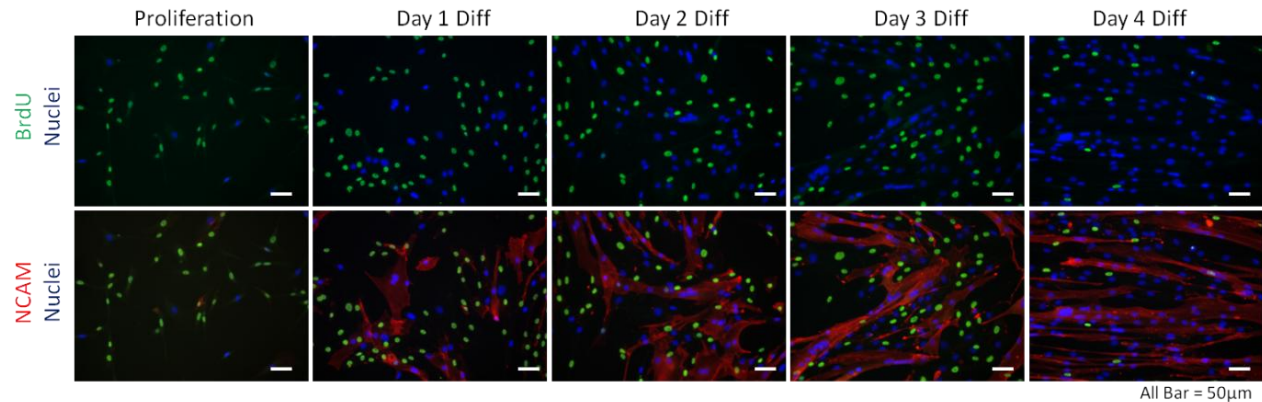


Figure 8: The Effect of Mitogen-reduced Media and Timing on Cell Cycle Analysis

2D Myoblast cultures incorporated with BrdU labeling reagent starting under proliferative conditions (far left) and following day 1-4 of differentiation (left to right). Top row stained for BrdU (green) indicating cells in S-phase of cell cycle whereas co-labeling of NCAM - a marker of early-stage myogenic differentiation, labeled differentiating cells. A decrease in proliferation and increase in differentiation is seen following extended culture in differentiation media.

Briefly, under standard proliferative conditions, 72% +/- 4% (standard error of the mean, SEM) of the cells were proliferating. Following a single day in DM, the subsequent percentage of proliferation cells decreased to 40% +/- 5% (SEM), and each subsequent day of differentiation (Days 2-4) decreased the proliferation percentage to 32% +/- 6%, 21% +/- 3%, and 9% +/- 2%, respectively. Furthermore, NCAM staining (a marker for early-stage myogenic differentiation), presented an inverse relationship with respect to differentiation timing, with proliferating cells exhibiting low levels of NCAM 8% +/- 7%, with subsequent days in differentiation (Days 1-4) showing increase in NCAM expression of 17% +/- 5%, 56% +/- 4%, 78% +/- 4% and 94% +/- 4%, respectively. A graphical display of the quantification is shown in *Figure 9* where statistical decreases in proliferation are observed between day 0 and day 1 of differentiation, and statistical increases in NCAM expression are seen between day 1 and day 2 of

differentiation (one-way ANOVA to conditions in same group, with Holm-Sidak post-hoc analysis $p < 0.05$).

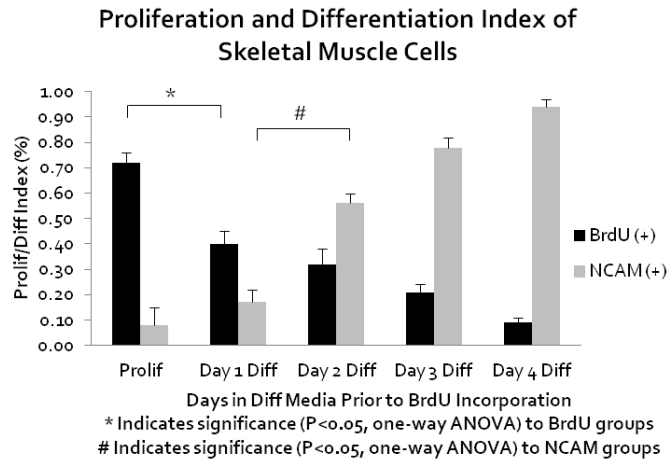


Figure 9: Quantification of the Effect Mitogen-reduced medium has on Myoblast Proliferation and Differentiation
The proliferation index of the myoblasts statistically decreases following transition to differentiation media, whereas NCAM expression statistically increases between days 1 and 2 of differentiation.

Translating this experiment to 3D was difficult, as there is no way to pre-differentiate cells in 3D, without actually forming a 3D tissue. However, 3D tissue rings that were comprised of cells pre-differentiated for 2 days, were fixed following 3 days in culture (and incorporation of the BrdU reagent 1 cell cycle prior to fixation in 3D), prepared for histological/IHC analysis, as previously described, and stained for proliferative marker BrdU. The 3 day 3D cultures contained very few BrdU-positive cells at day 3 in culture (3.9% +/- 1.2%, $n > 6$), indicating that the cells continue to differentiate and exit cell cycle, (as the percentage of BrdU-positive cells has decreased from the percentage of proliferating cells at the time of cell seeding (Day 3 differentiation BrdU - 32%, previously shown), as shown and quantified in *Figure 10*. Furthermore, comparing the effect of 3 days of mitogen-reduced differentiation between 2D cells and 3D tissue culture, *Figure 10* indicates that there is a statistically-significant reduction in BrdU-positive cells between 2D and 3D culture, confirming that cells do not continue to proliferate at the same rate in 3D, or return to a proliferative state in 3D, as compared to 2D cultures, following transition from a 2D to 3D culture platform. Finally, this confirms that the tissues are of a size that allows for

sufficient diffusion of nutrients such that external signaling, namely the change to the mitogen-reduced culture medium, has an effect of the entire tissue, not just cells on the periphery of the tissue.

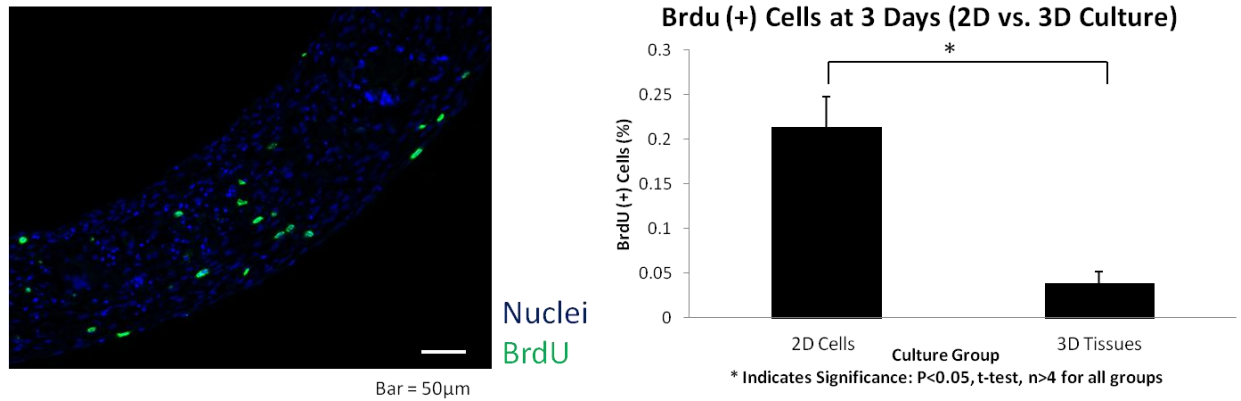


Figure 10: Proliferating Cells following 3 Days of 3D Culture

Day 3 tissue ring with BrdU-positive cells (green) labeled, counterstained with all nuclei (blue) (left). Quantification of the 3 day BrdU-positive cells comparing 2D vs. 3D differentiation (right) indicates that 3D cultures statistically reduce cell proliferation.

3.3.5. Differentiation Prior to Ring Seeding Improves Ring Formation Efficiency

In addition to showing that the mitogen-reduced differentiation medium directs the cells to exit replicative cell cycle and enter a terminal differentiation pathway, as shown by the increased NCAM protein expression, the induction of differentiation also played a role in the success rate of tissue formation. As show in *Figure 11*, cells that were taken directly from MGM and seeded into rings only formed at a 10.8% +/- 15% efficiency, whereas, following subsequent days in differentiation media of 1, 2, 3, and 4 days preceding cell harvesting and ring tissue formation, the formation efficiency changed to 45.2% +/- 0.134, 93.7% +/- 0.045, 87.4% +/- 0.076, and 69.3% +/- 0.092, respectively. As such, the highest ring formation efficiency, exceeding 93% efficiency, resulted from a 2 day pre-3D ring seeding differentiation of the cells.

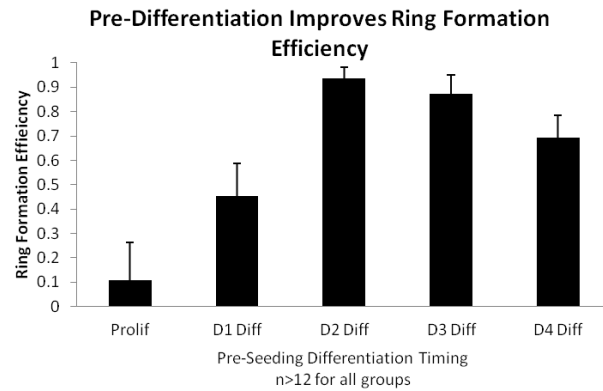


Figure 11: The Effect of Pre-differentiation on Ring Formation Efficiency

Pre-differentiation of the myoblasts prior to 3D tissue seeding improves ring formation efficiency, Optimal formation efficiency occurs following 2 days of differentiation. Criteria for successful ring formation involved observing a contiguous tissue ring at 48 hrs. post-seeding.

3.3.5.1. Skeletal Muscle Myoblasts Self-Assemble into Contiguous Tissue Rings

Following the pre-seeding differentiation, the formation efficiency of 3D skeletal muscle tissue rings significantly improved. Following seeding into annular wells, cells self-assembled into contiguous 3D tissues. Following 7 days in culture, tissues were fixed, processed, sectioned, and stained for H&E. The morphological image of the 3D tissues show that the majority of the cells are participating in tissue compaction, as cells can be observed aligning circumferentially around the tissue ring, as shown in *Figure 12*.

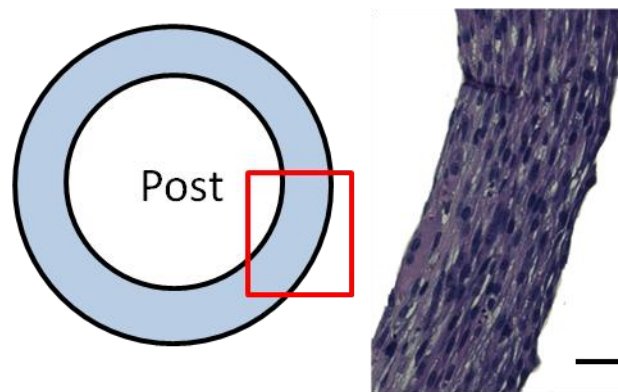


Figure 12: Contiguous Tissue Ring Formed Around Central Post Following 7 Days Culture

Contiguous tissue is observed with contractile nuclei aligning circumferentially around the central post. Bar = 50µm.

3.3.6. Minimizing Cell Number Decreased Tissue Ring Necrosis

Forming 3D skeletal muscle tissue rings comprised of fewer than 500,000 cells was possible. As shown in *Figure 13*, H&E images of 500,000 and 400,000-cell tissue rings can be formed and cultured without protocol change, as previously described.

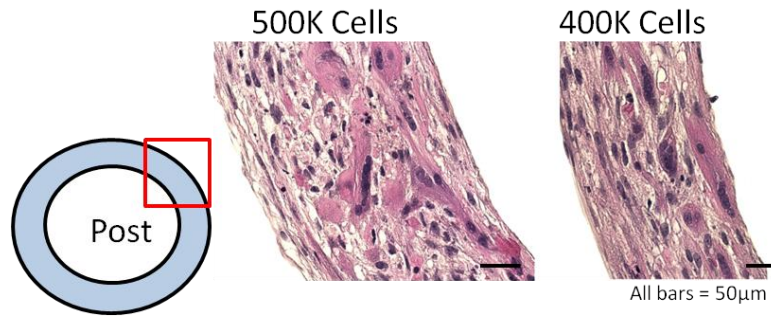


Figure 13: Tissue Rings Formed with Varying Cell Numbers

Tissues formed with 500,000 cells have visible necrosis and malaligned nuclei towards the center of the tissue, whereas a reduction in cell number to 400,000 cells decreases necrosis and increases circumferentially-aligned nuclei. Necrosis was defined as nuclei that are not participating in circumferential alignment.

There is a clear decrease in tissue ring thickness observed with the tissues that contain fewer cells. Following multiple iterations of ring formation using fewer cells, quantification of ring formation efficiency was calculated and displayed in below in *Figure 14*. Briefly, the ring formation efficiency for rings seeded with 500,000 cells was 92.1% +/- 3.7% and only decreased to 83.4% +/- 7.0% when the seeding density was decreased by 20% to 400,000 cells. However, when the seeding density is decreased to 300,000 cells, the formation efficiency statistically decreases to 29.1% +/- 4.7% (Student's t-test, n>12).

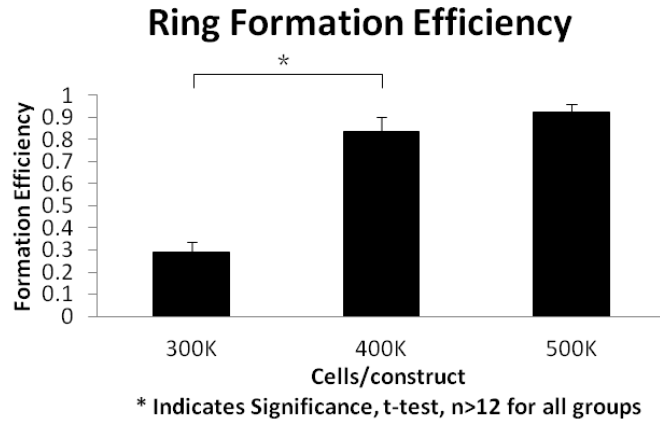


Figure 14: Ring Formation Efficiency with Varying Cell Seeding Numbers

The efficiency of the tissue ring formation does not statistically decrease following reduction of cell seeding number to 400,000 cells, but a further reduction to 300,000 cells statistically decreased formation efficiency.

Furthermore, quantification of the percentage of malaligned nuclei was conducted. There was a decrease in the malaligned nuclei (greater than 45° away from circumferential tangent) as the cell number was decreased, as shown in *Figure 15*. Briefly, the percent of diameter containing malaligned nuclei statistically decreased from 37% in 500,000 cell tissue rings to 14% in 400,000 tissue rings ($p < 0.05$, $n > 12$, Student's t-test), indicating that a higher percentage of the overall cells are both receiving nutrients and participating in the compaction and alignment of cells in the tissue ring when the overall cell number was decreased to 400,000 cells.

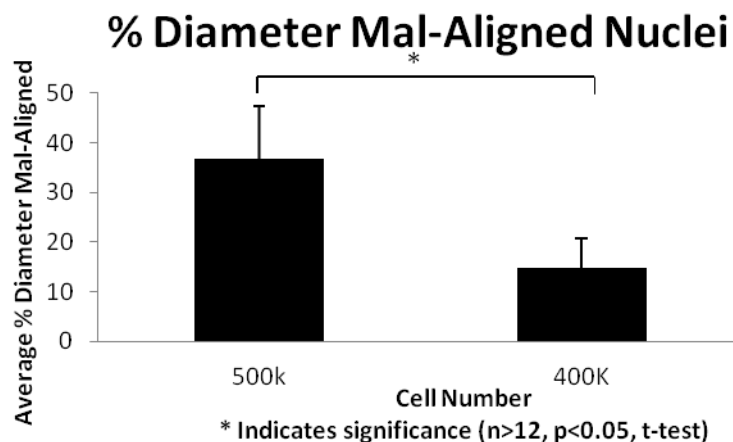


Figure 15: Percentage of Diameter of Malaligned Nuclei with Decreasing Cell Number

The percentage of the diameter of the nuclei not aligned with the circumference of the ring decreases following the reduction of cell seeding number to 400,000 cells. * indicates statistical significance ($p < 0.05$, Student's t-test, $n > 12$).

The 300,000 cell rings had the highest percentage of functional and healthy cells, (as defined previously, based on nuclear alignment being lower than 45° away from circumferential tangent) as evident by both morphological analysis and the lowest percentage of malaligned nuclei. However, the formation efficiency of the 300,000 cell tissues was much lower when compared to the 400,000 cell tissues (29% versus 83%), likely due to the inability of such a low cell number within an unchanging well geometry placing a limit on necessary cell-cell contacts needed for contiguous tissue formation. As such, rings with a higher percentage of healthy cells but still form with a high rate of efficiency, the 400,000 cell tissue rings, generate a better analogue of functional unit of skeletal muscle tissue.

3.3.7. Fibroblasts Improve Tissue Compaction and Nuclear Alignment

As discussed previously, the incorporation of fibroblasts into these myoblast 3D constructs at the time of 3D tissue seeding may have a dual-benefit. Firstly, fibroblasts have been previously shown to aid in the generation of highly-aligned tissues due to their contractility, both in 2D and in 3D [6, 7]. Secondly, fibroblasts readily synthesize ECM protein, and participate in the generation of ECM during native skeletal muscle development and repair processes [7, 26]. The incorporation of fibroblasts may increase the alignment of the overall 3D ring tissue while simultaneously providing a means for which ECM protein can be synthesized endogenously during 3D tissue culture.

Initial investigations into fibroblast incorporation involved culturing myoblasts and fibroblasts separately, as previously described, and then combining them into a heterogeneous mixture at defined ratios at the time of 3D ring tissue seeding. Initially, a murine immortalized myoblast line, C2C12, was used as model myoblast cells while human dermal fibroblasts (CRL-2097) were cultured as previously described, and following harvesting, were mixed with the myoblasts at specific ratios, yielding tissue rings that contain either 0%, 25%, 50%, or 75% fibroblasts, all while maintaining a total cell number of 500,000 cells. Tissue rings were cultured for 7 days and then analyzed morphologically with an H&E stain.

Initial validation of the fibroblast incorporation was completed using immunohistochemical analysis of the C2C12:CRL-2097 tissue rings with staining for human nuclear antigen and detection using HRP substrates, coupled with a Harris Hematoxylin nuclear counterstain, as previously described, was completed to allow for species-specific identification of the human fibroblasts from the murine myoblasts within the same tissue ring. Human nuclear staining allowed for the visualization and quantification of the percentage of human nuclei within each tissue with detection of human nuclei identified using IHC with hydrogen peroxidase DAB (brown) detection, as described previously, with all other nuclei counterstained with hematoxylin (blue), as shown in *Figure 16*.

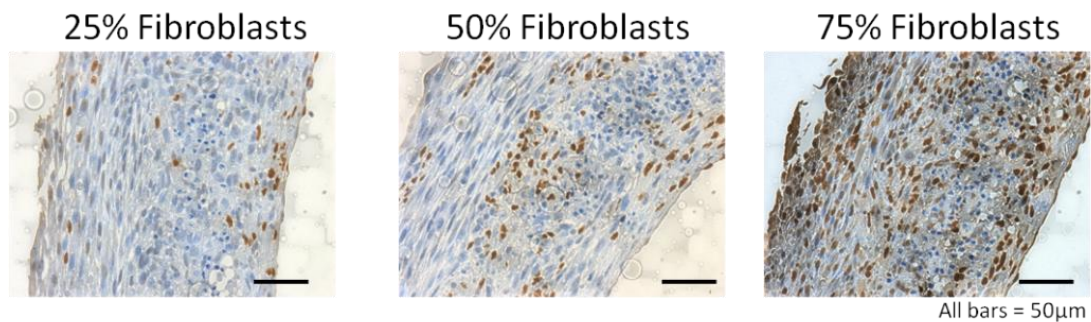


Figure 16: Fibroblast Incorporation Into Myoblast Rings
Hematoxylin and Eosin sections of tissue rings with varying percentages of fibroblasts. Selectively labeled fibroblasts (brown - DAB) compared to non-fibroblast nuclei (blue) indicate that fibroblasts seeded, persist in culture following 7 days.

Additional quantification of the percentage fibroblasts was completed at 7 days by quantifying the ratio of brown-stained human nuclei (fibroblasts) compared to the total number of nuclei (brown + blue nuclei). This ratio indicated whether the fibroblasts persist and remain in the 3D tissue rings following 3D culture or if a certain cell type was selectively lost from the 3D tissue following long-term culture. Shown below in *Figure 17* is quantification of the fibroblast ratio, red hash lines indicate the original percentage seeded into the tissue rings and indicates that for 25 and 50% fibroblasts, the resulting fibroblast percentage is close to the seeded percentage (28.0 +/- 6.3% and 51.3% +/- 10.1%, respectively). For the 75% fibroblasts, a slight decrease in fibroblast percentage is observed, although,

future work will show that the 75% fibroblast to myoblast ratio tissue constructs were not used for any analysis, therefore, this discrepancy is not relevant to this project.

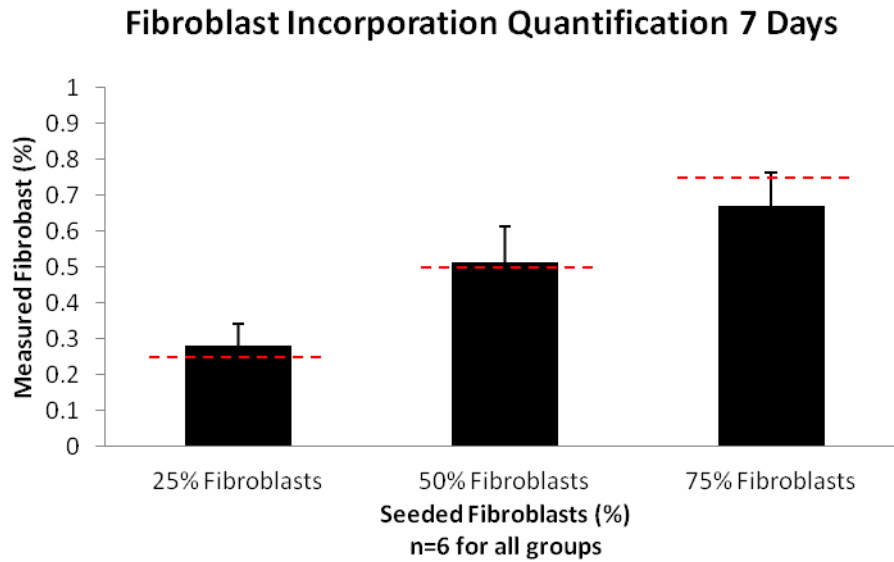


Figure 17: Fibroblast Incorporation Quantification of 7 Day Tissue Rings
Quantification of the percentage of fibroblasts that remain in the tissue ring following 7 days in culture. Red dash lines indicate the original percentage of fibroblasts seeded into the tissue rings. n=6 for all groups.

Qualitative analysis of tissue ring thickness confirmed that the presence of only 25% fibroblasts decreased the thickness of the rings, without changing the overall number of cells that were seeded, with such observation likely attributed to the contractile nature of the fibroblasts and their ability to compact a 3D tissue to a higher degree than myoblasts alone.

Following the addition of fibroblasts, both a decrease in ring thickness and decrease in tissue necrosis was observed. Unlike the entirely myoblast tissues, tissues containing minimally 25% fibroblasts have a lower percentage of nuclei that are maligned with the circumference of the ring. Nuclear alignment was quantified, as previously described, and following the addition of only 25% fibroblasts a statistical increase in percentage nuclei aligned within 0-30 degrees of circumferential tangent was observed, as shown in *Figure 18* below ($p < 0.05$, t-test, $n > 4$ for all groups). No statistical change in percent nuclei aligned between 30-90 degrees was determined, indicating that there are a small

percentage of the overall cells within the tissue constructs that are not actively participating in the contractile alignment.

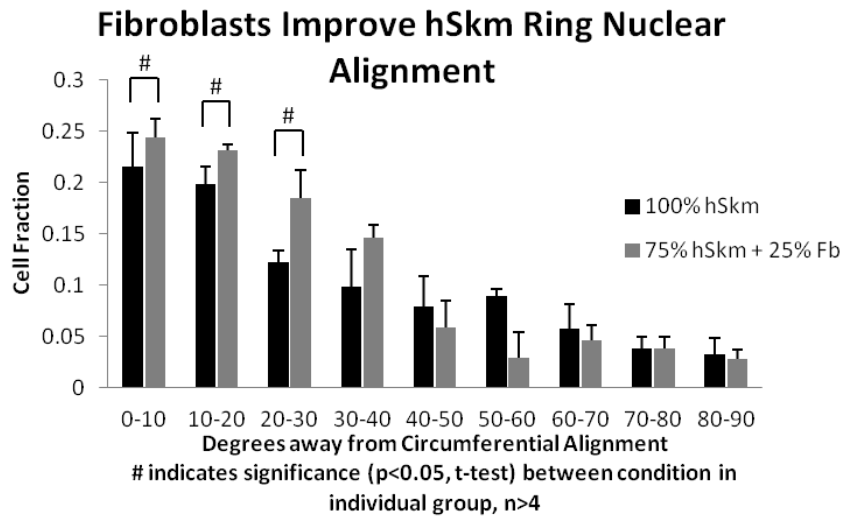


Figure 18: Ring Nuclear Alignment Following 25% Fibroblast Addition

Quantitatively, nuclear alignment for entirely myoblast tissue rings - black and myoblast:fibroblast rings - grey. The addition of fibroblasts increases the nuclear alignment for groups between 10-40°, # indicates statistical significance, ($p < 0.05$, $n = 4$, Student's t-test) comparing ring composition treatments within each angle group.

Finally, to determine if the presence of 25% fibroblasts has an effect on maturation of the 3D tissues following 14 days in culture, tissues cultured with and without 25% fibroblasts were fixed, prepared for histological/IHC analysis, as previously described, and stained for myosin heavy chain. These data indicated that there was no decrease in the percent of myosin-positive cells, despite the overall reduction of myoblasts within the construct, due to the fibroblast cell addition, as shown below in *Figure 19*. In fact, the percentage of myosin-positive cells (defined as total cells/tissue ring within or adjacent to contractile myosin protein production) statistically-increases in the constructs supplemented with fibroblasts ($p < 0.05$, t-test, $n = 4$ for all groups). This may indicate that the presence of the fibroblasts within the 3D tissue construct had an instructional benefit to mediate or facilitate improved differentiation of myoblasts to produce contractile protein - such observation has been observed previously in a different skeletal muscle tissue platform [6, 19].

Percent Myosin (+) cells

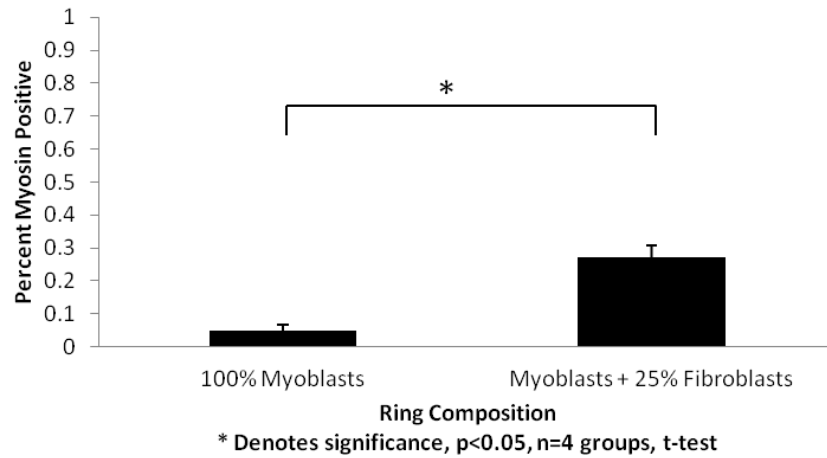
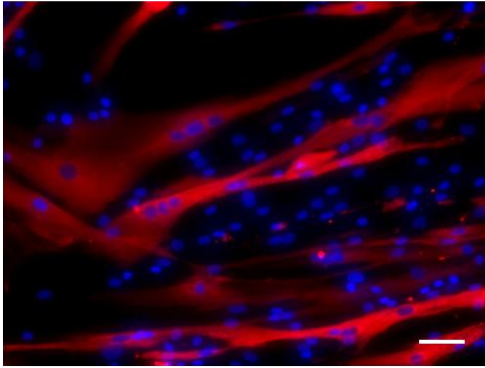


Figure 19: Fibroblast Supplementation Increase Myosin in 3D

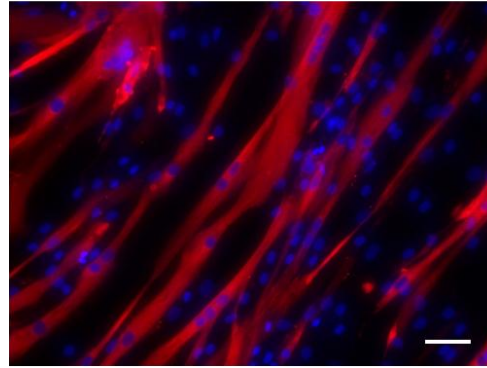
The addition of 25% fibroblasts to 3D tissue rings statistically improved the percentage of myosin-positive cells following 14 days of culture, * indicates significance, $p < 0.05$, Student's t-test, $n = 4$ groups.

Furthermore, corresponding 2D differentiation controls consisting of either 100% myoblasts or the 75:25 myoblast:fibroblast heterogeneous blend from the same culture of cells (to maximize correlation), were prepared for 2D differentiation, as described above, and cultured concurrently in 2D differentiation conditions for 14 days. Immunofluorescent images shown below in *Figure 20* indicate that there is no loss in overall myogenic differentiation when 2D myoblast cultures are supplemented with fibroblasts prior to differentiation. In fact, despite the 33% reduction in cells capable of differentiating and synthesizing myosin protein, there is no qualitative change in myogenic differentiation, indicating that the fibroblasts do not have an inhibitory effect on myoblast differentiation, and in fact, may mediate an increase in differentiation (qualitative postulation only).

100% Myoblasts



Myoblasts + 25% Fibroblast



All Bar = 50 μ m

Figure 20: 14 Day 2D Differentiation of Myoblasts and Fibroblast-Supplemented Myoblast Cultures
14 day differentiation of pure myoblast cultures (left), compared to co-cultures containing 25% fibroblasts indicate that the myosin production (red) is not reduced despite the reduction in myogenic-competent cells.

3.4 Discussion

3.4.1. Growth Factors Coupled with Selective Sub-Culturing Maintain Myogenic Potential

Our culture method permits roughly 17 passages of expansion while maintaining a high myogenic potential. We are the first to report on the identification of a non-adherent sub-population of skeletal muscle myoblasts following induction into our mitogen-rich medium (defined previously). Furthermore, we are the first to show that by selectively sub-culturing only the non-adherent population forward, not only are the cells viable, but a new multiple population of cells (adherent and non-adherent) arise, allowing for continued exponential expansion up until 1 passage prior to cell senescence, allowing us to practically enrich the myogenic lifespan of the primary culture substantially.

Furthermore, we have demonstrated the power that our mitogen-rich growth medium has on maintaining and generating a myogenic population of cells and that terminally differentiated cells can be re-activated into myogenic cells. Briefly, expanded skeletal muscle myoblasts in our previously defined growth medium were terminally differentiated (as described previously), for 14 days (with complete differentiation confirmed using ICC staining). Following 14 days of differentiation, the cells were transitioned back into the mitogen-rich growth medium, where a select population of non-adherent cells arose. Such population of cells were then expanded and implanted into an animal model muscle injury. Subsequent myofiber was promoted by the reactivated human skeletal muscle cells, and confirmed with IHC staining following an additional 14 days, as shown in Figure 21.

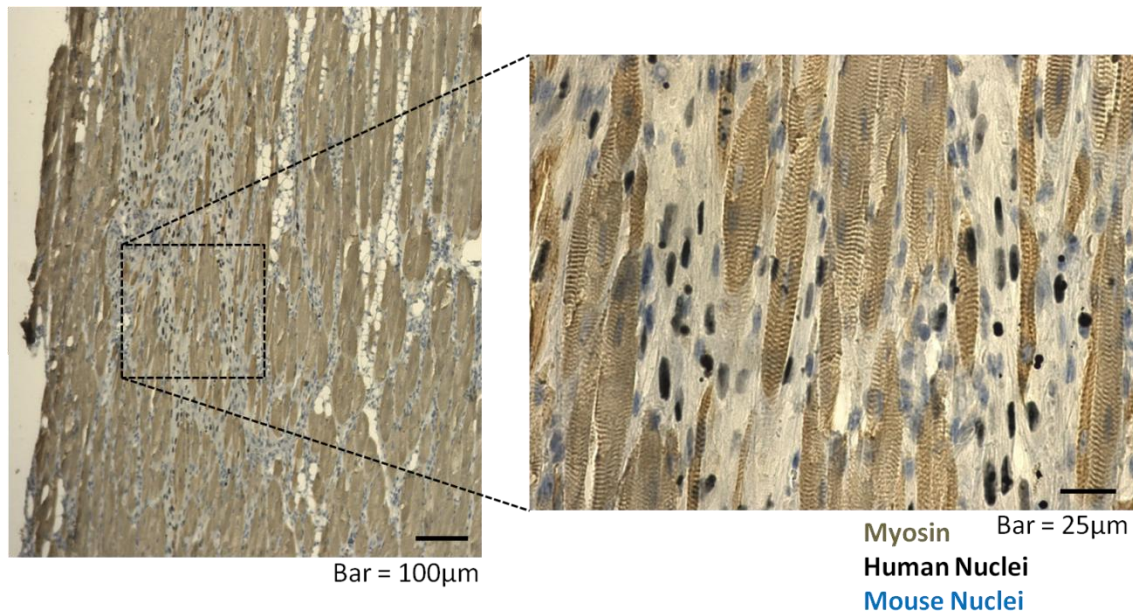


Figure 21: Human Myoblast Cells Implanted into Mouse Following Muscle Injury

Implanted human myoblasts (stained dark grey) are actively participating in regeneration of a muscular injury in the Tibialis Anterior of a SHO Mouse. Prior to implantation, myoblasts were terminally differentiated for 14 days and then reactivated with our defined growth factor-rich proliferative medium. Implanted human nuclei were visualized (dark grey), with myosin protein stained in brown and native murine nuclei counterstained in blue.

A challenge associated with the isolation, and subsequent *in vitro* expansion of primary adult skeletal muscle myoblasts involves maintaining a stem-like population of highly myogenic cells for an extended time period. *In vivo* maintenance of both activation, proliferation, and self-renewal is not yet fully understood, but interplay between notch receptors, nitric oxide, and a variety of growth factors (HGF, IGF-1, and FGF-2), play a varying role in satellite cell function, *in vivo* [27, 28]. Furthermore, such factors are transient and varying based on the location and function of the muscle, *in vivo*, further complicating the succinct understanding of satellite cell culture and control, *ex vivo* [29]. So far, sufficiently understanding the critical signaling interplay involving the generation and propagation of human satellite cells *ex vivo* has yet to be completed, as replication of the complex *in vivo* environment and subsequent crosstalk, coupled with a succinct antibody for detection of human satellite cells, does not exist [27]. This niche, as described previously, functions as a homeostatic environment for the maintenance and self-renewal of satellite cells, *in vivo*[28]. To date, properly replicating such

environment *ex vivo*, has yet to be completed, yielding researchers to attempt to emulate the environment and signaling cues as best as they can, to replicate the environment [28, 30].

Unfortunately, removal of the satellite cells from their innate niche via isolation leads to terminal and irreversible differentiation of the progenitor cell population within a few passages. As such, the current state of human satellite cell isolation and culture results in the rapid loss of myogenic potential *in vitro* [30, 31]. Recent work demonstrated that mouse satellite cells can be expanded for 6 passages while maintaining myogenic capacity on laminin-521 coated surfaces (a salient native skeletal muscle ECM protein), but only tested freshly-isolated human myoblasts for differentiation potential - indicating that the researchers could not expand the human myoblasts in culture [32]. Similar recent work demonstrated that human satellite cells initially expand at an exponential rate for 4 passages, and then enter a terminally-slowing linear growth phase, reducing the myogenic potential, as confirmed by ICC staining coupled with gene expression quantification of decreases in stem-like factors [33]. Such data clearly shows that a lack of a succinct culture platform (either by niche or culture modulations) does not exist to propagate human satellite cells *ex vivo* for extended culture, thus making it difficult for scale-up for large scale diagnostic testing. All current work to date has utilized adherent skeletal muscle myoblasts (regardless of culture method or substrate coating), and have globally observed a consistent loss in myogenic potential prior to 5 passages, *in vitro* [30, 31]. This limitation in maintaining the myogenic potential of human myoblasts, *in vitro*, highlights the need for a culture platform that permits extended use of myogenically-competent cells on the benchtop.

In summary, this culture system can provide researchers with a more clinically-relevant system capable of exponential scale-up of primary human skeletal muscle progenitor cells, *in vitro*. We have been able to expand a primary isolation of human skeletal muscle cells and selectively propagate a more progenitor like sub-population of cells such that the myogenic potential of the culture is maintained up until one passage prior to senescence. Such defined culture conditions have the potential to provide

researchers with a more clinically-relevant platform for the development of a mimetic model of skeletal muscle, and potentially defining the methodology for a patient-specific disease model of skeletal muscle.

3.4.2. Myoblasts Fail to Self Assemble in 3D Culture

During initial tissue formation experiments, tissue rings seeded with entirely myoblast constructs consistently failed to form contiguous tissue rings. This contradicts previous research that utilizes the same mold system to create 3D vascular tissue, in which cells were harvested and seeded into tissue rings directly from a high-mitogen proliferation media [18]. However, in the case of these myoblasts, we hypothesized that the high concentration of mitogens and growth factors present in the growth medium inhibited the myoblasts from making initial and crucial cell-cell contacts - a necessary function of initial myoblast differentiation. As such, despite literature indicating that the transition from 2D to 3D culture initiates myogenic differentiation and furthermore, results in increased mRNA levels of actin and myosin protein [34], in our culture system such process competes with the residual highly mitogen-rich growth factors present in the proliferation media, potentially delaying the onset of 3D differentiation cues and signaling [35]. To date, self assembly of skeletal muscle tissues still involve the aid of an exogenous ECM gel to mediate 3D tissue formation, perhaps imparting crucial environmental cues onto the myoblasts to exit replicative cell cycle [6].

3.4.3. Mitogen-reduction Induces 2D Terminal Differentiation

Initial BrdU staining of proliferating cells indicate that less than 100% of the cells are BrdU(+), indicating that a small proportion of the cells are not actively proliferating. However, it is unclear whether or not the cells are in a quiescent state or have exited cell cycle spontaneously, possibly indicating senescence. We postulated that the cells are not senescent, as the culture was maintained without decrement of doubling time for 10 additional passages. The role of having a small portion of

non-BrdU (+) cells in the cultures used to form 3D tissue rings was not investigated, however, no observed pitfall associated with this cell type was noted.

Similarly, following 4 days of differentiation, subsequent BrdU incorporation demonstrated that there were still some proliferating cells. This was attributed to the presence of the growth factors in the mitogen-rich growth medium maintaining a small percentage of the cells in a proliferative state, despite the reduction in mitogens. Furthermore, in primary cell cultures, there are likely a small population of cells (e.g. true progenitor cells) that cannot differentiate, and as such remain BrdU (+) due to the mitogen-rich culture medium. However, when translated to 3D cultures, similar-timing was employed in which 3D cultures were fixed following 4 days of differentiation, and subsequent BrdU staining and incorporation revealed that a fewer percentage of cells were actively proliferating. This coincides with past research that has shown that the transition from 2D monolayer culture to 3D culture along promotes cell exit from replicative cell cycle and the initiation of terminal differentiation [34, 35].

Perhaps the most crucial observation of this experiment involves the data presented in *Figure 10*, in which, following the same time of myoblasts differentiation in 2D vs. 3D, the 3D tissue constructs resulted in statistically fewer proliferating cells, indicating that the tissues proliferate less than 2D cultures under the same conditions. While the diffusion of nutrients is likely done without a gradient loss, (observation due to the lack of tissue necrosis), it is likely that the transition from 2D monolayer culture to 3D tissues has an innate ability to direct myoblasts out of cell cycle and initiate terminal differentiation [34, 35].

3.4.3.1. Correlation from 2D Pre-Differentiation to 3D Improvement in Ring Formation Efficiency

The pre-seeding differentiation improves 3D ring formation efficiency and correlates to previously-described data studying 2D differentiation. This improvement can be attributed to the mitogen-reduced differentiation medium inducing cells out of cell cycle and entering the terminal

differentiation pathway, during which, one of the first components of myogenic differentiation involves fusion with neighboring cells, thus promoting cell aggregation and subsequent contiguous 3D tissue formation [28].

Cells contact and form contiguous 3D tissues around the central post when seeded into the annular wells. There does appear to be minor necrosis towards the center of the tissue, as qualitatively identified as nuclei that appear more rounded in shape and not participating in the circumferential contraction of the ring. Such necrosis is perhaps expected as the tissue exceeds published literature values of nutrient free-diffusion limitations, approximated at 150 μ m, correlating to the maximal distance highly-metabolic tissue is from vascularization, *in vivo* with similar published observations of nutrient diffusion through 3D tissues confirming that approximately 150 μ m is the free diffusion limitation of nutrients [36, 37]. Necrosis is observed towards the inner radius of the tissue, correlating with the fact that the outer face of the ring is in direct contact with media, while the inner face of the ring is only in contact with hydrated agarose - potentially limiting the amount of free diffusion and subsequent availability of nutrients, hence necrosis is observed closer to the inner portion of the tissue rings.

Interestingly, there appears to be an additive effect of differentiation induction that is compounded by both the mitogen reduction along with the transition to 3D culture. This observation has been previously observed during *in vitro* culture of myoblasts, where the physiological and mechanical environment provided to the myoblasts due to a 3D culture results in increased differentiation and maturation, as compared to traditional 2D monolayer culture [34, 38].

3.4.4. Rationale for Fibroblasts Improving Tissue Compaction and Cellular Alignment

Past work has demonstrated that there is a clear benefit to including ECM-producing fibroblasts into myoblast cultures to improve maturation and furthermore increased tight tissue compaction along with cellular alignment [6]. Additionally, prior work has indicated that the presence of fibroblasts within

myoblast 3D constructs decreased the degeneration of tissues constructs up until 18 days along with promoting myotubes of both longer length and thicker diameter (both features of more mature, native-like skeletal muscle [6]).

As a result of this fibroblast incorporation study, data indicates that the beneficial role of fibroblasts is first observed following only the addition of 25% fibroblasts to the 3D myoblast ring culture. To further maximize maturation potential of the myoblasts to mature and generate more mimetic tissue analogues, the percentage of fibroblasts is minimized, once the beneficial result is observed. While adding more fibroblasts, (e.g. 50%- or 75%-fibroblast tissue rings) is possible, there is no observed increase in alignment or tissue compaction when compared to the 25% fibroblast rings, yet such higher-fibroblast rings likely decreased overall tissue maturation due to the fewer number of myoblasts within these rings. Past work has utilized an increased number of fibroblasts, with benefit being demonstrated following the inclusion of 50% fibroblasts to the myoblast culture (no lower percentages of fibroblasts were presented) [6]. However, this prior work utilized a fibrin gel to aid in tissue formation, resulting in an excess of ECM protein, and as such, may have played a role in masking the beneficial effects of the fibroblast inclusion [6]

Additionally, for our tissue rings that contained a greater number of fibroblasts (50% and 75%), there appears to be selective grouping and homing of fibroblasts to certain layers within the tissue ring. Such layering can be attributed to the selective cadherin expression levels of the two cell populations [39].

Finally, the inclusion of fibroblasts into the tissue ring culture system better emulates how native ECM is synthesized during *de novo* formation and regeneration. This salient difference in ECM protein source (compared to past research that utilizes exogenous fibrin [8] or collagen [11, 14] gels to provide myoblasts with ECM), may result in a better model of native skeletal muscle. Furthermore, this more precise model may result in more predictive data for skeletal muscle myopathies such as Ullrich or

Bethlem muscular dystrophy, which originate from malfunctions in collage VI synthesized by muscle interstitial fibroblasts [26].

3.5 References

1. Juhas, M. and N. Bursac, *Engineering skeletal muscle repair*. Curr Opin Biotechnol, 2013. **24**(5): p. 880-6.
2. Malik, V., L.R. Rodino-Klapac, and J.R. Mendell, *Emerging drugs for Duchenne muscular dystrophy*. Expert Opin Emerg Drugs, 2012. **17**(2): p. 261-77.
3. Porter, J.D., et al., *A chronic inflammatory response dominates the skeletal muscle molecular signature in dystrophin-deficient mdx mice*. Hum Mol Genet, 2002. **11**(3): p. 263-72.
4. Sacco, A., et al., *Short telomeres and stem cell exhaustion model Duchenne muscular dystrophy in mdx/mTR mice*. Cell, 2010. **143**(7): p. 1059-71.
5. Martin, N.R., et al., *Factors affecting the structure and maturation of human tissue engineered skeletal muscle*. Biomaterials, 2013.
6. Li, M., et al., *The role of fibroblasts in self-assembled skeletal muscle*. Tissue Eng Part A, 2011. **17**(21-22): p. 2641-50.
7. Gillies, A.R. and R.L. Lieber, *Structure and function of the skeletal muscle extracellular matrix*. Muscle Nerve, 2011. **44**(3): p. 318-31.
8. Huang, Y.C., et al., *Rapid formation of functional muscle in vitro using fibrin gels*. Journal of Applied Physiology, 2005. **98**(2): p. 706-713.
9. Hinds, S., et al., *The role of extracellular matrix composition in structure and function of bioengineered skeletal muscle*. Biomaterials, 2011. **32**(14): p. 3575-83.
10. Boonen, K.J., et al., *Interaction between electrical stimulation, protein coating and matrix elasticity: a complex effect on muscle fibre maturation*. J Tissue Eng Regen Med, 2011. **5**(1): p. 60-8.
11. Cheema, U., et al., *3-D in vitro model of early skeletal muscle development*. Cell Motil Cytoskeleton, 2003. **54**(3): p. 226-36.
12. Cronin, E.M., et al., *Protein-coated poly(L-lactic acid) fibers provide a substrate for differentiation of human skeletal muscle cells*. Journal of Biomedical Materials Research Part A, 2004. **69A**(3): p. 373-381.
13. Partridge, T.A., *The mdx mouse model as a surrogate for Duchenne muscular dystrophy*. FEBS J, 2013. **280**(17): p. 4177-86.
14. Mudera, V., et al., *The effect of cell density on the maturation and contractile ability of muscle derived cells in a 3D tissue-engineered skeletal muscle model and determination of the cellular and mechanical stimuli required for the synthesis of a postural phenotype*. J Cell Physiol, 2010. **225**(3): p. 646-53.
15. Vandenburg, H., et al., *Drug-screening platform based on the contractility of tissue-engineered muscle*. Muscle Nerve, 2008. **37**(4): p. 438-47.
16. Mak, I.W.V., I. Evaniew, and M. Chert, *Lost in translation: animal models and clinical trials in cancer treatment*. Am J Transl Res, 2014. **6**(2): p. 114-118.

17. Kinney, M.A., et al., *Engineering three-dimensional stem cell morphogenesis for the development of tissue models and scalable regenerative therapeutics*. *Ann Biomed Eng*, 2014. **42**(2): p. 352-67.
18. Gwyther, T.A., et al., *Engineered vascular tissue fabricated from aggregated smooth muscle cells*. *Cells Tissues Organs*, 2011. **194**(1): p. 13-24.
19. Brady, M.A., M.P. Lewis, and V. Mudera, *Synergy between myogenic and non-myogenic cells in a 3D tissue-engineered craniofacial skeletal muscle construct*. *J Tissue Eng Regen Med*, 2008. **2**(7): p. 408-17.
20. Murphy, M.M., et al., *Satellite cells, connective tissue fibroblasts and their interactions are crucial for muscle regeneration*. *Development*, 2011. **138**(17): p. 3625-37.
21. Page, R.L., et al., *Restoration of skeletal muscle defects with adult human cells delivered on fibrin microthreads*. *Tissue Eng Part A*, 2011. **17**(21-22): p. 2629-40.
22. Witten, C.M., R.D. McFarland, and S.L. Simek, *Concise Review: The U.S. Food and Drug Administration and Regenerative Medicine*. *Stem Cells Transl Med*, 2015. **4**(12): p. 1495-9.
23. Deyo, R.A., *Gaps, tensions, and conflicts in the FDA approval process: implications for clinical practice*. *J Am Board Fam Pract*, 2004. **17**(2): p. 142-9.
24. Shansky, J., et al., *Paracrine release of insulin-like growth factor 1 from a bioengineered tissue stimulates skeletal muscle growth in vitro*. *Tissue Eng*, 2006. **12**(7): p. 1833-41.
25. Zou, Y., et al., *Muscle interstitial fibroblasts are the main source of collagen VI synthesis in skeletal muscle: implications for congenital muscular dystrophy types Ullrich and Bethlem*. *J Neuropathol Exp Neurol*, 2008. **67**(2): p. 144-54.
26. Boldrin, L., F. Muntoni, and J.E. Morgan, *Are human and mouse satellite cells really the same?* *J Histochem Cytochem*, 2010. **58**(11): p. 941-55.
27. Dumont, N.A., et al., *Satellite Cells and Skeletal Muscle Regeneration*. *Compr Physiol*, 2015. **5**(3): p. 1027-59.
28. Cosgrove, B.D., et al., *A home away from home: challenges and opportunities in engineering in vitro muscle satellite cell niches*. *Differentiation*, 2009. **78**(2-3): p. 185-94.
29. Danoviz, M.E. and Z. Yablonka-Reuveni, *Skeletal muscle satellite cells: background and methods for isolation and analysis in a primary culture system*. *Methods Mol Biol*, 2012. **798**: p. 21-52.
30. Montarras, D., et al., *Direct isolation of satellite cells for skeletal muscle regeneration*. *Science*, 2005. **309**(5743): p. 2064-7.
31. Penton, C.M., et al., *Laminin 521 maintains differentiation potential of mouse and human satellite cell-derived myoblasts during long-term culture expansion*. *Skelet Muscle*, 2016. **6**(1): p. 44.
32. Charville, G.W., et al., *Ex Vivo Expansion and In Vivo Self-Renewal of Human Muscle Stem Cells*. *Stem Cell Reports*, 2015. **5**(4): p. 621-32.
33. Chiron, S., et al., *Complex Interactions between Human Myoblasts and the Surrounding 3D Fibrin-Based Matrix*. *PLoS One*, 2012. **7**(4).
34. Elliott, N.T. and F. Yuan, *A review of three-dimensional in vitro tissue models for drug discovery and transport studies*. *J Pharm Sci*, 2011. **100**(1): p. 59-74.
35. Lovett, M., et al., *Vascularization Strategies for Tissue Engineering*. *Tissue Eng Part B* 2009. **15**(3): p. 353-370.
36. Corstorphine, L. and M.V. Sefton, *Effectiveness factor and diffusion limitations in collagen gel modules containing HepG2 cells*. *J Tissue Eng Regen Med*, 2011. **5**(2): p. 119-29.
37. Liao, H. and G.Q. Zhou, *Development and progress of engineering of skeletal muscle tissue*. *Tissue Eng Part B Rev*, 2009. **15**(3): p. 319-31.
38. Foty, R.A. and M.S. Steinberg, *Cadherin-mediated cell-cell adhesion and tissue segregation in relation to malignancy*. *Int. J. Dev. Biol*, 2004. **48**: p. 397-409.

Chapter 4: The modulations of culture conditions, supplements, and tissue shape improve tissue integrity and enable long-term culture while increasing contractile and ECM protein production.

4.1 Introduction

In previous studies, we demonstrated that 3D skeletal muscle tissue rings can be generated and certain culture parameters could be modulated to improve both tissue formation and differentiation potential. Although tissue rings were generated, limitations involving ring failure before 10 days of culture, coupled with insufficiently mature ECM protein available to facilitate maturation and finally sub-native levels of maturation, required further improvements and optimization of culture conditions.

To improve long term ring culture, we investigated the role that relieving static tissue stress had on promoting sustained culture, *in vitro*. It is well understood that physical cues play a crucial role on guiding myoblast differentiation, and that the application of biomimetic cues including dynamic motion, improve muscle maturation [1, 2]. During fetal development, skeletal muscle undergoes phases of contraction and relaxation (via contraction of the antagonistic muscle), indicating that dynamic stimuli is crucial to muscle embryogenesis [3]. Our system currently cultures the tissue rings in a static system, and such static culture has lead to consistent tissue failure during early stages of culture. One of the motivations of this study was to investigate the potential of creating a dynamic-like culture system for which the tissue rings can mature on.

Additional investigation on culture modulations involved the addition of pro-ECM producing supplements. Past work has demonstrated that ascorbic acid 2-phosphate is an essential cofactor in hydroxylation of prolines in collagen and helix formation and furthermore stimulates collagen synthesis, *in vitro* [4, 5]. Furthermore, previous work has demonstrated that the addition of ascorbic acid increased the collagen production of tissue engineered benchtop constructs [6]. As our tissue constructs were failing during maturation, coupled with substantial literature that indicates the importance of cell-ECM

bonds to promote maturation [4, 7-9], an additional motivation of this study was to investigate the role that ascorbic acid supplementation has on increasing ECM production and the extension of long-term tissue viability.

Finally, prior research has demonstrated that IGF-1 is a potent activator of new protein synthesis and inhibits protein degradation [10, 11]. IGF-1 supplementation has been shown to increase the diameter of myotubes in 3D benchtop cultures, indicating that such supplementation could help bridge the gap between the current differentiation potential of benchtop skeletal muscle constructs and native skeletal muscle [10].

As such, the goal of this chapter was to investigate the role that a redesigned tissue culture mold that allows for tissue relaxation during formation and maturation, coupled with ascorbic acid 2-phosphate and IGF-1, have on the morphology and functionality of the tissue rings. Such modulation and supplementations were shown to improve long-term tissue longevity along with an increased production of ECM proteins and mature cell-ECM connections, along with increased myogenic maturation.

4.2 Methods

4.2.1. Mold Redesign with Slanted Wells and Sloped Posts

To develop a different tissue culture platform capable of relieving tissue tension, the following process was completed. Using the original ring molds as benchmarks for overall tissue size and well volume, the software Solidworks® was used to create a different seeding platform. Similar to the original post design, positive acrylonitrile butadiene styrene (ABS) plastic molds were printed from the Solidworks drawings using an in-house Objet® 3D printer. Since the plastic should not be repeatedly exposed to the high heat and pressure within an autoclave due to potential warping, negative PDMS molds were cast into the plastic, which were then autoclave-sterilized and used as a mold for casting 2% agarose in DMEM, as previously described.

The redesign maintained a well with a central post, but with a few modifications. Firstly, the shape of the well surrounding the post was redesigned to end in a sharp point at the bottom of the post, namely to reduce the cell number needed to direct cell-mediated self assembly. This further enabled the ultimate diameter of the tissues to be controlled by the number of cells seeded into the wells. The previous mold design consisted of an annular well that created a large surface area for which cell aggregation occurred within - necessitating the need for an abundance of cells seeded per tissue ring. Secondly, the posts were redesigned from a cylindrical shape to a tapered conical shape, such that the bottom of the posts - where the tissue initially forms - maintains the original diameter of 2mm, but the post tapers down by a defined margin moving upwards. Two different continuously-tapered designs were engineered, one containing a tapered angle of 87.5° and the other containing a tapered angle of 85°. A schematic of the redesigned molds is show below in *Figure 22*.

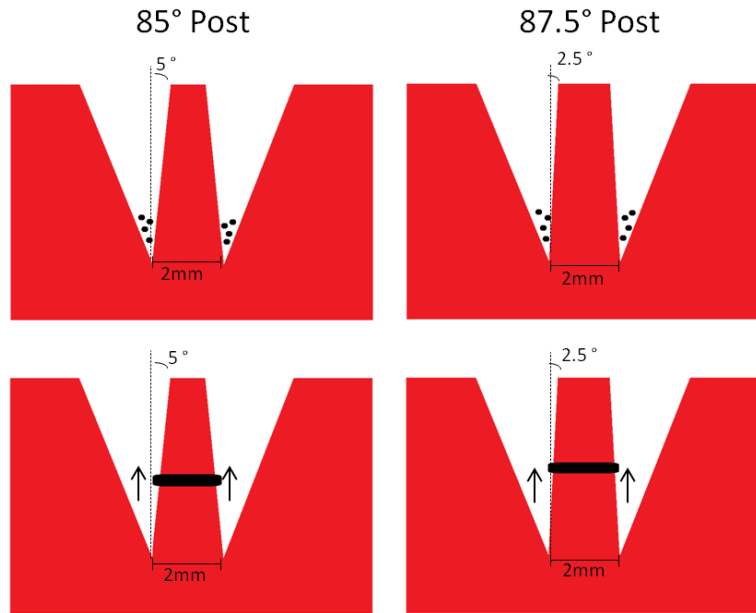


Figure 22: Post Redesign Incorporating Conical Posts and Sloped Wells

Both angles of the redesigned molds contain conical posts with defined tapers of either 5° or 2.5°. Further modification replaced the annular wells with sloped wells, allowing for the reduction in cells required for contiguous tissue formation.

Once the new agarose molds were cast (termed "85° molds" or "87.5° molds" - based on the taper), initial volumetric calculations were completed to determine the maximal amount of volume that can fit into the new well geometry. By incorporating Trypan blue (a deep blue dye) into PBS and maximally filling wells, it was possible to determine the maximum volume the new wells can hold - thus maximizing the volume of media that the cells could be resuspended into, prior to 3D tissue ring seeding.

4.2.1.1. Modifications to 3D Tissue Seeding Protocol

To test the efficacy of the new mold redesign on tissue ring formation, both homogeneous skeletal muscle myoblasts and heterogeneous myoblast: fibroblast cultures were seeded into the new tissue molds. Once again, since this mold is geometrically different from the original annular well mold, an optimization study was completed to determine the minimal number of cells necessary to form contiguous tissue, while maintaining a high degree of formation efficiency.

4.2.1.2. Redesigned Mold Tissue Migration Along Sloped Posts

To determine if the tissues actually contracted up the conical posts, tissues were seeded into the new redesigned wells and allowed to aggregate into tissues and cultured for 14 days. Following the culture period, tissues were fixed, processed, and sectioned onto microscope slides, as previously described. An H&E stain allowed for the inner diameter of the tissue rings to be measured, allowing for a calculation of the amount of contraction that the rings underwent following the 14 days of culture on the two different conical posts, allowing for quantification of final ring inner diameter.

4.2.1.3. Redesigned Mold Tissue Longevity and Myosin Production

To determine if the new mold redesigns increase the percentage of tissues that maintain contiguity following 14 days in culture, heterogeneous myoblast-fibroblast tissue rings were seeded into both new tissue ring mold variations and cultured for 14 days. Statistics regarding ring formation efficiency and the timing of any ring failure were collected and quantified to determine if the new posts improve the longevity of the tissues in culture over 14 days.

To determine if the new mold redesigns increase the amount of contractile myosin protein production, tissues were fixed at 14 days and prepared for IHC staining, as previously described and stained for myosin heavy chain. Comparisons were made between the number of myosin-positive cells between the original annular well/cylindrical post molds and the new angled post molds, to determine if the new post geometry was a better platform to direct a higher percentage of cells to differentiate and begin forming contractile myosin protein.

4.2.2. Ascorbic Acid 2-Phosphate Supplementation

Previous work has indicated that fibroblasts can be instructively directed to synthesize an increased amount of ECM through the use of supplementation with ascorbic acid. Ascorbic acid has been shown previously to act as an essential cofactor for hydroxylation of prolines in collagen and helix formation, and enable secretion [4, 6]. To determine if ascorbic acid increased the overall ECM

production during 3D ring tissue culture, L-ascorbic acid 2-phosphate (a stable derivative of ascorbic acid) was supplemented into the culture medium during each feeding (daily), starting at day 3 in 3D culture. The supplementation of ascorbic acid was intentionally delayed for 3 days to ensure that myoblasts have sufficient time to fuse together - ascorbic acid has been previously demonstrated to attenuate cell-cell fusion - a critical early-step in myoblast differentiation into multinucleated myotubes [12].

Benchmarks based on past literature were used as a starting point for determining the concentration needed to improve ECM production, whereas ranges between 50-250 $\mu\text{g}/\text{ml}$ of ascorbic acid has been shown to have a beneficial effect on increasing ECM production, however, the application that required between 50-100 $\mu\text{g}/\text{ml}$, involved skeletal muscle research and was employed on tissue that was of a similar size and morphology to our 3D tissue rings, whereas other applications involved cardiac muscle and thus the benchmarks generated from their research - while experimentally useful - may not be translatable to the tissue ring project [4, 13-15]. While benchmarks were useful starting points, tissues similar to our 3D self-assembled rings have yet to be experimentally tested in literature to determine the optimal ascorbic acid concentration for increased ECM production. The following concentrations were tested to determine the minimal ascorbic acid necessary to improve ECM production: 25, 50, 100, and 250 $\mu\text{g}/\text{ml}$, and were compared to unsupplemented controls. L-ascorbic acid 2-phosphate (a stable derivative of ascorbic acid) (at the aforementioned concentrations) was dissolved in the differentiation media and added to the tissue rings starting at day 3 with repeated re-dosing with every daily feeding for the remaining time in culture.

Following culture, fixation and preparation for histological/IHC analysis, as previously described, the following ECM proteins were assayed for, as shown in *Table 1*. Two collagens (Collage IV and Collagen VI) and Laminin-211 (all proteins found in native skeletal muscle) were assayed for to determine if ascorbic acid increases the synthesis of these important skeletal muscle ECM proteins.

4.2.3. IGF-1 Supplementation

Previous work has further indicated that certain exogenous supplements, such as IGF-1, can improve differentiation and contractile protein production by increasing myotube maturation. As discussed previously, the use of IGF-1 on benchtop 3D models of skeletal muscle has profound benefits in terms of increasing myotube diameter, which can lead to a 3D *in vitro* tissue that better emulates the contractile function and strength of native skeletal muscle [10, 11]. Prior work has shown that a concentration of 100ng/ml IGF-1 results in a statistical increase in myotube diameter [10]. To improve myotube maturation in culture, IGF-1 was supplemented into the tissues starting at day 3 at a concentration of 100ng/ml, replenished with each daily feeding. Tissue rings were cultured for 14 days, and then fixed and analyzed as previously described, to identify increases in myotube diameter when compared to unsupplemented tissue ring controls. Staining for myosin heavy chain was completed as previously described, and myotubes (as defined by myosin-positive structures containing 3 or more nuclei), were measured for diameter, allowing for quantifications to be compared to unsupplemented control tissue constructs.

4.2.4 Statistics

For all experimentation, sample sizes of tissue rings are reported: tissues numbers exceeded 6 tissues for myosin protein quantification and myotube diameter quantification, exceeded 16 for all longevity experiments and formation efficiency data, exceeded 12 for the 300,000-cell ring formation efficiency, and equaled 8 for ring diameter calculations. All experimentation was completed at least in duplicate and the two groups of (6 tissue minimums) were averaged prior to statistical analysis. All data are presented as mean \pm Standard Error of Measurement (SEM). For analysis requiring statistical inference, a Student's t-test was used to determine significance between individual test groups, (at a critical p-value <0.05).

4.3 Results

4.3.1. A Mold Redesign Prevents 3D Muscle Tissues Cultured Failure

The first part of this study investigated the feasibility of improving long-term tissue culture longevity by using a redesigned tissue mold seeding platform that allowed the tissue rings to concentrically relax during maturation.

4.3.1.1. *Tissues Cultured in Annular Molds Consistently Fail During Culture.*

Previous data has indicated that the 3D tissue rings could be maintained in culture while maintaining tissue integrity for 7 days with minimal observed failure (less than 10% - and such failure is attributed to human error of poor ring seeding and was consistent across all tissue seeding groups, where an observed variable distribution of cells was observed circumferentially around the tissue ring, that led to rapid ring failure (before day 2 in 3D culture). Unfortunately, 7 days was insufficient time for these 3D tissue rings to mature - in fact, past research has indicated that substantially more culture time (up to 30 days), may be necessary to promote native levels of tissue maturation and contractile function, as complete regeneration has been shown to take upwards of 4 week within an *in vivo* setting [16]. We observed that our tissues began to thin in one region of the ring, leading to necking and ultimately failure of the ring between 7-10 days in culture, as shown in *Figure 23* below, where, regardless of the seeding condition (myoblasts or fibroblast-supplemented myoblast rings), a significant proportion of rings failed (67% and 60% respectively for the myoblast and fibroblast-supplemented myoblast rings) within 14 days of seeding. Note that the graph in *Figure 23* begins at day 2 of 3D culture at which time point such values were normalized to 100%, to remove the tissue rings that failed prior to 2 days from analysis, as this was attributed to human error in the ring seeding method.

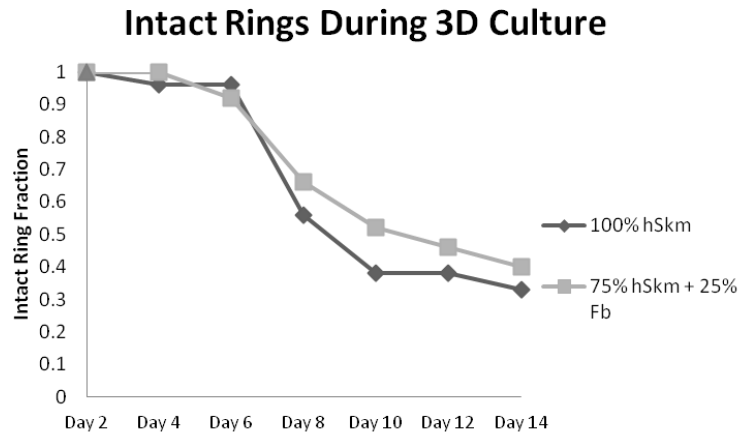


Figure 23: Ring Failure During 3D Culture

Significant ring failure - over 50% of the formed rings - occur between 7-10 days in culture for both myoblast rings and rings that contain fibroblasts, n>16 for all conditions.

Once failure occurred between days 7-10 in culture, the tissue no longer consisted of a contiguous ring, but rather a crescent-shaped tissue which, due to the intrinsic function of both skeletal muscle or fibroblast cells. These tissues rapidly contracted further and resulted in a spherical tissue within the annular wells of ring mold, thus losing their anchorage and original tissue shape.

This trend and timing of ring failure was consistent between both homogenous myoblast rings, along with the heterogeneous myoblast: fibroblast rings. For all conditions, the formation efficiency exceeded 90%, indicating that there was not an issue with repeatability or user error during the process of 3D ring tissue seeding. Between days 1-6, of the 90% of rings that successfully formed, only 9% failed, indicating that the cellular aggregation and initial days of 3D differentiation did not lead to tissue failure. Such stages of maturation (days 1-6) include initial cellular alignment and fusion (markers of early-stages of differentiation), but do not include the production of any functional contractile proteins, with the correlative relationship completed in 2D, where myosin staining was barely evident at 7 days, (*Figure 24-left*) but became more prominent at 14 days (*Figure 24-right*), with myosin heavy chain visualized in red while all nuclei are visualized in blue. As such, work to address this issue of tissue self-induced failure must be completed to allow for extended, *in vitro* culture of these 3D tissue constructs.

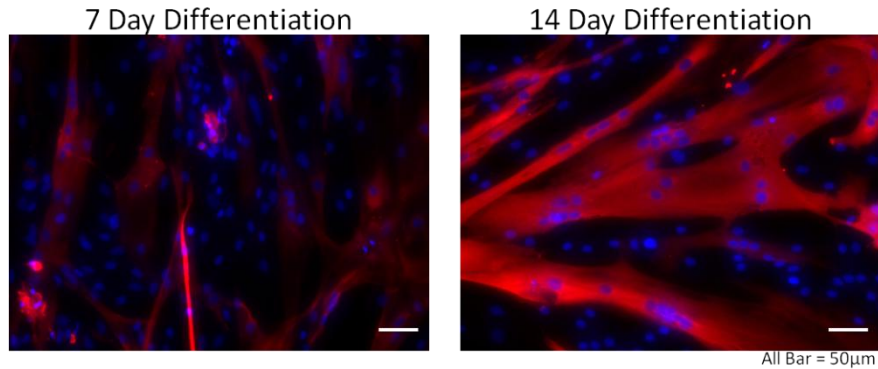


Figure 24: 2D Myoblast Differentiation for 7 and 14 Days

Myosin protein production is minimal following 7 days of differentiation (left), but is significantly increased at 14 days (right).

However, the repeatable and consistent failure that begins around day 7 coincides with the beginning of myosin protein production. To improve ring longevity in culture, the tension must be reduced or the ECM protein production increased, to allow for passive force transmission - as the ECM is capable of absorbing passive force transmission - thus preventing overall tissue failure.

4.3.1.2 Mold Redesign Results in Contiguous 3D Tissues

To reduce the overall tension of the 3D tissue rings during culture, a different seeding platform was developed, such that the tension that the tissue ring imparts on itself, is reduced. As described previously, the new tissue molds contained a slanted well - more precisely funneling media and cells towards the central post - reducing the cell number requirement. Furthermore, the posts were redesigned from a cylindrical shape to a conical shape with two different defined tapers, 85°, and 87.5°. As described previously, there is no difference in the post diameter (2mm) at the bottom of the well (the location where the cells self-aggregate into 3D tissue. However, there is a continuous taper (consisting of two different slopes for the 85° and the 87.5° post designations) that allowed for the tissues to move upwards as they contract during continued culture.

Initial calculations of the maximum volume that the new wells were capable of holding was completed. Due to the changing geometry, it was determined that the new wells can hold maximally 37.5µl of volume. Exceeding this volume, e.g. attempting to load 40µl into the wells resulted in media

flowing over the lip of the well, indicating that a portion of the cells would be lost if all of the media did not remain in the well. As such, all seeding densities was adjusted such that the prescribed number of cells were resuspended in 37.5 μ l of media, and such concentration were seeded into each redesigned well.

Initial 3D tissue generation experiments were completed using both of the new angle wells. Seen below in *Figure 25*, the ring formation efficiency (quantified by the number of intact rings at day 2 in 3D culture) is actually increased slightly from 92.1% +/- 4.5% for the annular wells to 93.6% +/- 4.1% and 95.0% +/- 4.0% for the 85° and the 87.5° wells respectively.

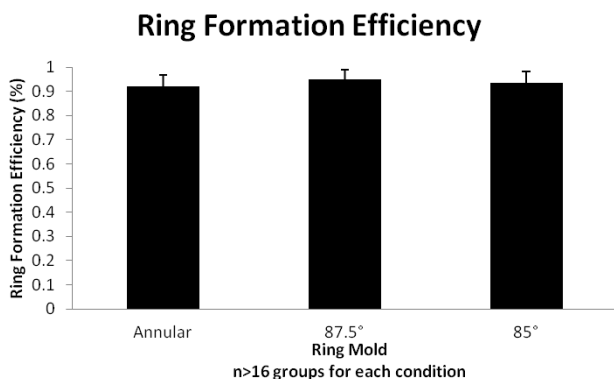


Figure 25: Ring Formation Efficiency for the Annular and New Angle Wells

Tissues seeded with new angled post wells do not reduce overall ring formation efficiency as compared to the formation efficiency from the original annular wells. All tissues seeded with myoblast:fibroblast mixtures (75:25), with 400,000 total cells seeded.

4.3.1.3 Change in Mold Design Allows for Cell Seeding Number Reduction

Due to the geometrical change in the shape of the well directing cells to a more focused area, we postulated that cells would aggregate easier into 3D tissue and potentially require fewer cells to do so. Another cell minimization experiment was conducted to determine if a fewer number of cells could be seeded into these new molds while still maintaining a high formation efficiency. As shown in *Figure 26*, we were able to decrease the total cell seeding number to 300,000 cells/tissue and result in a statistically-improved formation efficiency of 65.7% +/- 4.1% and 93.7% +/- 4.4% for the 85° and 87.5°

post wells respectively, compared to only 29.1% +/- 4.7% for the annular wells, when only 300,000 cells are seeded ($p < 0.05$, t-test, $n > 12$ for all groups).

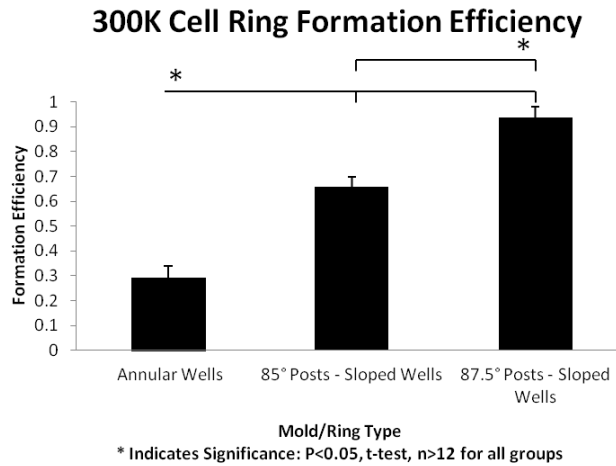


Figure 26: Ring Formation Efficiency with 300,000 Cells Seeded

The change to the angled sloped post wells statistically-increases the ring formation efficiency when 300,000 cells are seeded, compared to the annular well molds ($p < 0.05$, t-test, $n > 12$ groups). All tissues seeded with myoblast:fibroblast mixtures (75:25), with 300,000 total cells seeded.

The conical posts have been shown to allow for tissue rings to contract up the posts throughout the 14 days in culture. Seen below in *Figure 27* are tissues cultured on the 87.5° conical posts, with the left tissue fixed following 2 days in culture and the right tissue fixed at 14 days in culture, demonstrating clear tissue migration up the conical post during the culture period, with the red arrows pointing to the white colored tissues on the agarose posts.

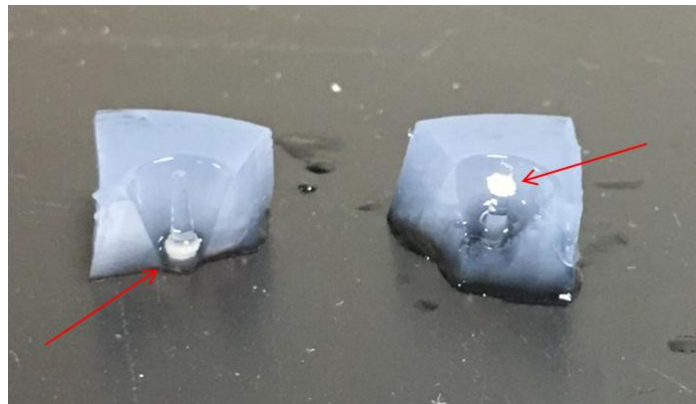


Figure 27: Tissue Rings on 87.5° Posts

Tissue rings fixed at day 2 (left) and day 14 (right) illustrate the migration of the tissues up the conical posts during the culture period (red arrows point to white colored tissues on agarose posts).

Morphological analysis of the 300,000 cell rings via H&E staining indicate that the tissue rings appear uniform in diameter and did not exhibit any signs of necking or necrosis following 14 days in culture. Two examples of tissue rings cultured for 14 days on both 85° and 87.5° posts are shown below in *Figure 28*. For all subsequent experiments involving the new angle molds, a seeding density of 300,000 cells/37.5 μ l was used, while with all comparative work done with the original annular post molds, seeding density remained unchanged from prior work at 400,000 cells/55 μ l.

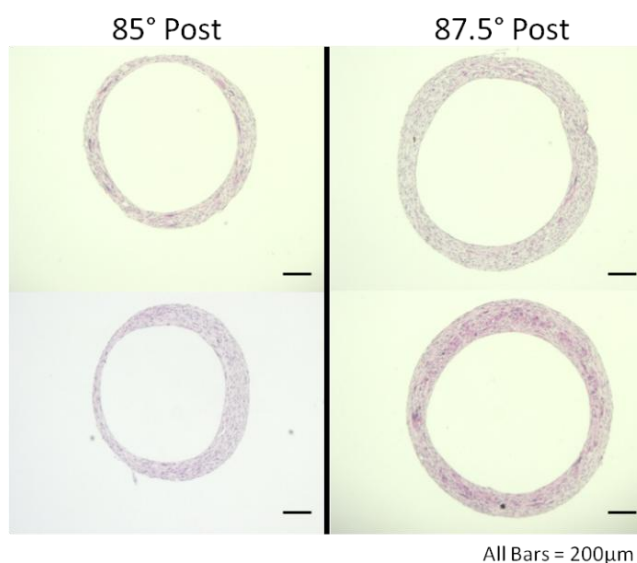


Figure 28: Hematoxylin and Eosin of New Angle Tissue Rings

Contiguous tissue formation is shown formed from 85° and 87.5° post molds. Increased necking is observed with 85° post tissues as compared to 87.5° post tissues. All tissues seeded with myoblast:fibroblast mixtures (75:25), with 300,000 total cells seeded.

To determine how much tissue contraction and subsequent migration upwards on the conical post occurred for rings seeded within each of the two new angled molds, tissues were fixed at 14 days, and prepared for histological analysis and stained with H&E, as previously described. Inner diameter measurements were taken to determine the percentage of initial tissue diameter that each tissue contracted during culture - as a comparison, tissues seeded using the original annular wells maintained a measured diameter of 2mm - the original post dimension, indicating that the tissue ring did not squeeze

or contract the agarose post during culture. A table of the inner diameters of the 85° and 87.5° tissue rings are shown in *Table 4*.

Table 4: Inner Ring Diameters From New Angle Tissue Ring Molds

Inner diameter of the 85° post tissues is slightly lower than 87.5° post tissues, due to the increases taper of the post design, resulting in smaller-diameter tissues (top row), with diameter comparisons made to original 2mm tissue rings (bottom row).

	85° Ring	87.5° Ring
Average Diameter (+/- Standard Dev) (mm)	1.03 mm (+/- 0.047)	1.25 mm (+/- 0.083)
Average Diameter compared to base (2mm diameter)	51.5%	62.6%

A graph comparing the diameter of the tissue rings formed with the new angle molds is shown in *Figure 29* with a comparative dashed line indicating the diameter of the original annular wells (2mm). A clear decrease in ring diameter indicates that the tissues contracted and migrated up the conical post, resulting in a smaller inner diameter, when compared to the annular well ring tissues, (n=8 for each condition).

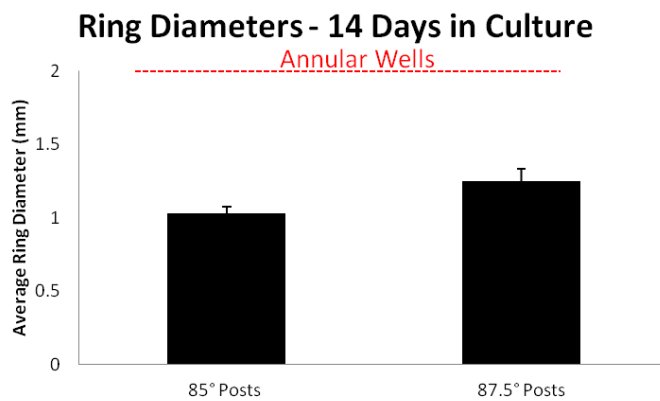


Figure 29: Ring Diameter From New Angle Tissue Rings Molds

Inner ring diameters for both 85° and 87.5° post tissues are both lower than that of original annular well mold tissues.

4.3.1.4 Mold Redesign Improves 3D Tissue Ring Longevity in Culture

To determine if the tension-reducing molds promoted improved tissue longevity during culture, statistics regarding ring failure were recorded. The new angled posts reduced the incidence of ring failure during the 14 days of culture when compared to the original annular well molds, with data reported for only the fibroblast-supplemented myoblast tissue rings, as prior data has indicated a clear benefit of the fibroblast inclusion, including a higher percentage of contiguous tissue rings during preliminary research. All experiments discussed forthcoming involved only the heterogeneous myoblast-fibroblast tissue rings. Rings cultured on the 85° posts had a 14 day retention rate of 60%, while the rings cultured on the 87.5° posts had an increased retention rate of 83%, compared to the original annular molds that only had a 14 day retention of 40%. The increased 14 day retention rate is shown below in *Figure 30*.

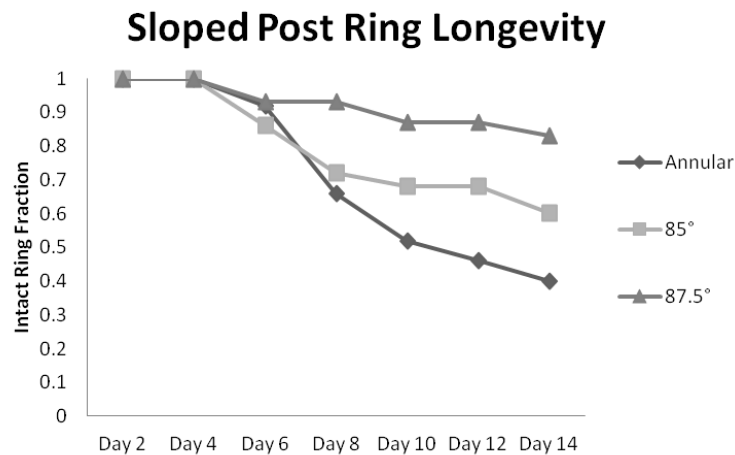


Figure 30: Ring Retention Annular vs. Sloped Post Tissue Rings

The longevity of both 85° and 87.5° post tissues is greatly improved as compared to original annular wells - a near 100% improvement is observed with the 87.5° post tissues, n>16 for all conditions.

4.3.1.5. Mold Redesign Results in Increased Myosin Protein Production

Finally, to determine if the new tension-reducing molds increase the contractile myosin protein accumulation, rings fixed at 14 days were stained for myosin heavy chain protein, as previously described. Seen below *Figure 31*, there were visible myosin-positive myotubes in for the new angle

tissue rings, with detection in violet purple. Further verification of the positive myosin staining is shown with correlative serial-sectioned hematoxylin and eosin stained tissue sections of the same region, where the multinucleated structures are clearly visible.

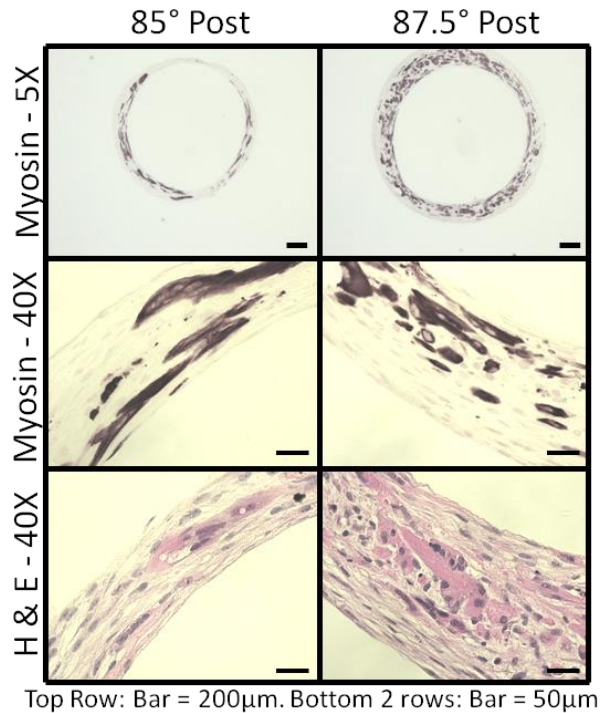


Figure 31: Myosin and Hematoxylin and Eosin Staining at 14 Days in New Angled Post Tissue Rings
 Full-thickness myosin protein production is observed with both 85° and 87.5° post tissues (top and middle). Comparative H&E staining of serial sections demonstrate that myosin-positive structures correlate with multinucleated structures.

Furthermore, quantification of the myosin-positive nuclei was done, as previously described to elucidate the role that the new angle posts - and hence the contractile motility of the tissue rings during maturation - had on the differentiation potential of the tissues. As shown below in *Figure 32*, a statistically-significant increase in the percentage of myosin-positive nuclei were observed with both of the new angle posts, when compared with the original annular well/cylindrical post molds (36.5% +/- 10.2% and 46.0% +/- 8.3% for the 85° and 87.5° post tissues respectively, compared to 26.9% +/- 3.8%, for the original annular well post tissues, $p < 0.05$, t-test, $n > 6$ for all groups).

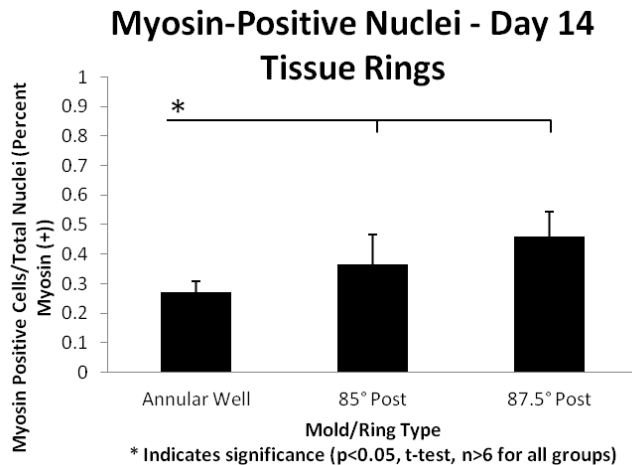


Figure 32: Myosin-Positive Nuclei 14 Days New Angle Posts

An statistical increase in myosin-positive protein is quantified for both the 85° and 87.5° post tissues when compared to the myosin nuclei from original annular well tissues.

4.3.2. Ascorbic Acid 2-Phosphate Improves ECM Production During 3D Culture

As mentioned previously, ascorbic acid has been shown to increase endogenous fibroblast ECM synthesis [6]. Following supplementation with 0, 25, 50, 100, and 250 $\mu\text{g/ml}$ L-ascorbic acid 2-phosphate, there were comparative differences in the amount of ECM protein expression at 14 days. Seen below in *Figure 33*, there was a qualitative difference in the relative expression of salient skeletal muscle ECM proteins including Collagen IV, VI, and Laminin-211 for constructs supplemented with 100 $\mu\text{g/ml}$ ascorbic acid when compared to the unsupplemented (control) tissues. Quantitative statistics recorded regarding ring retention and longevity during culture indicated that the addition of ascorbic acid, in any of the tested concentrations, did not decrease the percentage of rings that maintain contiguity up to 14 days, indicating that the ascorbic acid does not affect ring retention and longevity during culture.

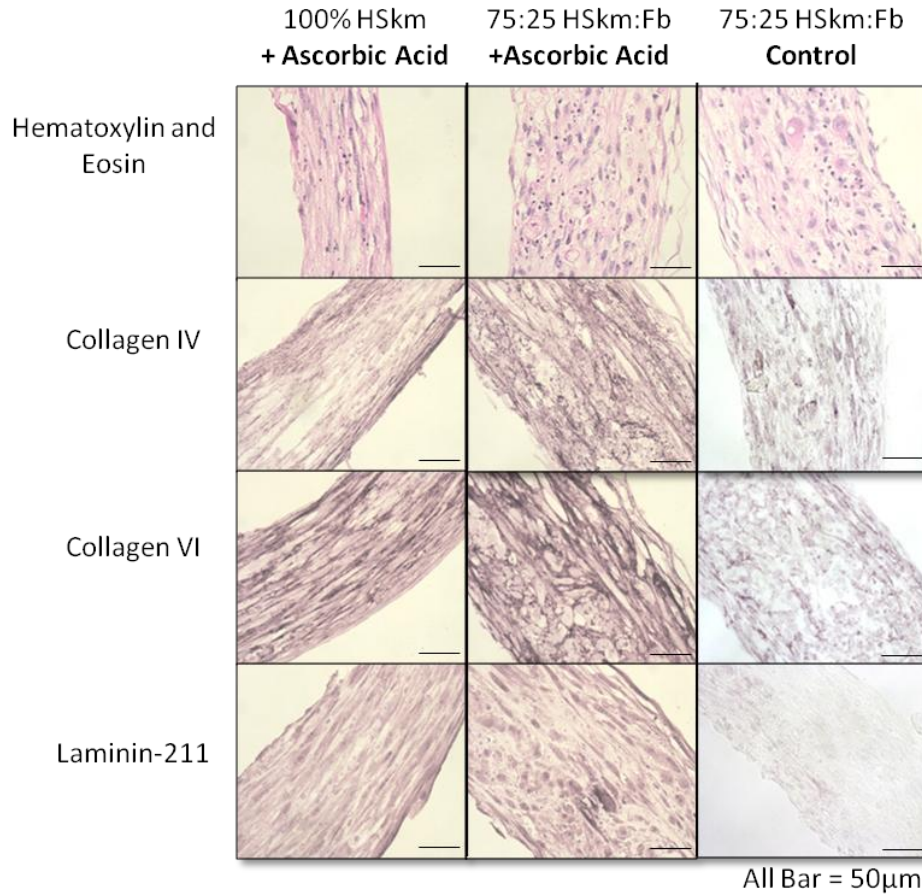


Figure 33: The Effects of Ascorbic Acid on ECM Synthesis

Ascorbic acid supplementation [100µg/ml] resulted in increased production of salient native skeletal muscle ECM proteins for constructs supplemented with or without fibroblasts (left and middle column), as compared to unsupplemented controls (right column).

For concentrations below 100 µg/ml, (25 and 50 µg/ml), increases in ECM protein accumulation compared to the control tissues were observed, however, the qualitative increases were less than the difference observed following the 100 µg/ml supplementation. Additionally, the highest concentration of ascorbic acid, 250 µg/ml, did not result in any additional increase in ECM protein staining, when compared to the 100 µg/ml. Seen below in *Figure 34*, are images from ascorbic acid supplementation of 50 µg/ml (left) and 250 µg/ml (right), stained for Collagen VI. The images indicated a clear difference in staining intensity between the 50 and 100 µg/ml, indicating that there is a clear benefit and cellular response from the additional ascorbic acid, however, there is no observed increase Collagen expression

when increasing the ascorbic acid to 250 $\mu\text{g}/\text{ml}$, indicating that the 100 $\mu\text{g}/\text{ml}$ condition is optimal for these 3D tissue rings.

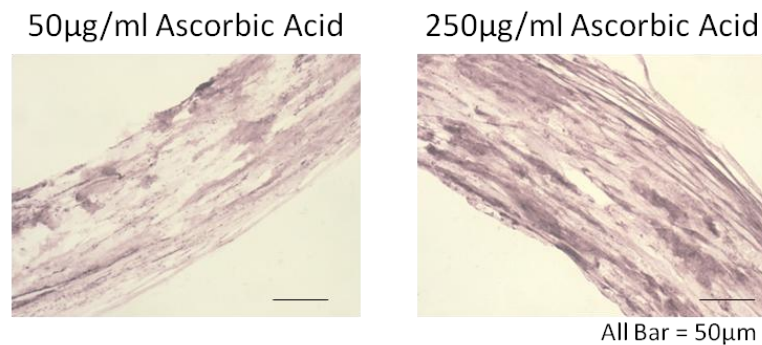


Figure 34: Lower and Higher Concentration Ascorbic Acid Supplementation
Reduced concentration of ascorbic acid (50 $\mu\text{g}/\text{ml}$ - left) resulted in lower ECM protein production, while increased ascorbic acid concentration (250 $\mu\text{g}/\text{ml}$) did not increase ECM production, as compared to the 100 $\mu\text{g}/\text{ml}$ supplementation.

4.3.3. IGF-1 Supplementation Improves Contractile Protein Production During 3D Culture

As mentioned previously, IGF-1 has been shown to improve myotube hypertrophy both *in vivo* and within *in vitro* 3D muscle tissue constructs, potentially creating benchtop skeletal muscle tissue that produces native levels of functionality and contractile protein production. The addition of 100ng/ml IGF-1 starting at day 3 and replenished with each daily feeding to our 3D tissue rings had a statistical effect on increasing the myotube diameter following 14 days in culture. There was no decrease in tissue ring retention over the 14 day culture period as a result of the IGF-1 supplementation.

Seen below in *Figure 35* the addition of 100ng/ml IGF-1 results in visible large multi-nucleated structures that align with the principal axis of strain, and can be observed both in horizontal sections along with cross-sections (X-SEC), where the cross-sectional view of the multinucleated myotube is visible, indicated by red arrows.

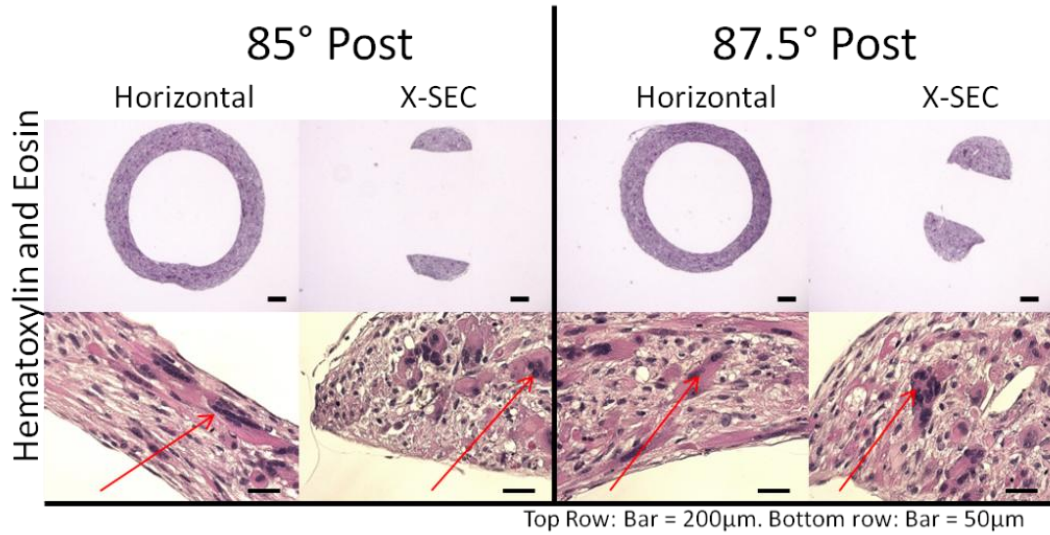


Figure 35: Hematoxylin and Eosin Images of IGF-1 Supplemented Tissue Rings
Horizontal and cross-sectional H&E images of tissue rings show visible multinucleated myotubes that have defined thickness in cross-section, as indicated by red arrows.

Furthermore, the following sequential serial sections of the same tissue rings were also stained for myosin protein to verify that the observed structures indicated in *Figure 35* were in fact multinucleated myotubes. As previously described, IHC staining for myosin with silver detection identified myosin-positive myotubes in *Figure 36* below, and the red arrows indicating the presence of multinucleated myotubes in *Figure 35* above can be clearly seen as myosin-positive in *Figure 36*.

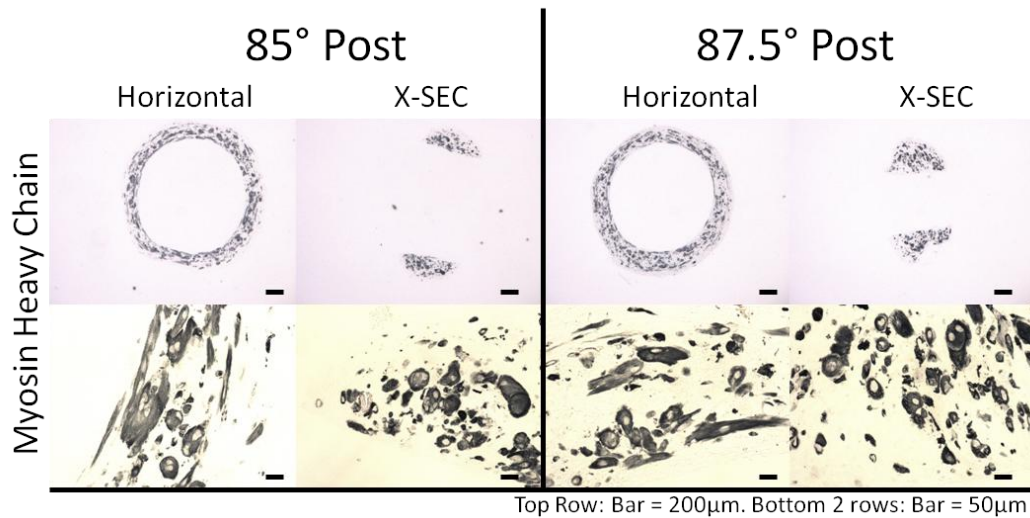


Figure 36: Myosin Staining of IGF-1 Supplemented Tissue Rings
Myosin heavy chain staining of tissue rings confirm that morphological multinucleated myotubes are in fact present in tissues. Full-thickness differentiation throughout the tissue ring is observed for both post tissue conditions.

Such identification allowed for the quantification of the average myotube diameter (with parameters for inclusion defined previously), as IGF-1 has previously been shown to increase the diameter of myotubes during maturation, enhancing the contractile force production of the tissue. Seen below in *Figure 37* is quantification of the diameter of multinucleated myotubes that fit our selection criteria (previously described). For the 85° post tissues, a non-significant increasing trend was observed, indicating that IGF-1 may be increasing the myotube diameter (17.0 μm +/- 5.3 μm vs. 17.7 μm +/- 6.7 μm for the control vs. supplemented respectively). However, the 87.5° post tissues resulted in a statistical increase in the diameter of all myotubes following IGF-1 supplementation (21.6 μm +/- 6.3 μm vs. 15.4 μm +/- 4.7 μm for the supplemented vs. control respectively, $p < 0.05$, t-test, $n > 6$ for all groups), indicating that IGF-1 did increase the average diameter of the myotubes during culture.

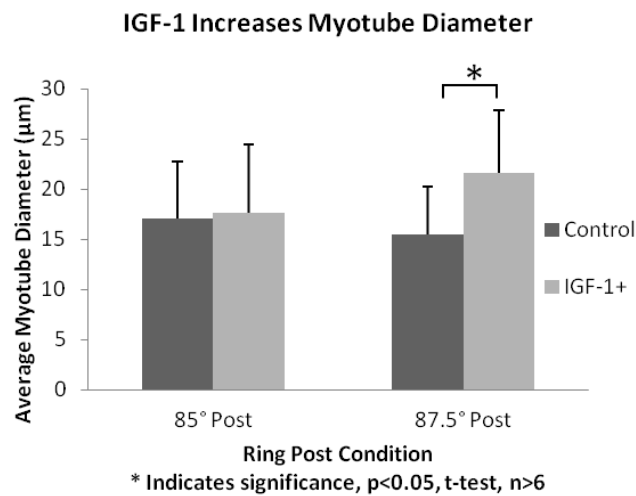


Figure 37: IGF-1 Increases Myotube Diameter
The diameter of the measured myotubes statistically-increases for tissues cultured in 87.5° post molds.

In conclusion of this experiment, IGF-1 supplementation was shown to increase myotube hypertrophy for both redesigned posts, however, the effect was more profound for the 87.5° post molds compared to the 85° molds.

4.4 Discussion

4.4.1. Allowing Tissue Constructs to Relax During Maturation Allows for Contractile Protein Development While Preventing Tissue Failure

Our data indicate that the tissue failure that occurred between 7-10 days in culture occurs during the preliminary production of myosin heavy chain protein, indicating that as myosin begins to be produced during maturation, the tissue cannot withstand the minute isometric contractile force that is created, yielding to necking and failure. Furthermore, our redesigned conical-shaped molds were shown to allow tissue relaxation and free migration up the conical post during tissue maturation, reducing incidence of ring failure, coinciding with prior work indicating that stiffness reduction decreases microtissue failure [17]. The posts were cast from 2% agarose, previously shown to be non-adhesive to cells, and as such, allowed for the tissues to not bond to the post, but instead freely migrate to relieve internal tension [18, 19].

This observed necking of the tissue, effectively thinning in one area of the circular tissue and thickening in the opposite has been previously discussed and characterized in constrained microtissues [17]. In such prior work, researchers concluded that cell-derived tension from contractile units can lead to tissue necking, and subsequent failure. Mathematical modeling of such failure exists, with the researchers generating constitutive equations to approximate the failure kinetics of constrained microtissues, and future work developing such models for our 3D tissue constructs could be completed, but is currently beyond the scope of the work presented. The researchers did indicate that solutions to tissue necking and failure include tuning the tissue stiffness, and/or modulating the ECM composition within the microtissues [17]. ECM modulation is discussed in the next section, whereas the tissue stiffness modulation was attempted in a different manner - namely we modulated the tissue mold to allow for tissue relaxation - effectively decreasing the tissue stiffness during growth and maturation.

The decrease in seeding volume by 33% from 55 μ l to 37.5 μ l was another concern to the researchers, as there would potentially not be sufficient nutrients available in the media to maintain cell viability during the first 24 hrs. of seeding (following 24 hrs, the entire system is flooded with media, making the reduced seeding volume negligible). While the volume of the media is decreased, it is decreased at the same ratio as that of the cell number, indicating that there is no decrease in available nutrients/cell basis. Seminal work by Jeff Morgan's group [20] demonstrated that cell aggregates could be formed in an array setting in a volume of media with similar cell to volume ratio and that the resulting spheroids created maintained viability [20]. More recent work from the same research group indicated that similarly-shaped tissues, termed toroids, could be formed with smaller cell numbers in smaller geometrical ring-shaped morphology with no loss in viability due to decreased nutrient availability, indicating further that decreasing cell number and media volume is not detrimental to the culture [18].

The amount of tissue contraction can be a measure of the force the tissue is capable of producing. One such manner to measure the force that such tissue constructs are capable of producing could involve simply measuring the diameter reduction that occurred during long-term culture. Such length-shortening relationships have been used successfully to quantify the strength of benchtop skeletal muscle microtissues by a pioneer in the field of skeletal muscle research, whereby mechanical data could be interpreted by the degree of beam bending by two flexible posts serving as anchor points for a skeletal muscle microtissue [21]. Similar mechanical models could be created based on the geometry of the cylindrical posts used in this work, if a different means of determining contractile force was necessary [17].

A more crucial question was to determine if there was a limit of the tissue contraction, e.g. were the tissues still under circumferential tension, or did they contract to a diameter that no longer results in anchored tissue. While it is challenging to quantify the degree of contractility due to the

movement of tissues up the conical posts, we can (and have) quantified the degree of diameter shortening that occurs when the tissues are allowed to freely contract, which was roughly 40%. Prior work by Lee et al. [22] demonstrated that skeletal muscle atrophy could be modeled using benchtop skeletal muscle bioartificial muscles (BAMs) anchored between two posts by reducing the length of the tissues by 50%, indicating that a further reduction of tissue diameter may induce atrophy in our tissue models, and correlating to our observation that following a 40% reduction in diameter, the tissue remains in a tensile state whereby further contraction is possible following the removal of anchorage [22].

Finally, it is challenging what mechanisms are influenced by the tissue contracting up the conical post during maturation. Prior work has shown that the application of mechanical stimuli improves the maturation of skeletal muscle tissue constructs when compared to tissues cultured under purely static conditions [23, 24]. Furthermore, during embryonic development, skeletal muscle undergoes substantial mechanical motion, thought to play a crucial role in the development of functional muscle tissue. We can conclude that the tissue contraction up the conical posts likely provides some cell motility that improves the differentiation and maturation potential of the tissue constructs, and that the contracted tissue is still under contractile tension, firmly anchored around the post. Active skeletal muscle motion during development has been well characterized during embryonic development [3].

4.4.2. The Increase in ECM Production Strengthens Cell-ECM Connections

The increase in ECM production observed following the addition of ascorbic acid correlated to prior work found in literature, where researchers utilized concentrations of ascorbic acid between 50-100 μ g/ml was added to increase the ECM production of skeletal muscle 3D tissue constructs [14, 15]. Our optimization study determined that there is a concentration-mediated response to ascorbic acid levels added to the culture medium which correlates to prior work that has used ascorbic acid to increase myogenic differentiation of skeletal muscle [25].

The addition of ascorbic acid to the culture medium also likely increased the production of collagen I, as observed in prior work that utilizes ascorbic acid to increase ECM production in skeletal muscle tissue constructs [14, 26]. Collagen I is found in native skeletal muscle, however, in higher abundance at myotendonous junctions closer to bone attachment points. While Collagen I is typically considered the collagen type that promotes scar formation, there is an interplay between the various types of collagen. Ascorbic acid has been shown previously to promote secretion of various types of collagen, however, especially during the early-stage of myoblast differentiation, the presence of any kind of collagen can increase crucial cell-ECM contacts and thus encourage native levels of differentiation and maturation [25, 27, 28].

Ascorbic acid has been previously shown to increase ECM production of resident fibroblasts within skeletal muscle. Interestingly, the ascorbic acid supplementation had an effect on entirely-myoblast tissues to a similar degree as the fibroblast-supplemented tissues. This could be due to the non-pure myoblast population that is used for experimentation. While prior work confirmed that this primary culture was at least 90% desmin-positive (a myogenic cell marker), the presence of a small percentage of non-myogenic cells may also be capable of synthesizing ECM protein. Additionally, the ascorbic acid may also stimulate secretion of ECM proteins from the myocytes.

4.4.3. Rationale for Myotube Diameter Increase Following IGF-1 Supplementation

Prior research has indicated that similar concentrations of IGF-1 have a beneficial effect on myotube differentiation, showing that 100ng/ml IGF-1 statistically increase myotube hypertrophy of myotubes within a 3D collagen gel model, compared to unsupplemented controls [10, 21]. Following IGF-1 supplementation in our tissue constructs, we calculated the diameter of the myotubes, and demonstrated that a statistical increase in diameter occurred following supplementation.

We did not report this data as being an indication of myotube hypertrophy as prior researchers have done, as we were unsure how to properly quantify hypertrophy, as doing so would require us to

normalize the diameter of each myotube to the number of nuclei within each myotube. Such calculation could allow us to determine if a normalized number of nuclei contribute to thicker myosin-positive myotubes. As mentioned previously, a limiting factor to benchtop skeletal muscle tissue models is the lack of myotubes reaching the diameter of native myotubes. Completing such hypertrophy calculation could be done, but was beyond the scope of this project, as we demonstrated a marked increase in maturation following IGF-1 incorporation.

4.5 Conclusion

In conclusion of this aim, several optimizations and improvements were made to the methodology and culture conditions of the 3D tissue rings that resulted in a tissue that better emulates the structure and function of native muscle. Firstly, a mold redesign resulted in tissues that can be generated with 33% fewer cells while maintaining the same rate of tissue formation success. Furthermore, the mold redesign yielded tissues that fail significantly less frequently during culture. This improvement in ring retention over the 14 day culture period creates a more high-content tissue generation platform as compared to previous work completed with the annular well/cylindrical post system. Finally, the new mold redesign improved the percentage of cells that stained positive for myosin protein following 14 days in culture. This increase in myosin nuclei may indicate that the ability of the tissue to contract up the conical post improves the ability of the cells to differentiate, as the conical posts allow for cell/tissue motility during culture vs. the original annular posts, where the tissue is cultured and matured in a completely static system.

The next component of this aim involving ascorbic acid supplementation was done to increase the amount of endogenous ECM protein that the fibroblasts synthesize during 3D culture. The data indicated that an optimal concentration of ascorbic acid (100 μ g/ml) resulted in a measurable increase in salient skeletal muscle ECM proteins following 3D culture. Such concentration was determined to be optimal as there was a measurable improvement in overall ECM protein production compared to the next lowest-tested concentration, while the next highest-tested concentration yielded no improvement on the ECM protein production, therefore, indicating that no further beneficial gain is accomplished by increasing the concentration of ascorbic acid.

The final culture modification involved IGF-1 supplementation to improve myotube hypertrophy following 3D culture. Following 100ng/ml IGF-1 supplementation a quantitative increase in myotube hypertrophy was observed with tissue within the 87.5° post molds, indicating that IGF-1 can modulate

the diameter of myotubes *in vitro* using our tissue culture system. Furthermore, such an improvement allows for these benchtop models of skeletal muscle to begin to close the functionality and contractile force production gap between native muscle and other skeletal muscle tissues models.

In summary, this aim presented categorical improvements to tissue formation mold and culture medium that facilitate the production of skeletal muscle tissue analogues that more closely mimic the morphology and functionality of native muscle better than existing models.

4.5 References

1. Cook, C.A., et al., *Characterization of a novel bioreactor system for 3D cellular mechanobiology studies*. Biotechnol Bioeng, 2016. **113**(8): p. 1825-37.
2. Cimetta, E., et al., *Enhancement of viability of muscle precursor cells on 3D scaffold in a perfusion bioreactor*. Int J Artif Organs, 2007. **30**(5): p. 415-28.
3. Racca, A.W., et al., *Contractility and kinetics of human fetal and human adult skeletal muscle*. J Physiol, 2013. **591**(12): p. 3049-61.
4. Zou, Y., et al., *Muscle interstitial fibroblasts are the main source of collagen VI synthesis in skeletal muscle: implications for congenital muscular dystrophy types Ullrich and Bethlem*. J Neuropathol Exp Neurol, 2008. **67**(2): p. 144-54.
5. Lamandé, S.R., et al., *The Role of the $\alpha 3$ (VI) Chain in Collagen VI Assembly: EXPRESSION OF AN $\alpha 3$ (VI) CHAIN LACKING N-TERMINAL MODULES N10–N7 RESTORES COLLAGEN VI ASSEMBLY, SECRETION, AND MATRIX DEPOSITION IN AN $\alpha 3$ (VI)-DEFICIENT CELL LINE*. Journal of Biological Chemistry, 1998. **273**(13): p. 7423-7430.
6. Nieponice, A., et al., *Development of a tissue-engineered vascular graft combining a biodegradable scaffold, muscle-derived stem cells and a rotational vacuum seeding technique*. Biomaterials, 2008. **29**(7): p. 825-33.
7. Kinney, M.A., et al., *Engineering three-dimensional stem cell morphogenesis for the development of tissue models and scalable regenerative therapeutics*. Ann Biomed Eng, 2014. **42**(2): p. 352-67.
8. Gillies, A.R. and R.L. Lieber, *Structure and function of the skeletal muscle extracellular matrix*. Muscle Nerve, 2011. **44**(3): p. 318-31.
9. Li, M., et al., *The role of fibroblasts in self-assembled skeletal muscle*. Tissue Eng Part A, 2011. **17**(21-22): p. 2641-50.

10. Shansky, J., et al., *Paracrine release of insulin-like growth factor 1 from a bioengineered tissue stimulates skeletal muscle growth in vitro*. *Tissue Eng*, 2006. **12**(7): p. 1833-41.
11. Sacheck, J.M., et al., *IGF-I stimulates muscle growth by suppressing protein breakdown and expression of atrophy-related ubiquitin ligases, atrogin-1 and MuRF1*. *Am J Physiol Endocrinol Metab*, 2004. **287**(4): p. E591-601.
12. Temu, T.M., et al., *The mechanism of ascorbic acid-induced differentiation of ATDC5 chondrogenic cells*. *American Journal of Physiology - Endocrinology and Metabolism*, 2010. **299**(2): p. E325-E334.
13. Balguid, A., et al., *Hypoxia induces near-native mechanical properties in engineered heart valve tissue*. *Circulation*, 2009. **119**(2): p. 290-7.
14. Kostrominova, T.Y., et al., *Ultrastructure of myotendinous junctions in tendon-skeletal muscle constructs engineered in vitro*. *Histol Histopathol*, 2009. **24**(5): p. 541-50.
15. Larkin, L.M., et al., *Structure and functional evaluation of tendon-skeletal muscle constructs engineered in vitro*. *Tissue Eng*, 2006. **12**(11): p. 3149-58.
16. Karalaki, M., et al., *Muscle regeneration: cellular and molecular events*. *In Vivo*, 2009. **23**(5): p. 779-96.
17. Wang, H., et al., *Necking and failure of constrained 3D microtissues induced by cellular tension*. *Proc Natl Acad Sci U S A*, 2013. **110**(52): p. 20923-8.
18. Napolitano, A., et al., *Scaffold-free three-dimensional cell culture utilizing micromolded nonadhesive hydrogels*. *BioTechniques*, 2007. **43**(4): p. 494-500.
19. Tanaka, N., et al., *Microcasting with agarose gel via degassed polydimethylsiloxane molds for repellency-guided cell patterning*. *Rsc Advances*, 2016. **6**(60): p. 54754-54762.
20. Napolitano, A.P., et al., *Dynamics of the self-assembly of complex cellular aggregates on micromolded nonadhesive hydrogels*. *Tissue Eng*, 2007. **13**(8): p. 2087-94.
21. Vandeburgh, H., et al., *Drug-screening platform based on the contractility of tissue-engineered muscle*. *Muscle Nerve*, 2008. **37**(4): p. 438-47.
22. Lee, P.H. and H. Vandeburgh, *Skeletal muscle atrophy in bioengineered skeletal muscle: a new model system*. *Tissue Eng Part A*, 2013. **19**(19-20): p. 2147-55.
23. Powell, C.A., et al., *Mechanical stimulation improves tissue-engineered human skeletal muscle*. *Am J Physiol Cell Physiol*, 2002. **283**(5): p. C1557-65.
24. Hicks, M.R., et al., *Mechanical strain applied to human fibroblasts differentially regulates skeletal myoblast differentiation*. *Journal of Applied Physiology*, 2012. **113**(3): p. 465-72.
25. Ikeda, K., et al., *Effects of heat stimulation and l-ascorbic acid 2-phosphate supplementation on myogenic differentiation of artificial skeletal muscle tissue constructs*. *J Tissue Eng Regen Med*, 2015.
26. Larkin, L.M., et al., *Functional evaluation of nerve-skeletal muscle constructs engineered in vitro*. *In Vitro Cell Dev Biol Anim*, 2006. **42**(3-4): p. 75-82.
27. Savini, I., et al., *Vitamin C homeostasis in skeletal muscle cells*. *Free Radic Biol Med*, 2005. **38**(7): p. 898-907.
28. Dumont, N.A., et al., *Satellite Cells and Skeletal Muscle Regeneration*. *Compr Physiol*, 2015. **5**(3): p. 1027-59.

Chapter 5: Functional contractile and mechanical properties are improved following culture and mold modifications

5.1 Introduction

The previous two chapters demonstrated the ability to generate benchtop 3D skeletal muscle tissues and established culture and mold modifications that improve tissue ring longevity along with maturation and production of ECM and contractile proteins.

Yet still, functional measurements have yet to be conducted to attempt to correlate the morphological improvements with physical structural and functional improvements. Past researchers have quantified the force of bioartificial muscle (BAM) tissue contractile measurements and have shown that measurable improvements in tissue structure and morphology result in increases in functional force generation. Specifically, fibrin-based tissue constructs have shown to generate tetanic force of approximately 120 μ N of force, yet, the tissue was already passively contracting between 400-700 μ N, indicating that close to 1N of force can be generated [1]. Furthermore, past work has indicated that subtle changes in tissue morphology, including increases in myotube diameter due to IGF-1 supplementation, can generate measurable contractile force generation [1].

To date, minimal work has been completed on testing and determining mechanical strength properties of engineered skeletal muscle tissue constructs. However, similar work has shown that engineered fibrin biopolymer microthreads can have tunable mechanical properties following subtle changes in scaffold crosslinking [2]. Substantial other work has shown that measurable mechanical strength properties of healthy human muscle can be generated, as that muscle displays an anisotropic behavior due to the linearly-aligned structure [3]. These past studies suggest that we can generate quantitative data through mechanically-testing our 3D tissue constructs to elucidate the role that certain mold and culture supplements have on increasing crucial cell-ECM bonds, and subsequently increasing gross tissue strength and ability to withstand a load [3].

Additional work to generate functional skeletal muscle data has utilized animal modeling. Such experiments have aimed to quantify the increase in skeletal muscle force production following an injury and subsequent clinical intervention. Variables including implanted scaffold crosslinking differences coupled with cell therapy have resulted in quantifiable and measurable differences in *in vivo* contractile force production [4, 5]. And while beneficial information is gathered from animal modeling, the purpose of this project was to avoid issues of poor clinical translation and as such, avoid the use of animal modeling to confirm tissue functionality. As such, the purpose of this study was to correlate the improvements in the observed tissue morphology due to the inclusion and optimization of culture supplements and mold architecture to functional mechanical strength and contractile force generation measurements.

5.2 Methods

5.2.1. Tissue Mechanical Strength Quantification

To determine the mechanical strength of the tissue rings, the following experimental protocol was conducted using the types of 3D tissues with the noted supplements, as shown in *Table 5* below, to elucidate the role that both the mold variation along with the culture supplements have on overall tissue mechanical strength.

Table 5: Ring Types and Supplements Used for Mechanical Testing

The four different conditions used for mechanical and contractile force testing. Regular ring molds and 87.5° post molds were used and each type of ring was either supplemented with ascorbic acid and IGF-1 or unsupplemented.

Ring Type	Supplements
Regular Annular Cylindrical	Ascorbic Acid + IGF-1
Regular Annular Cylindrical	None
87.5° Conical	Ascorbic Acid + IGF-1
87.5° Conical	None

Following 14 days in culture, ring thickness of the remaining intact tissues were initially measured while the ring remained on the agarose post, and then carefully removed from the post using a 1.0mm flamed-pulled and polished glass capillary, to ensure that the ring integrity wasn't damaged during the handling process. To maintain physiologic conditions, rings were moved to a dish containing DPBS maintained at 37°C.

To measure the mechanical strength of the tissues, an Instron ElectroPuls E1000 electrodynamic mechanical testing machine was used. A 1 Newton (1N) force transducer was mounted to the anchored side, while the opposite side actuates linearly. Briefly, two separate flame-pulled and polished glass capillary tubes were bent such that the tips of the two glass pieces could be used to hold the ring from opposite directions. The glass was bent in so that the ring could be incubated in a small dish of DPBS heated to 37°C while suspended atop a small jack between the actuator heads. Seen below in *Figure 38* (with a higher magnification, side-view image shown in *Figure 39*) is an image of the complete setup showing the linear actuator head on the left with the fixed anchor attached to the 1N force transducer on the right, with the ring setup shown in the middle.



Figure 38: Mechanical Testing Setup

Two glass hooks bent into a dish of warmed DPBS on an elevated stand. Tissue rings are anchored between the two hooks. The left hook linearly actuates, placing tension on the tissue ring, while the right hook is affixed to a 1N force transducer to record the force applied to the tissue ring.

A different perspective of the mechanical stimulation setup demonstrated that the tissue ring is submerged in warmed DPBS and firmly attached to the two glass hooks, allowing for linear actuation and subsequent mechanical testing and data generation.

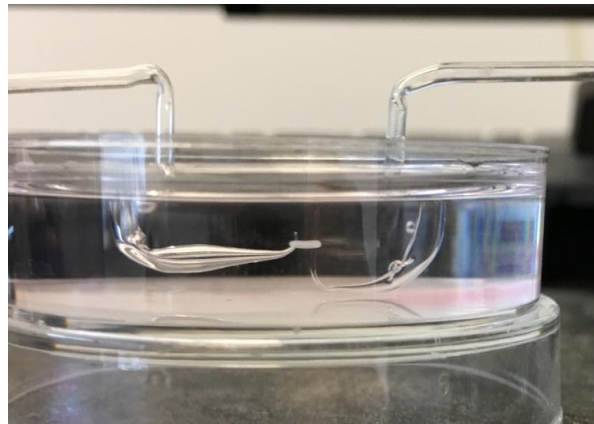


Figure 39: Side-View of Mechanical Testing Setup Showing Ring Anchored Between Glass Hooks
The tissue ring can clearly be seen affixed between the two glass hooks. No part of the glass hooks make contact with the Petri dish, ensuring accurate force readings due to the tissue.

5.2.1.1. Mechanical Testing Parameters

Once the tissue was carefully loaded onto the glass posts submerged in the DPBS, the following mechanical testing protocol was completed, based on similar testing conducted by a collaborator [6]. The tissue rings were initially pre-cycled to possibly align fibrils along the principal axis of strain, prior to strain-to-failure testing. Following the pre-cycling, the rings were pulled to failure at a constant strain rate of 10mm/min. Following each ring failure, the "Grips" were returned to their original starting position and the experiment repeated with the next sample. Raw data including time, force, and extension were collected and used to analyze and calculate mechanical strength parameters including both failure stress and strain, along with elastic modulus.

Following each failure test, the tissue rings were immediately removed from the DBPS and fixed in a tube containing 4% paraformaldehyde, and then prepared for histological/IHC analysis, as previously described.

For each group of tissues, several parameters aimed at elucidating the role that variations in medium supplements and mold design had on overall tissue strength were calculated and reported. For parameters such as load at failure and strain at failure, corrections to the values were made prior to any analysis to normalize the relative force and strain values between the two different tissue groups that contain both a different cell number and initial inner ring diameter. For example, the redesigned molds have 33% fewer cells, therefore, in order for accurate comparisons between mechanical data generated from the measurement of the overall tissue, e.g. force at failure - the force that the tissues are capable of withstanding -to be made, the force values must be corrected by the aforementioned 33% ratio to allow for group to group comparisons. A similar correction was done for the strain at failure, as the starting inner diameter of the tissue rings made using the two different tissue molds is different by almost 50%. Therefore, values generated previously for average ring diameter were used to provide more accurate initial inner diameter measurements. For mechanical data that does not rely on global measurements, e.g. stress at failure, elastic modulus, etc. histological analysis of each ring subjected to mechanical testing allowed for ring diameter measurements, and thus proper calculations of mechanical properties that are functions of the ring geometry.

5.2.2. Active Tetanic Contractile Force Quantification

To measure the contractile force that these 3D ring tissues were capable of generating, an electrical stimulation was coupled with a highly sensitive force transducer, as described below. Briefly, a wire myograph (DMT 610M) was used as a platform for measuring contractile force production. This wire myograph consists of a stainless steel chamber that contains two tissue supports (pins) that are positioned within the chamber. The myograph also contains a heating element that maintains the

stainless steel well at 37°C. Furthermore, this myograph has an oxygen infusion setup that bubbles oxygen into the well, to ensure that the fluid within the well that the ring is submerged into remains highly oxygenated. Both the heat and oxygenation are crucial for generating a contraction from live tissues. To ensure maximal tissue contraction, a defined potassium-rich physiologic salt solution buffer (K-PSS buffer) previously used to generate maximal tissue contraction was used (*Table 6*) [7].

Table 6: 60mM K-PSS Bicarbonate Buffer Recipe

The buffer used for facilitating tissue contraction when using the myograph unit, the millimolarity of the chemicals along with the weight in grams needed to make 1L of buffer [7]

Chemical	Molecular Weight	mM	g/L
NaCl	58.45	74.7	4.37
KCl	74.557	60	4.47
KH ₂ PO ₄	136.09	1.18	0.16
MgSO ₄ - 7H ₂ O	246.498	1.17	0.29
NaHCO ₃	84.01	14.9	1.25
Dextrose	180.16	5.5	1.00
CaNa ₂ Versenate (EDTA)	372.2	0.026	0.0097
CaCl ₂	110.99	1.6	0.235

A concentrated solution of the K-PSS buffer was made using 80% of the final working volume to enable the addition of fresh 1.0M solution of CaCl₂ (110.00/CaCl₂ - H₂O = 147.026) immediately prior to use. To make complete buffer, 1.6mL of the 1.0M CaCl₂ was slowly added to the 80% volume of K-PSS while vigorously stirring. Once dissolved, the final volume of the K-PSS buffer was brought up to 1L, and stored at 4°C for no more than 2 weeks, following which, fresh CaCl₂ was added to make fresh K-PSS buffer.

Similar to the Instron setup, the wire myograph is capable of measuring the isometric contractile force on the tissue ring, as one of the two grips contains a highly-sensitive calibrated force transducer with a resolution of 10µN. The two tissue pins can be manually actuated to facilitate initial tissue loading and subsequent tension generation prior to electrically stimulated tissue contraction.

To facilitate an action potential and subsequent contraction of the myotubes within our 3D tissue rings, a custom-modified electrical stimulation platform was incorporated within the myograph. Briefly, a BIOPAC MP-100 system (BIOPAC Systems, Inc., Goleta, CA) was used to apply a 4V electrical stimulation with a 4 ms pulse duration, with 20ms pulse intervals, to generate a tetanic contraction of the 3D tissue ring. Such conditions have been used previously to generate an action potential and measurable tetanic contractile force using a similar force transducer setup, from the tibialis anterior muscle of a mouse [4]. An Image of the DMT Myograph and a schematic of the electrode placement is shown in *Figure 40*.

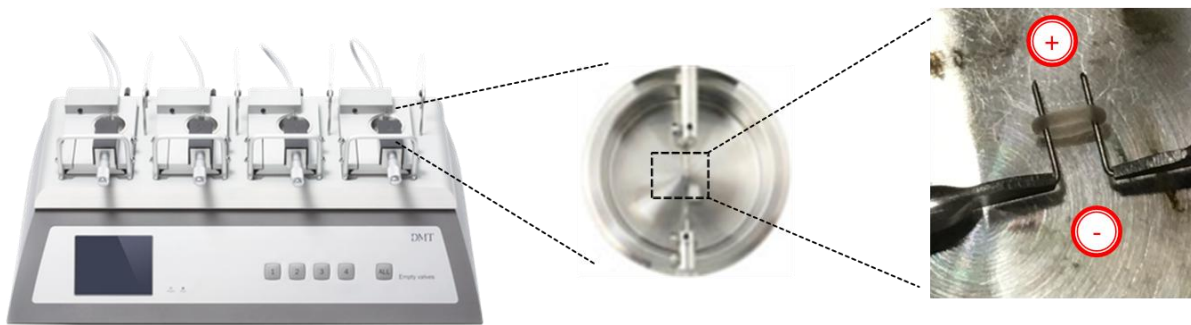


Figure 40: Image and Schematic of DMT Myograph and Electric Field Setup

The DME myograph showing the interface screen and 4 individual testing wells (left). An individual testing well (center), with a higher-magnification image showing the tissue ring anchored between the two stainless steel hooks with a schematic of the electric lead placement perpendicular to the tissue (right).

Similar to the mechanical testing setup, the tissue rings were carefully removed from the agarose posts, submerged in DPBS and looped around the two sets of pins (*Figure 40 right*). During active recording by the force transducer, positive and negative stainless steel electrodes were submerged into the buffer containing the tissue ring and maintained on either side of the tissue ring, creating an electrical field across the tissue ring, perpendicular to the direction of contraction. Tissue contraction was actively measured and recorded by the DMT software for the duration of the test. Following contractile force measurements, the tissues were immediately fixed in 4% paraformaldehyde and prepared for histological/IHC analysis, as previously described.

5.2.3. Statistics

For all experimentation, sample sizes of tissue rings are reported here: For mechanical testing of the tissue rings, a total of 4 replicates of each test were completed, with each group containing a minimum of 6 tissue rings (a minimum of 24 tissue rings total/condition). For tetanic contraction of the tissue rings, a total of 3 replicates were completed, with each group containing a minimum of 4 tissue rings (a minimum of 12 tissue rings total/condition). All data is presented as mean \pm Standard Error of Measurement (SEM). For analysis requiring statistical inference, a Student's t-test was used to determine significance between individual test groups, (at a critical p-value <0.05).

5.3 Results

The purpose of this study was to quantify the functionality of the 3D tissue rings, and attempt to correlate categorical improvements seen morphologically following culture and mold modifications to the mechanical properties and contractile functionality of the 3D ring tissues. To complete this aim, first, mechanical strength properties were generated by subjecting the tissue rings to a tensile failure test, and second by electrically stimulating a tetanic contraction and measuring the resultant force production of the tissue rings.

5.3.1. Culture Mold and Supplement Modifications Improve Functional Mechanical Strength and Tensile Properties of 3D Tissue Rings

Tissues were cultured for 14 days in their defined mitogen-reduced differentiation medium, with certain groups supplemented, as defined previously in *Table 5*. To minimize tissue failure during manipulation, care was taken to not pinch or forcibly manipulate the tissues during handling. Any ring failure that occurred prior to the tissue ring entering the elastic region (e.g. during or prior to the tissue completing the "toe" region of the characteristic stress-strain graph) was removed from the mechanical analysis, as either a defect in the tissue, or a defect caused by handling and mounting affected tissue integrity, and defined as outlier data. A characteristic load vs. time (red) and extension vs. time (blue) graph of a tissue ring pulled to failure at a constant rate of 10mm/min is shown below in *Figure 41*.

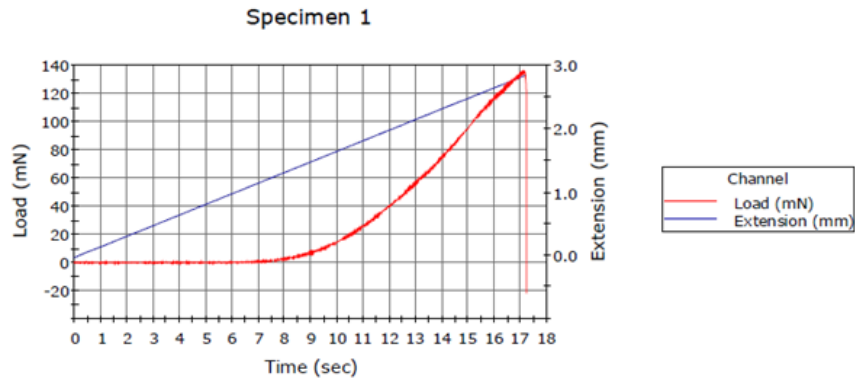


Figure 41: Load vs. Extension Graph

Characteristic load vs. time and extension vs. time graph for a tissue ring pulled to failure at 10mm/min.

Initial mechanical analysis of the tissue rings indicated that the failure force for rings containing ascorbic acid and IGF-1 was statistically greater than comparable rings not containing those two supplements. Regular annular ring molds containing ascorbic acid and IGF-1 resulted a failure load of 126mN +/-51mN, compared to non-supplemented regular annular tissue rings, which resulted in a failure load of 3mN +/- 0.7mN. Similarly, the 87.5° post rings supplemented with ascorbic acid and IGF-1 resulted in a maximum failure load of 102mN +/- 44mN, compared to the unsupplemented tissues that had a failure load of 2.6mN +/- 0.9mN. For both the regular annular and 87.5° post tissues, a statistical increase in failure load was observed following the addition of ascorbic acid and IGF-1, $p < 0.05$, Student's t-test, $n > 4$ groups/condition. A graph summarizing the above data of the failure load is shown in *Figure 42*.

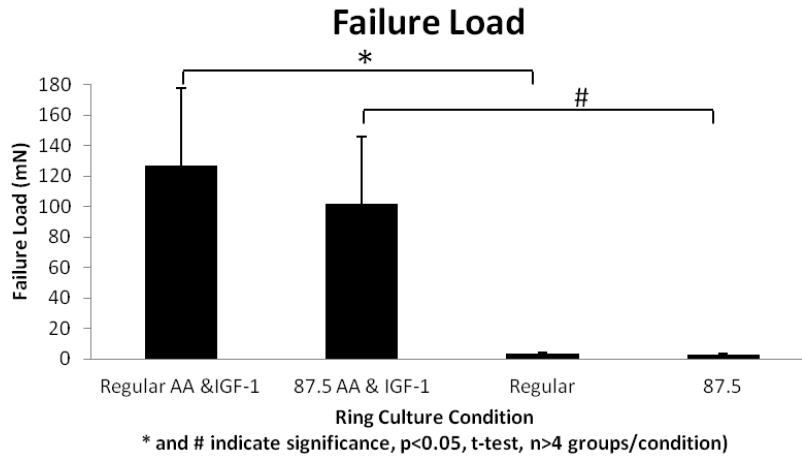


Figure 42: Failure Load of Tissue Rings

The failure load of the supplemented tissues (both annular and 87.5° post tissues) are statistically higher than comparative unsupplemented tissues.

To demonstrate that the cross-sectional areas of the ring tissues were minimally impacted by the addition of the supplements, calculated cross sectional areas are shown below in *Figure 43*. Additionally, qualitative decreases in cross-sectional areas are observed with the 87.5° sloped post tissues, validating the methodology that utilized 33% fewer cells to form those tissues, compared to the regular annular tissues.

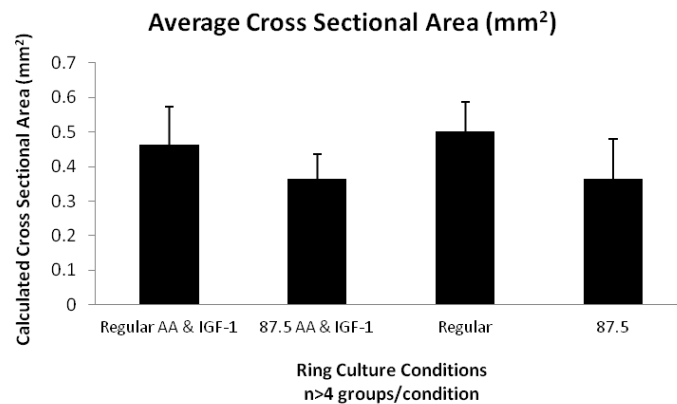


Figure 43: Cross-Sectional Area of Tissue Rings

The cross-sectional areas are qualitatively consistent between groups, with observed decreases between regular and 87.5° tissue rings due to the 33% decrease in cell seeding number.

The maximum extension of the four different tissue groups was also tested. For the regular annular tissues, no statistical difference was observed between rings supplemented with ascorbic acid and IGF-1 compared to unsupplemented rings, (2.62% +/- 0.31% vs. 2.70% +/- 0.25%, respectively).

However, the 87.5° post tissues supplemented with ascorbic acid and IGF-1 did demonstrate a decrease in percentage extension compared to the unsupplemented tissues, (1.52% +/- 0.33% vs. 2.58% +/- 0.38%, respectively), $p < 0.05$, Student's t-test, $n > 4$ groups/condition. A graph summarizing the failure extension is shown in *Figure 44*.

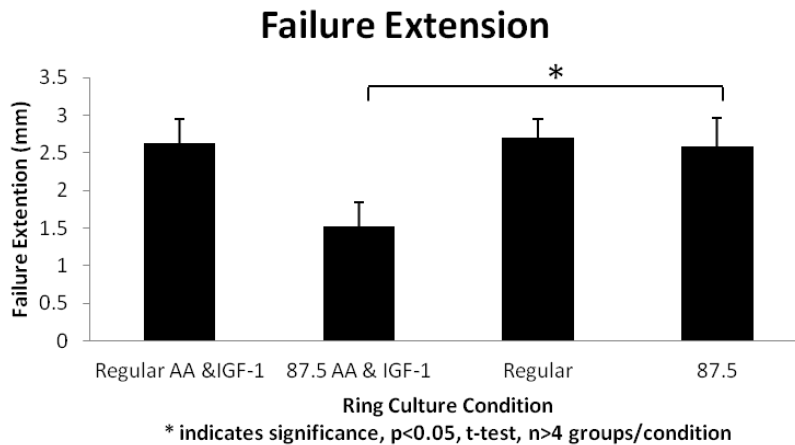


Figure 44: Failure Extension of Tissue Rings

The failure extension of the supplemented 87.5° post tissues was statistically lower than comparative unsupplemented controls, whereas regular annular well tissues did not results in a change in failure extension.

Calculations of tissue mechanical properties were also completed to better correlate the relationship between the two different tissue models. The ultimate tensile strength (UTS) was calculated by determining the area of tissue subjected to mechanical loading. As tissue rings were approximated as cylinders and thus containing circular cross-section, only the ring diameter was needed to calculate the cross-sectional area of the tissue (*Figure 43*). As the ring was looped around the posts, shown in *Figure 39*, the area subjected to the mechanical loading was doubled, as the load was distributed between two sides of the tissue ring during mechanical testing.

The UTS of the regular annular rings supplemented with ascorbic acid and IGF-1 was statistically greater than the unsupplemented rings, (253 kPa +/- 93 kPa vs. 9 kPa +/- 3 kPa, respectively). Similarly, the 87.5° sloped post tissues supplemented with ascorbic acid and IGF-1 demonstrated a statistical increase in UTS compared to the unsupplemented tissues, (232 kPa +/- 77 kPa vs. 5 kPa +/- 1 kPa),

$p < 0.05$, Student's t-test, $n > 4$ groups/condition. In both cases (annular regular and 87.5° sloped), the increase in UTS was greater than 1 order of magnitude, indicating that the addition of the two supplements greatly increased the tensile strength of the tissues, independent of the tissue size. A graph summarizing the UTS of the tissues is shown in *Figure 45*.

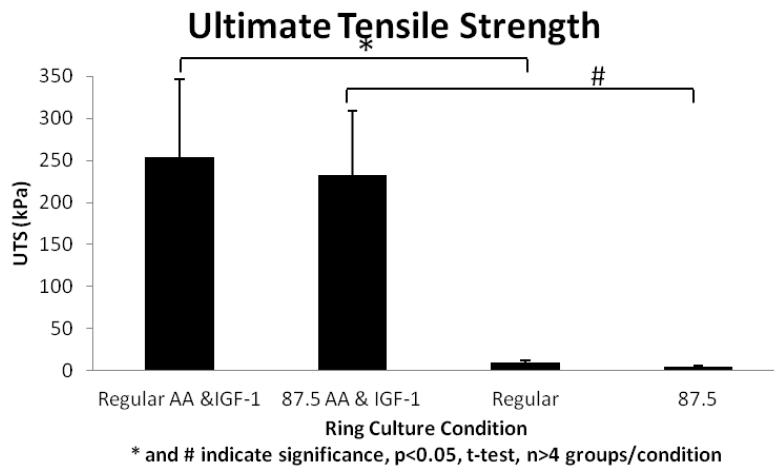


Figure 45: UTS of Tissue Rings

The Ultimate Tensile Strength of the supplemented tissues (both 87.5° and regular annular post tissues was statistically higher than comparative unsupplemented controls.

The failure strain of the tissue was also calculated to determine if the tissues of different size, (the 87.5° posts have a diameter of roughly 60% of that of the regular annular tissues following 14 days of culture), have a different strain profile following tensile testing. Similar to the extension data, the failure strain of the supplemented vs. unsupplemented regular annular tissues was statistically unchanged, (83% +/- 10% vs. 82% +/- 6%, respectively). However, the 87.5° posts that were supplemented as described previously, did have a statistically lower strain at failure compared to the unsupplemented tissues, (62% +/- 14% vs. 86% +/- 9%, respectively, $p < 0.05$, t-test, $n > 4$ groups/condition). A graph summarizing the failure strain is shown in *Figure 46*.

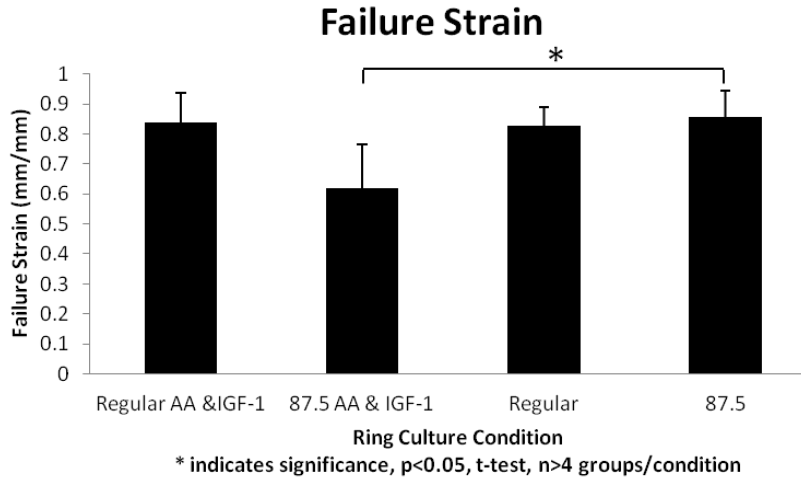


Figure 46: Failure Strain of Tissue Rings

The failure strain of the supplemented 87.5° post tissues was lower than comparative unsupplemented controls whereas regular annular post tissues did not have a statistically-significant difference between supplemented and unsupplemented tissues.

5.3.2. Active Tetanic Contractile Force Production is Increased for Supplemented Tissues

Tissues were cultured for 14 days in their defined culture medium, as shown previously in *Table 5*. The same tissue conditions used for the generation of mechanical data presented in the previous section were used for the contractile function generation experiment, to further allow for cross-condition correlations to be drawn with regards to the contractile force production between the various conditions. As described previously, tissues were carefully removed from the agarose posts and loaded onto the small wire posts of the DMT myograph, an image of a tissue ring on the myograph, as shown in *Figure 40 (right)*. Following tetanic stimulation and subsequent tissue contraction, contractile force production values were measured.

A similar trend was observed with the contractile force production as seen with the mechanical testing, in which the tissue rings supplemented with ascorbic acid and IGF-1 displayed a statistically higher contractile force production, as compared to the similar unsupplemented tissues. For the regular annular rings, the average measured tetanic contractile force for the supplemented vs. unsupplemented tissues was 2.6 mN +/- 1.1 mN vs. 0.03mN +/- 0.04mN, respectively. For the 87.5° post rings, a similar statistically-significant trend was observed, (1.6 mN +/- 1.0mN vs. 0.02mN +/- 0.01mN), for the

supplemented vs. unsupplemented tissues, respectively ($p < 0.05$, t-test, $n > 8$). For the unsupplemented tissues, the amount of contractility observed was measured at the lower limits of the force transducer resolution, whereas the supplemented tissues resulted in a measurable and clear isometric tissue contraction. A graph summarizing the tetanic tissue force for each of the 4 groups is shown in *Figure 47*.

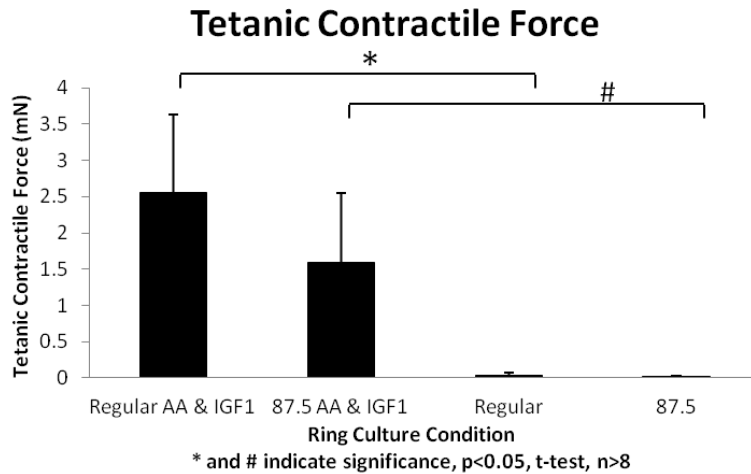


Figure 47: Tetanic Contractile Force of Tissue Rings

Tetanic contractile force production for supplemented tissues (both 87.5° and regular annular post tissues was statistically greater than comparative unsupplemented tissues.

The tensile stress of the tissue contractile force production was also calculated. Due to the relatively similar size (and subsequent cross-sectional area of the tissues, regardless of the groups/supplements), the trends observed in the tetanic contractile force (*Figure 47*) mimicked the calculated tensile stress shown in *Figure 48*.

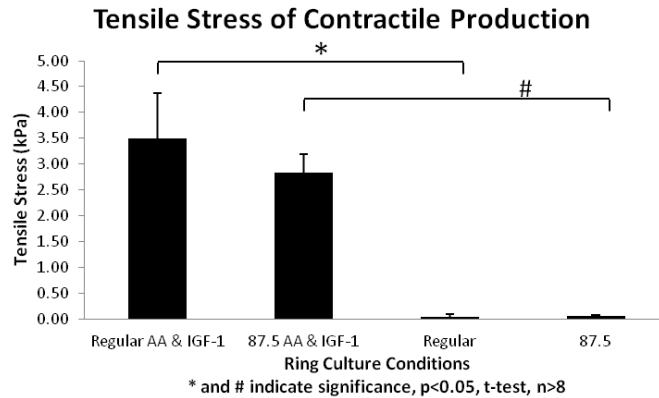


Figure 48: Tensile Stress of Contractile Force Production
Tensile stress of the contractile force production of the tissues following electrical stimulation indicate that the supplemented tissues (both regular and 87.5°) had a higher stress than unsupplemented tissues.

5.4 Discussion

5.4.1. Culture Mold Modifications Improve Mechanical Strength and Tensile Properties of 3D Tissue Rings

Prior to mechanical testing, qualitative observations were made regarding the compaction of the tissue rings following removal from the anchored agarose posts. For all tissues types and supplementations, following the removal from the agarose posts, the tissues quickly compacted into spheres within 3-5 minutes, indicating that the tissues maintain the ability to compact. Future work could investigate quantification of compaction speed and relate such values to cell power, however, this was not completed in the present work.

Our data showed clear differences between the unsupplemented controls and the ascorbic acid/IGF-1 supplemented tissue rings for both the regular and 87.5° tissue rings. Perhaps most prominently, the failure loads of supplemented tissues were over an order of magnitude higher than unsupplemented controls. This, and other mechanical data presented in this section, was an interesting observation, as there was very minimal observed differences in both tissue morphology and contractile

protein production. This finding indicates that the ECM that the cells are facilitated to produce by the ECM, coupled with the myotube diameter increase with the IGF-1 result in tissues that are capable of withstanding substantially more force prior to failure. While the addition of ascorbic acid does not result in a morphological observed difference in tissue structure, as shown by the hematoxylin and eosin staining, the increase in more mature ECM proteins as mediated by ascorbic acid supplementation appear to significantly increase the capability of the tissue to withstand load, whereas unsupplemented tissues sheared and failed at much lower force values. Past research has highlighted the importance of a sufficiently mature ECM to facilitate native levels of functionality [8].

In terms of extension, the extension for the regular tissue rings with and without supplements were roughly the same, indicating that the addition of supplements did not affect the extension of the tissues when subjected to failure strain. However, the 87.5° tissue rings demonstrated a decrease in failure extension for the tissues supplemented with ascorbic acid and IGF-1. This suggests that the supplements are increasing more cell-cell binding forces, and decreasing cell-ECM slipping, as there is less extension within identical tissues with the same cell number.

As the tissues with and without supplementation within the same group (either regular or 87.5 ° tissues) were indiscernible in size, shape, and morphology, calculated mechanical properties including UTS and failure strain mimicked trends seen with raw mechanical data values. However, it is important to note that the 87.5° tissue rings contained 33% fewer cells, therefore, having fewer cells participating in mechanical testing and analysis. Not surprisingly, the failure load of the 87.5° tissues were lower than the regular mold tissues due to the decrease in cell number. When the UTS data was calculated factoring in the cross sectional area of the tissues, it is important to note that despite 33% fewer cells, the UTS of the supplemented 87.5° tissues is not statistically different than the supplemented regular tissues.

Additionally, the failure loads are raw data values that do not consider the tissue size or shape. As such, by normalizing the failure load to correct for the 33% reduction in cell number participating in the mechanical testing shown in *Figure 49* below, is generated. The corrected failure load values, shown in red indicate that the 87.5° tissues are able to withstand more force when subjected to uniaxial failure testing.

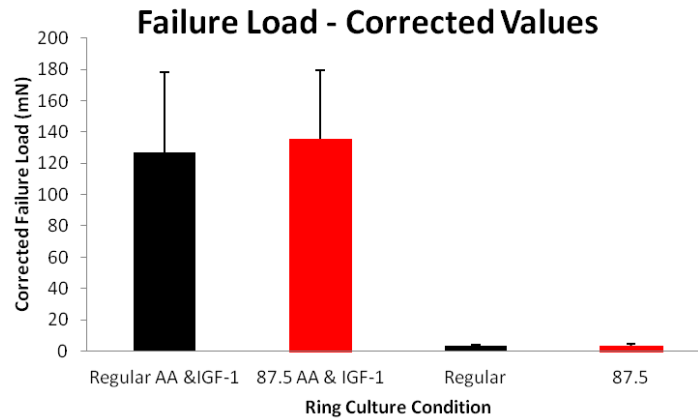


Figure 49: Failure Load of Tissue Rings

Corrected for cell seeding number to normalize mechanical testing values to cell number.

These data indicate that there is a clear increase in overall tissue strength and capability to withstand load between regular and 87.5° supplemented tissues, such that the supplementation coupled with the conical posts increased the strength of the tissues to a higher degree than the regular post tissues.

Largely, mechanical strength experiments have been limited to engineered biomaterials [2] or a variety of healthy tissues [3], as more direct comparisons can be made to normal or native tissue structures and strength. To date, minimal work has been completed on engineered skeletal muscle tissue constructs, as mechanical data generated may not have any correlative benchmarks, and as such, most researchers have attempted to quantify function using electrically-mediated contractile force production assays.

5.4.2. Contractile Function is Improved and Correlated with Culture Mold and Supplement Modifications

Our research and experimentation determined that following ascorbic acid and IGF-1 supplementation, measurable increases in tetanic contractile force production was determined and measured between 1-2.5mN of force, whereas unsupplemented tissues did not generate measurable contractile force.

Significant past research has also measured the contractile force of both native skeletal muscle and 3D benchtop tissue models of skeletal muscle. To provide a categorical benchmark to native muscle, past research has indicated that a native muscle fiber consisting of a cross sectional area of between 4,000 and 12,000 μm^2 in area produce an average of 0.5-2mN contractile force [9]. To determine mechanical properties of our tissue rings, the cross sectional area was calculated. On average, the cross sectional area of our microtissues approximated 400,000 μm^2 indicating that our microtissues are over an order of magnitude lower than native muscle. This observation is not surprising, considering that these tissues have only been cultured for 14 days and lack additional components, including tendons, vasculature, and innervation, all of which play a role in native levels of functionality and force transmission [10]. Furthermore, our tissue constructs lack completely matured myotubes, as noted by the lack of both sarcomeric myosin within the myotubes along with the centrally-aligned nuclei, both indicators of incomplete maturation of the myotube.

Throughout literature, researchers have also measured the contractile force of 3D skeletal muscle tissue constructs [1, 11]. One research group generating collagen-gel based linearly-aligned microtissues between two anchored posts determined that the maximum tetanic contractile force approximated 0.1-0.15mN [1, 11]. While these measurements are below the tetanic force production of our tissue constructs, it is important to note the following: These measurements were acquired without removing the tissue from the culture platform containing two posts, as such, the tetanic force is only

recorded as the addition of the active from the current passive force being imparted onto the posts, which was measured numerous times by the researchers, and generally fell between 0.5-1mN [1, 12]. In our experiments, to measure contractile force, the tissue was removed from the original culture platform and hooked up to a force transducer.

In another example of measured force of 3D skeletal muscle tissue constructs, contractility of 3D tissue constructs generated from monolayer culture of myoblasts directed to detach from the culture surface and form contiguous tissue around two minutia pins, was investigated [13, 14]. As described previously, these 3D tissue constructs range between 300-500 μ m in diameter (also resulting a cross sectional area on average very similar to our tissues) and contain a significant percentage of exogenous ECM which facilitated 3D tissue formation. Following tetanic force stimulation, the 3D constructs produced an average of 0.3mN force [14].

We postulated that our tissue constructs generated slightly more measurable tetanic contractile force than prior benchtop skeletal muscle tissue models, despite being similar in size to many of the aforementioned examples. One such rationale for this discrepancy could involve the presence of such a high degree of exogenous ECM protein in the other tissue constructs. Since ECM naturally acts as a shock absorber to force transmission, the overabundance of ECM present in those constructs could be absorbing force transmission during myotube contraction.

Additionally, both histological and immunostained images of other tissue constructs demonstrate that the myotubes present are very thin and sparse in appearance, compared to the myotubes generated with our tissue assembly/maturation process which contain a greater number of nuclei and are thicker in diameter when compared to previous literature, which quantified the myotube diameter maximally at 6 μ m [11], whereas we observed myotube diameters exceeding 20 μ m. This difference in myotube diameter could be another reason for the increased force production following tetanic contraction.

5.5. Conclusions

Overall, we have made categorical improvements to tissue morphology by modulating the culture and growth conditions of the 3D tissues. It is important to note that such improvements, made by either changing the mold shape and/or by optimizing pro-maturation and pro-ECM producing supplementation played a drastic role in subsequent tissue contractile function. Of most note, the addition of ascorbic acid and IGF-1 had a very minimal effect on the gross tissue morphology - as determined using H&E histochemistry. However, the addition of IGF-1 had a significant, but minimally-noticeable effect on increasing the diameter of the myotubes. Past researchers have not focused on optimizing the culture or growth conditions to generate more mimetic tissue, and often have been content with the proof-of-concept experimentation that results in contiguous 3D tissue formation, regardless of the methodology used. What we have demonstrated here is that even though the culture and supplement improvements have minimal morphological visual benefit within the 3D tissue, in fact the benefit is drastically seen when the tissues are mediated to contract. Past researchers have used only one measurement (e.g. force production) to determine success of an experiment, whereas we used a multitude of benchmarks, notably, 2D and 3D culture, coupled with morphological and immunostaining, to determine the effect that experimental variables have on tissue production and maturation. We then correlated the improvements to significant increases in contractile tissue function.

In conclusion, our multi-pronged approach to developing and optimizing benchtop tissue constructs appear to result in tissue that more closely approximates native skeletal muscle morphology and function than previous tissue constructs. While we still may be close to an order of magnitude away from native muscle force production, we have improved force production significantly, compared to prior work. In general, past researchers have not investigated similar types of optimization and

verification systems, potentially limiting the resulting contractile force production of their tissue constructs.

5.6. References

1. Vandenburg, H., et al., *Drug-screening platform based on the contractility of tissue-engineered muscle*. Muscle Nerve, 2008. **37**(4): p. 438-47.
2. Grasman, J.M., et al., *Crosslinking strategies facilitate tunable structural properties of fibrin microthreads*. Acta Biomater, 2012. **8**(11): p. 4020-30.
3. Tan, K., et al., *Characterising skeletal muscle under large strain using eccentric and Fourier Transform-rheology*. J Biomech, 2015. **48**(14): p. 3788-95.
4. Grasman, J.M., et al., *Rapid release of growth factors regenerates force output in volumetric muscle loss injuries*. Biomaterials, 2015. **72**: p. 49-60.
5. Page, R.L., et al., *Restoration of skeletal muscle defects with adult human cells delivered on fibrin microthreads*. Tissue Eng Part A, 2011. **17**(21-22): p. 2629-40.
6. Gwyther, T.A., et al., *Engineered vascular tissue fabricated from aggregated smooth muscle cells*. Cells Tissues Organs, 2011. **194**(1): p. 13-24.
7. Craige, S.M., et al., *NADPH Oxidase 4 Promotes Endothelial Angiogenesis Through eNOS Activation*. Circulation, 2011. **124**(6): p. 731-740.
8. Gillies, A.R. and R.L. Lieber, *Structure and function of the skeletal muscle extracellular matrix*. Muscle Nerve, 2011. **44**(3): p. 318-31.
9. Clafin, D.R., et al., *Effects of high- and low-velocity resistance training on the contractile properties of skeletal muscle fibers from young and older humans*. J Appl Physiol, 2011. **111**(4): p. 1021-30.
10. Mertens, J.P., et al., *Engineering muscle constructs for the creation of functional engineered musculoskeletal tissue*. Regenerative Medicine, 2014. **9**(1): p. 89-100.
11. Shansky, J., et al., *Paracrine release of insulin-like growth factor 1 from a bioengineered tissue stimulates skeletal muscle growth in vitro*. Tissue Eng, 2006. **12**(7): p. 1833-41.
12. Powell, C.A., et al., *Mechanical stimulation improves tissue-engineered human skeletal muscle*. Am J Physiol Cell Physiol, 2002. **283**(5): p. C1557-65.
13. Larkin, L.M., et al., *Structure and functional evaluation of tendon-skeletal muscle constructs engineered in vitro*. Tissue Eng, 2006. **12**(11): p. 3149-58.
14. Weist, M.R., et al., *TGF-beta1 enhances contractility in engineered skeletal muscle*. J Tissue Eng Regen Med, 2012.

Chapter 6: Downstream Translation of Benchtop Muscle Technology

6.1 Overview

Additional work presented in this chapter investigated the initial downstream translations of the developed tissue generation technology and aimed to show that feasibility of future work is possible. Following the development, optimization and functional force generation readout of this healthy skeletal muscle 3D model, challenges still remain prior to this technology being transferred into a more clinically-applicable model for use as a candidate drug screening and testing tool capable of replacing poorly-predictive pre-clinical animal modeling and the inability to determine non-target drug side effects, that currently increases the time, cost, and lack of drug efficacy during development [1].

Feasibility studies investigating the possibility of increasing the cell-ECM connections and hence increasing the maturation potential of these tissue constructs have been researched. Furthermore, preliminary research into the generation of tissue rings using a diseased (dystrophic) cell line have also been investigated, allowing us to determine if a correlation between culturing healthy normal muscle tissue and dystrophic muscle tissue exists with respect to culture and tissue mold seeding conditions.

6.2 Collagen Gel

Prior work has demonstrated that the use of an exogenous ECM protein such as collagen [2, 3] and fibrin [4], can be used to translate 2D monolayer cultures to 3D tissue cultures. While this method provides the myoblasts with an abundance of exogenous ECM protein for which crucial cell-ECM connections necessary for native levels of regeneration, can be made, drawbacks of current ECM-gel platforms involve the presence of substantial undigested matrix that results in a cell density lower than that of native regenerating muscle, inhibiting native functionality generation [5].

We have modified our seeding parameters to attempt to introduce exogenous ECM protein in our tissue rings without sacrificing the high cell density needed for tissue maturation. Using a similar culture and tissue seeding protocol, cells were expanded and pre-differentiated in 2D culture prior to trypsinization and harvesting. For proof of concept testing, an immortalized murine myoblast cell line (C2C12), a common myoblast cell line used in muscle research [6-9], was used for experimentation due to low cost and ease of culturing, *in vitro*. Different from prior work, where cells were resuspended in culture medium, cells were resuspended at the same seeding densities in Collagen type 1 (Advanced BioMatrix), pH 7.4 chilled on ice. The cell-gel solution was gently pipetted into the wells of the tissue ring molds and gently mixed to ensure uniform circumferential cell distribution. Following seeding, the tissue molds were incubated at RT for 1 hr (a deviation from prior work which induced immediate polymerization at 37°C) to prevent collagen gelation. We hypothesized that delaying gelation would allow the cells to settle to the bottom of the well and aggregate in a higher density. Following 1 hr, half of the volume of the collagen gel was gently manually pipetted off the top of tissue mold, following which, tissues were transferred to 37°C to promote gelation. Similar to past work, tissues were flooded with differentiation following 24 hrs in culture and fed daily, according to protocols presented in previous chapters.

Results of such study indicate that, despite cells being resuspended in a uniform gel, the delayed polymerization allows for cell aggregation at the bottom of the well, and following 14 days in culture, a high cell density tissue ring is observed. In fact, due to the dual benefit of the exogenous ECM providing early time point cell-ECM binding, the cell number seeded into the tissue wells were decreased by 50% to 200,000 cells/ring (for the annular well tissue molds), and still, contiguous tissue formation occurred. Seen below in *Figure 50*, H&E images of tissue rings following 14 days of culture formed with exogenous collagen gel, seeded with either 200,000 or 400,000 cells/ring.

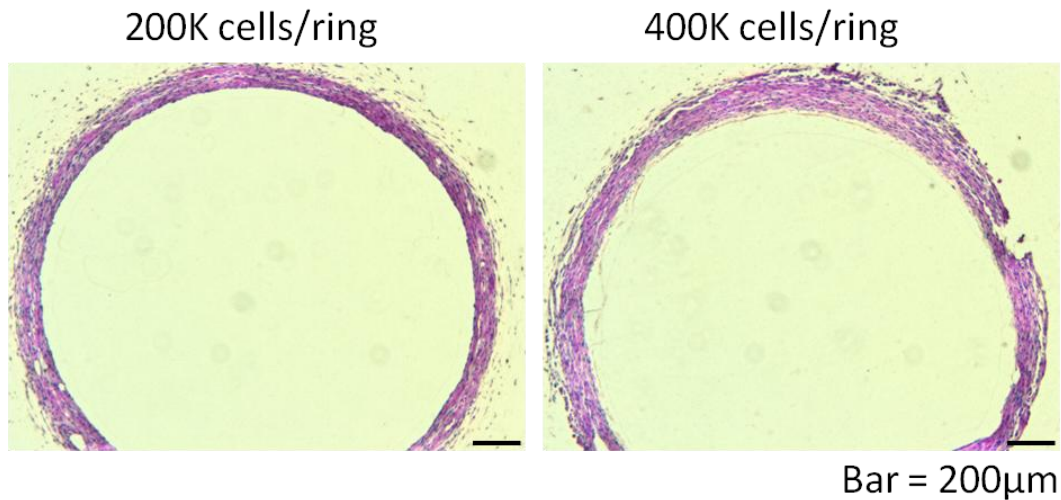


Figure 50: H&E Images of Collagen Gel Rings

Tissue rings formed following re-suspension in collagen gel. A high cell density tissue ring is produced due to the delayed gelation step and a reduction in cell seeding number due to the presence of collagen gel is possible.

Further investigation into the benefit of incorporating exogenous ECM protein into the culture during tissue formation was completed by staining for myosin heavy chain protein, using the same methods as described previously. Seen below in *Figure 51*, myosin heavy chain protein staining on sequential sections (from *Figure 50*, above) of collagen-gel tissue rings, with myosin protein visualized in brown, with nuclei counterstaining in hematoxylin. As indicated by the red arrows, striations in the myosin-positive myotubes are visible in the 200,000-cell collagen gel tissue rings. We postulated that the increased in maturation compared to prior work, as indicative by the striations, are a result of the presence of the ECM protein, an observation that has been well researched in literature [10, 11].

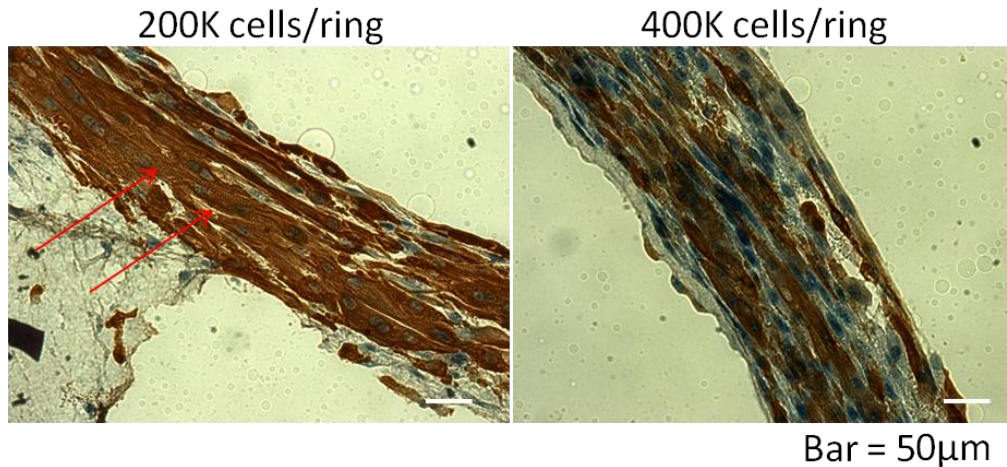


Figure 51: Myosin Heavy Chain Staining of Collagen-Gel Tissue Rings
 Visible striations are seen in the 200,000-cell tissue rings indicating increased maturation following culture.

Future work could investigate the role that providing human cell tissue rings with exogenous ECM has on maturation. Furthermore, this preliminary work only utilizes a single ECM protein (collagen), whereas substantial past work has demonstrated that there is likely a symbiotic benefit of numerous ECM proteins, as such proteins, especially basement membrane proteins (collagen IV, VI, laminin-211), play a crucial role in myoblast differentiation and native levels of maturation.

6.3 Dystrophic Tissue Generation

To date, we have presented work to generate a benchtop model of healthy human skeletal muscle, and postulate that such methodology for tissue creation and subsequent culture could be translated more precisely to a dystrophic model system. Preliminary work has investigated the feasibility of forming tissue rings using previously defined culture protocols from a dystrophic cell line. A disease model of human FSHD cells were acquired from the Coriell Cell Repository and expanded under standard adherent culture conditions, as prescribed by the supplier to be used for 2D and 3D experimentation in the lab setting.

Initial expansion for 2 passages yielded a substrate-adherent population of fibroblastic-appearance cells. Subsequent washing and transition to a mitogen-reduced differentiation medium

(Differentiation Medium - previously defined), resulted in the exit of replicative cell cycle and transition to myogenic differentiation. Seen below in *Figure 52* FSHD cells differentiated for 14 days with nuclei (blue) and myosin heavy chain (green) labeled, as described in previous protocols. Terminal differentiation of the FSHD cells demonstrate a decreased myogenic potential of the *in vitro* culture, as a significant proportion of the cells are not actively participating in the differentiation, as evident by the lack of myosin protein.

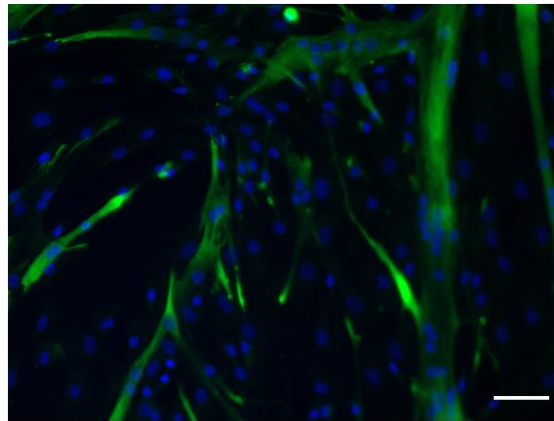


Figure 52: 14 Day Differentiation of FSHD Cells

Terminal differentiation of FSHD cells demonstrates a decreased differentiation capacity compared to primary human myoblast cell lines. Bar = 50 μ m

Further preliminary work sought to determine if 3D tissue rings could be formed using the human FSHD-diseased cells. Similar to past work, cells were pre-differentiated for 2 days in 2D culture prior to being seeded into tissue rings. The cells formed contiguous tissue rings, using the same parameters for both the original annular well molds and the conical post molds, as described previously, and were subjected to the same culture conditions as past work, to minimize experimental variation. As seen below in *Figure 53*, H&E images of the tissue rings, contiguous tissue formation is possible and uniform aggregation of the cells around the central post is observed for both groups.

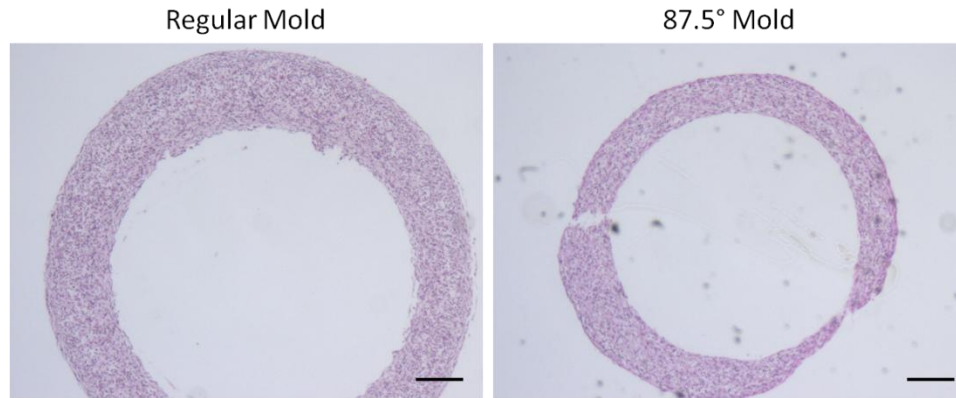


Figure 53: FSHD Tissue Rings

Contiguous tissue formation of FSHD cells into 3D tissue rings is possible for both annular well and 87.5° sloped post molds. Bar = 200 μ m.

Initial analysis indicate that there are differences in cellular alignment compared to healthy primary human-based tissue rings, however, preliminary experimentation with the FSHD cells did not investigate the beneficial effect of fibroblast inclusion, as such may skew data on 3D tissue formation and aggregation. There is a visible difference in tissue ring inner diameter - indicating that in a similar fashion to the healthy primary tissue rings, the FSHD tissue rings contracted and migrated up the conical post of the 87.5° post mold. Once again, this cell motility indicates that the cells are actively undergoing remodeling and migrate as a single contiguous tissue during the 14 days of 3D culture.

6.4 Conclusions

We have completed preliminary research to investigate the feasibility of incorporating exogenous ECM protein into tissue constructs without sacrificing the cell density necessary to promote maturation of the tissue constructs. We have also shown that the inclusion of exogenous collagen protein may result in more maturation of the myotubes, as indicative of the sarcomeric structure visible following 14 days of 3D culture. Furthermore, the translation of the culture system to a dystrophic system demonstrates initial capability to produce guided self-assembled tissues that have the potential to model a disease phenotype, *in vitro*.

6.5 References

1. Pinnapureddy, A.R., et al., *Large animal models of rare genetic disorders: sheep as phenotypically relevant models of human genetic disease*. Orphanet J Rare Dis, 2015. **10**: p. 107.
2. Vandeburgh, H., P. Karlisch, and L. Farr, *Maintenance of highly contractile tissue-cultured avian skeletal myotubes in collagen gel*. In Vitro Cell Dev Bio, 1988. **24**(3): p. 166-74.
3. Vandeburgh, H., et al., *Drug-screening platform based on the contractility of tissue-engineered muscle*. Muscle Nerve, 2008. **37**(4): p. 438-47.
4. Huang, Y.C., et al., *Rapid formation of functional muscle in vitro using fibrin gels*. Journal of Applied Physiology, 2005. **98**(2): p. 706-713.
5. Gillies, A.R. and R.L. Lieber, *Structure and function of the skeletal muscle extracellular matrix*. Muscle Nerve, 2011. **44**(3): p. 318-31.
6. Khodabukus, A. and K. Baar, *Regulating fibrinolysis to engineer skeletal muscle from the C2C12 cell line*. Tissue Eng Part C Methods, 2009. **15**(3): p. 501-11.
7. Nagamine, K., et al., *Micropatterning contractile C2C12 myotubes embedded in a fibrin gel*. Biotechnol Bioeng, 2010. **105**(6): p. 1161-7.
8. Patz, T.M., et al., *Two-dimensional differential adherence and alignment of C2C12 myoblasts*. Materials Science and Engineering: B, 2005. **123**(3): p. 242-247.
9. Langelaan, M.L., et al., *Advanced maturation by electrical stimulation: Differences in response between C2C12 and primary muscle progenitor cells*. J Tissue Eng Regen Med, 2011. **5**(7): p. 529-39.
10. Kroehne, V., et al., *Use of a novel collagen matrix with oriented pore structure for muscle cell differentiation in cell culture and in grafts*. J Cell Mol Med, 2008. **12**(5A): p. 1640-8.
11. Heher, P., et al., *A novel bioreactor for the generation of highly aligned 3D skeletal muscle-like constructs through orientation of fibrin via application of static strain*. Acta Biomater, 2015. **24**: p. 251-65.

Chapter 7: Conclusions and Future Work

7.1 Overview

In conclusion to this in depth study, we have presented concise methodology towards the development of a biomimetic 3D benchtop model of human skeletal muscle through the use of guided non-adhesive molds capable of promoting cell-cell self-assembly. We have shown that we can reproducibly generate 3D tissues and that certain optimized parameters including pre-differentiation, minimization of the cell number, and inclusion of ECM-synthesizing fibroblasts have been shown to improve tissue formation and cell alignment while decreasing tissue necrosis. Furthermore, we have demonstrated that further mold modifications coupled with culture supplementations increase production of pro-maturation and pro-ECM proteins and result in tissue morphology that better emulates native muscle during development and regeneration. Finally, we have shown that measured increases in contractile and ECM proteins along with observed differences in various tissue mold configurations correlate to statistical increases in both mechanical strength of the tissues, along with tetanic contractile force production. In conclusion, we have developed a model of human skeletal muscle that better approximates native muscle structure and functionality compared to the current gold-standard.

The following section highlights future directions of this research that allow the methodology and techniques used to create muscle models to be translated to a diseased model system while simultaneously investigate high-throughput methodologies to make this tissue generation platform more desirable for pre-clinical screening assays for candidate drug efficacy aimed at replacing poorly-predictive pre-clinical animal modeling. Additionally, the development of a mimetic skeletal muscle tissue model can also serve to elucidate side effects of non-target drugs during the early stages of benchtop drug discovery.

7.2 Future Work

7.2.1 Translating Model into a High-Throughput System

Current 3D skeletal muscle tissue model generation is conducted in a 6-well plate format and utilize between 300- and 400,000 cells/tissue and roughly 20 ml of media per tissue per the 14 days of culture time. While the cell and media need have been minimized for this model, their quantity is still far greater than current benchtop high-throughput assay systems which utilize high-content based screening systems including microarray chips and high-density well plates. Compared to microarray systems that were initially developed for gene expression analysis, where thousands of distinct and ordered loci (termed microspots) can be printed on a single glass microscope slide and are capable of returning outputs including metabolism and drug resistance, our system still remains orders of magnitude larger [1, 2]. Furthermore, many high-content screening systems utilize microwell plates that are more useful for drug to drug and drug dosing experiments, where certain analysis tools including colorimetric or molecular-based assays can be employed on the entire plate at the same time, minimizing time and cost associated with analysis [3].

The majority of current high-throughput assay systems still utilize 2D cell cultures, and are focused on "one gene" or "one protein" targets on the benchtop [3]. Furthermore, benchtop 2D cultures fail to recapitulate the 3D *in vivo* niche, nor do they consider the overall tissue or organ effect or interactions that the therapeutic may have on other systems in the body [1, 3]. Overall, the benefit of high-throughput organ-on-a-chip technology is well understood, and can provide initial cues predictive cues towards effective therapeutics, there still lacks a connection between such screening methods and the complexity and structure of native tissue.

As such, future work will aim to bridge the gap between current predictive benchtop models that more precisely mimic native function, and the clear high-throughput/cost effective screening systems currently employed with microarray screening systems. Future directions for this project aim to

decrease the tissue size and the overall cell and media requirement for building mimetic tissue constructs and translating such tissue constructs to a high-throughput 3D tissue generation and screening system, reducing the need for poorly-predictive animal models being used to bridge the gap between current high-throughput screening and clinical trials.

7.2.2. Translating to a Linearly-Aligned Model System

Our current 3D tissue generation platform produces ring-shaped tissues that are circumferentially-anchored around a central agarose post. Such geometrical shape has been useful for preliminary testing and optimization of culture conditions, as the simplified geometry results in a high degree of tissue formation and ease of culture *in vitro*. The ring tissues could be removed from the post, severed, stretched, and re-anchored in a linear fashion between two anchor points, but doing so would not precisely recapitulate the native myotendinous junctions, and likely present other mechanical challenges, requiring the cells within the tissue to realign in a linear-fashion between two anchor points following the transition to a linear system.

Ultimately, translation of the 3D self-assembly tissue method to a linearly-aligned mold system would more precisely mimic native tissue morphology. Substantial research has demonstrated that such linearly-aligned and anchored tissue constructs are possible [4-7], yet such examples utilize exogenous ECM gel to aid in tissue formation and do not utilize cell self-assembly to result in native tissue cell density and morphology.

Future work will aim to generate a small mold capable of generating linearly-aligned tissue anchored between two fixed posts in a high-content well system to facilitate use as a high-throughput benchtop assay.

7.2.3. Dystrophic Modeling - Translation

This study has defined culture methodology for the generation of a more mimetic model of skeletal muscle structure and function than previous examples. However, a healthy model of skeletal muscle tissue will not aid in the development of a drug or therapeutic to treat skeletal muscle diseases or disorders.

Ultimately (with preliminary data presented in Chapter 6 above), translation to tissue generation using the same methodology needs to be adapted to a diseased cell line model. Our preliminary work demonstrated that while tissue formation utilizing our defined culture methodology is possible, the resulting tissue structure demonstrated that some further culture and mold optimizations may be required to generate mimetic diseased microtissues on the benchtop. Interestingly, this difference highlights the fact that certain variables, including cell type and culture methodology can greatly impact the resulting 3D tissues, providing further rationale for utilizing a clinically-relevant cell source for drug screening and testing.

Such translation and subsequent validation of the tissue morphology and function will facilitate the pre-clinical testing of therapeutics in a more precise manner than using animal models. Furthermore, more specific drug-development and treatment targeting can be completed by using patient-specific cells to generate benchtop tissues, alleviating potential differences in cell source variation that we observed (despite not changing cell species). While time consuming, recent research indicates that specific targeting of combinatorial therapeutics can be done in an optimal fashion by adapting a custom treatment to specific patients.

7.2.4. Mechanical and Electrical Conditioning to Improve Maturation

Prior work had demonstrated that conditioning of benchtop 3D engineered skeletal muscle tissue constructs can improve their maturation potential. To generate muscle tissue that functions similarly to native tissue, an understanding and application of salient cues including mechanical and

electrical stimuli that are imparted on tissue during development and formation, is necessary. Specifically, controlled mechanical stimulation (stretch) coupled with electrical stimulation (pacing) is likely necessary to emulate native tissue embryogenesis and regeneration [8].

Mechanical stimulation has been well understood to play a role in muscle myogenesis whereas conversely, decreases in muscle use have been shown to lead to decreased muscle mass and ultimately atrophy [9]. For engineered skeletal muscle tissue constructs, mechanical stimulation in the form of passive and cyclic stretch-relaxation has previously been shown to improve the maturation, including an increase in myofiber diameter by 12% and an increase in 40% of overall myosin area [5].

Electrical stimulation applied to 3D skeletal muscle microtissues following 2 days in culture has been shown to increase expression levels of myosin heavy chain, as compared to un-stimulated controls [10]. As such, ongoing work is focusing on adapting a mechanical and electrical stimulation device to our 3D tissue constructs to further improve the maturation of the tissue constructs closer to that of native muscle.

7.3 Contribution to Science

This study focuses on the generation of benchtop 3D skeletal muscle tissue constructs. Further culture and mold optimizations improve tissue morphology and function to associated values closer to that of native skeletal muscle, as compared to previous "gold-standards" of *in vitro* skeletal muscle tissue models. These tissue constructs can be used as benchtop models of skeletal muscle, allowing researchers to better understand muscle development and regeneration and provide a platform for efficacy testing of therapeutic treatments. Similarly, an atrophy model of skeletal muscle could be generated [11] by removing tissue anchorage during culture, providing a tool for better understanding the effect of either low-gravity (space travel), or lack of use (tissue/bone immobilization), potentially providing clinicians with a tool for addressing muscle loss following injury.

Future work could investigate incorporation of a vascular network and/or innervation to create a more mimetic system capable of recapitulating the various other component of native muscle. Minimal prior research has preliminarily researched the role that certain growth factor (FGF-2) supplementation has on inducing re-innervation of muscle following implantation [12]. Additional work aims to investigate the process of angiogenesis, as there is currently no system capable of incorporating both innervation and angiogenesis, severely limiting the tissue model to completely recapitulating the native skeletal muscle niche [13]. Furthermore, adaptation of such a system could involve assembling individual functional units into a larger structure that could be used as a model or therapeutic for muscle regeneration - although other crucial issues would have to be addressed, including patient-specific cell sourcing, for such a therapeutic to be feasible for human therapy.

Histological analysis allows for the confirmation of mimetic structure, while immunoassays and functional tests utilizing uniaxial straining or electrical stimulation coupled with wire myography allows for the determination of tissue functionality - a crucial readout for confirming functional improvements in tissue contractile force production.

Further adaptation of this mold utilizing diseased-tissue cell sources could provide clinicians with a benchtop testing tool for the development of therapeutics for muscular diseases such as muscular dystrophy. Recent work in this field has noted that more precise mimetic benchtop 3D models of tissues are capable of providing more precise and relevant pre-clinical data, as compared to the current standard of utilizing animal models for pre-clinical testing.

In conclusion, this novel benchtop model of skeletal muscle tissue, generated by guided self-assembly results in a more mimetic minimal functional unit of tissue, compared to recent work. As such, this model system can be appropriately adapted to streamline candidate drug discovery and therapeutic development for various muscular diseases.

7.4 References

1. Russo, G., C. Zegar, and A. Giordano, *Advantages and limitations of microarray technology in human cancer*. *Oncogene*, 2003. **22**(42): p. 6497-507.
2. Schena, M., et al., *Quantitative Monitoring of Gene Expression Patterns with a Complementary DNA Microarray*. *Science*, 1995. **270**(5235): p. 467-470.
3. Berthuy, O.I., et al., *Multiplex cell microarrays for high-throughput screening*. *Lab Chip*, 2016. **16**(22): p. 4248-4262.
4. Shansky, J., et al., *Paracrine release of insulin-like growth factor 1 from a bioengineered tissue stimulates skeletal muscle growth in vitro*. *Tissue Eng*, 2006. **12**(7): p. 1833-41.
5. Powell, C.A., et al., *Mechanical stimulation improves tissue-engineered human skeletal muscle*. *Am J Physiol Cell Physiol*, 2002. **283**(5): p. C1557-65.
6. Cheema, U., et al., *3-D in vitro model of early skeletal muscle development*. *Cell Motil Cytoskeleton*, 2003. **54**(3): p. 226-36.
7. Brady, M.A., M.P. Lewis, and V. Mudera, *Synergy between myogenic and non-myogenic cells in a 3D tissue-engineered craniofacial skeletal muscle construct*. *J Tissue Eng Regen Med*, 2008. **2**(7): p. 408-17.
8. Rangarajan, S., L. Madden, and N. Bursac, *Use of flow, electrical, and mechanical stimulation to promote engineering of striated muscles*. *Ann Biomed Eng*, 2014. **42**(7): p. 1391-405.
9. Wisdom, K.M., S.L. Delp, and E. Kuhl, *Use it or lose it: multiscale skeletal muscle adaptation to mechanical stimuli*. *Biomech Model Mechanobiol*, 2015. **14**(2): p. 195-215.
10. Langelaan, M.L., et al., *Advanced maturation by electrical stimulation: Differences in response between C2C12 and primary muscle progenitor cells*. *J Tissue Eng Regen Med*, 2011. **5**(7): p. 529-39.
11. Lee, P.H. and H. Vandenburgh, *Skeletal muscle atrophy in bioengineered skeletal muscle: a new model system*. *Tissue Eng Part A*, 2013. **19**(19-20): p. 2147-55.
12. Iwata, Y., et al., *Fibroblast growth factor-2 enhances functional recovery of reinnervated muscle*. *Muscle Nerve*, 2006. **34**(5): p. 623-30.
13. Mertens, J.P., et al., *Engineering muscle constructs for the creation of functional engineered musculoskeletal tissue*. *Regenerative Medicine*, 2014. **9**(1): p. 89-100.

Appendix

Hematoxylin and Eosin Staining Protocol

** Tissues sectioned onto positively-charged microscope slides**

Prior to staining, bake slides at 60°C - 1 hr. or until water is evaporated. Cool to RT in Fume Hood

** Filter Harris Hematoxylin prior to use**

** Always stain control slides**

- 1) Deparaffinize in Xylene I - 5 min
- 2) Deparaffinize in Xylene II - 5 min
- 3) Deparaffinize in Xylene III - 5 min
- 4) Incubate in 100% Alcohol - 5 min
- 5) Incubate in 100% Alcohol - 5 min
- 6) Hydrate in 95% Alcohol - 5 min
- 7) Hydrate in 95% Alcohol - 2 min
- 8) Hydrate in 70% Alcohol - 1 min
- 9) Hydrate in cool running water - 5 min
- 10) Stain in Harris Hematoxylin - 10 min
- 11) Rinse in cool running water until clear - 1 min
- 12) Differentiate in 0.1% Acid Alcohol - 2 quick dips
- 13) Rinse in cool water - 3 quick dips
- 14) Blue in 0.001% Ammonia Water - 30 sec
- 15) Rinse in cool running water - 10 min
- 16) Incubate in 95% Alcohol - 2 min
- 17) Counterstain in Eosin - 2 min
- 18) Dehydrate in 95% Alcohol - 30 sec
- 19) Dehydrate in 95% Alcohol - 30 sec
- 20) Dehydrate in 100% Alcohol - 30 sec
- 21) Dehydrate in 100% Alcohol - 2 min
- 22) Dehydrate in 100% Alcohol - 5 min
- 23) Clear in Xylene IV - 3 min
- 24) Clear in Xylene V - 3 min
- 25) Clear in Xylene VI - 5 min - Can be left in last Xylene for days without effect

Coverslip with 2-3 drops of Cytoseal XYL after wiping away excess Xylene

Dry slides at 37°C for 1 hr prior to imaging

Store slides at RT

Pre-IHC Tissue Hydration Protocol

**** Tissues sectioned onto positively-charged microscope slides****

****Prior to staining, bake slides at 60°C - 1 hr. or until water is evaporated. Cool to RT in Fume Hood****

**** Always stain control slides****

- 1) Deparaffinize in Xylene I - 5 min
- 2) Deparaffinize in Xylene II - 5 min
- 3) Deparaffinize in Xylene III - 5 min
- 4) Incubate in 100% Alcohol - 5 min
- 5) Incubate in 100% Alcohol - 5 min
- 6) Hydrate in 95% Alcohol - 5 min
- 7) Hydrate in 95% Alcohol - 2 min
- 8) Hydrate in 70% Alcohol - 1 min
- 9) Hydrate in 50% Alcohol - 1 min
- 10) Hydrate in running di Water - 10 min
- 11) Incubate in di Water - at least 15 min or until ready for antigen retrieval

IHC Staining Protocol - HRP Polymer Detection

- 1) Place slides into a suitable rack for antigen unmasking in pressure cooker and keep in dH₂O until the pressure cooker is ready.
- 2) Add 15 ml of Vector antigen unmasking solution to 1.5 liters of distilled water and place in pressure cooker. Place lid on loosely and set cooker on a hot plate and turn heat to high setting.
- 3) When solution reaches a boil, add slides and lock the lid.
- 4) When the steam begins to escape from the valve, start timer and cook for 10 min (can vary time between 3 and 20 min - depending on level of antigen unmasking required - cooking for the minimal time necessary for antigen unmasking will minimize background staining).
- 5) Remove from heat and run pressure cooker under cool tap water to cool.
- 6) Release pressure using valve, open cooker and rinse slides in tap water for 5 min.
- 7) Completely dry slide and using ImmEdge hydrophobic pen, outline tissue to be stained. Add ~20ul of PBS to the slide (making sure to keep the pen outlines free of fluid until they completely dry. Once dry, wash tissue with PBS (~100ul).
- 8) Quench endogenous peroxidase activity by incubating with 0.5ml 3.0% H₂O₂ at RT for 30 min (change 3.0% H₂O₂ at 15 min). Use fresh H₂O₂ to maximize quenching.
- 9) Wash 2 times with PBS (2 min).
- 10) Incubate with kit-specific blocking - 2.5% normal serum solution (20 min)

NOTE: Use reagents from kit specific to host species of primary antibody.

- 11) Aspirate blocking (DO NOT WASH) and incubate with primary Ab diluted according to specific Ab diluted in PBS/Tween + 2.5% horse serum for 30 min at RT (45 min for stronger signal).

1. Using Pap Pen: ~100ul/tissue section; or
2. Using coverslipping method: ~10 µl/tissue section on a 18x18 mm coverslip and cover with a wet paper towel to prevent evaporation; or
3. Using Thermolectron IHC chambers with ~100 µl/tissue section

- 12) Wash 3 times in PBS (5 min). Do not allow samples to dry between washes.
- 13) Incubate with ImmPRESS solution for 30 min at RT (45 min for stronger signal).

NOTE: Use reagents from kit specific to host species of primary antibody
(This must be from the same kit as step #17).

4. Using Pap Pen: ~100ul/tissue section; or
5. Using coverslipping method: ~10 µl/tissue section on a 18x18 mm coverslip and cover with a wet paper towel to prevent evaporation; or
6. Using Thermolectron IHC chambers with ~100 µl/tissue section

- 14) Wash 3 times with PBS.

- 15) Prepare enzymatic ImmPACT peroxidase substrate according to Vector Labs instructions and incubate until desired darkness (see instructions for each kit for approximate time - develop under microscopic observation - stop reaction by diluting substrate in tap water). Time positive control slide until desired darkness and match timing to test slides.

Harris Hematoxylin Counterstain (if not desired, skip to step #27):

- 16) Incubate slides in Harris Hematoxylin (2 min) - filter prior to use.
- 17) Rinse slides in running cold tap water (2 min).
- 18) Blue slides in 0.1% Ammonium Hydroxide (Ammonia Water, 15-20 sec).
- 19) Rinse in tap water (2 min).
- 20) Incubate slides in 95% ethanol (1 min).
- 21) Dehydrate slides in 95% ethanol (2 min).
- 22) Dehydrate slides in 100% ethanol (2 min).
- 23) Dehydrate slides in 100% ethanol (2 min).
- 24) Dehydrate slides in 100% ethanol (5 min).
- 25) Clear slides in Xylene IV (3 min).
- 26) Clear slides in Xylene V (3 min).
- 27) Clear slides in Xylene VI (5 min). Slides can remain in last Xylene for days without effect
- 28) Permanently mount slides using Cytoseal XYL. Let slides dry overnight in 37°C oven.